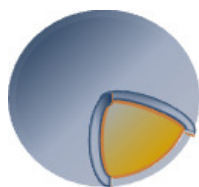# UNIVERSITA' DEGLI STUDI DI NAPOLI

FEDERICO II

Dipartimento di Ingegneria Chimica, dei Materiali e della Produzione industriale

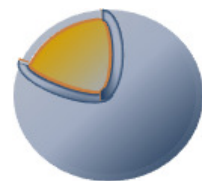*Ph.D. PROGRAMME IN MATERIALS AND STRUCTURAL ENGINEERING*

XXV CYCLE

Ph.D. Thesis

RAFFAELE VECCHIONE

BIODEGRADABLE NANOCAPSULES PRODUCED VIA LAYER-BY-LAYER TECHNIQUE ON OIL BASED TEMPLATES

TUTOR

Chiar.mo Prof. PAOLO A. NETTI

COORDINATOR

Chiar.mo Prof. GIUSEPPE MENSITIERI

To my Grandfather Raffaele

Table of Contents

CONTENTS   PAGE

Preface

Scientists are people who keep their juvenile desire to give an explanation to all and keeping discovering always something new. Since I was a child I have been very curious about everything wishing to find out explanations and solutions. However, just after my degree in Materials Engineering I chose to start working for companies even though always covering positions as a researcher. Then, following my real nature, after almost 9 years I left a permanent position accepting a temporary one to join a multidisciplinary group which deals with one of the most fascinating fields regarding bio-interfaces. Specifically, I was involved in the development of new smart nano-capsules for nano-biotechnologies. In my opinion, nothing is comparable to a job that allows discovering something useful for humankind and I am proud of my choice.

The objective of this work was to provide biodegradable nanocapsules produced layer-by-layer on oil based templates, demonstrating therefore nanoemulsion capability, once properly optimized, to be used at the same manner of solid templates but with unparalleled advantages compared to them. Indeed, they do not need to be removed after capsule preparation, they can embed high payloads of active substances and drugs and may then be exploited in a variety of bio-technology fields such as nano-food, nutraceutics, cosmetics, cosmeceutics, and, above all, nanomedicine including drug delivery and imaging for diagnostics.

In synthesis, the first chapter of the thesis is an overview on nanotechnologies mainly applied to nanomedicine but also to fields like food and cosmetics. The second chapter deals with preparation and characterization of monodisperse and biodegradable oil in water nanoemulsions characterized by a tunable stability over time. A third chapter follows regarding the development of monodisperse biodegradable nanocapsules by using previous oil in water nanoemulsions as template. This chapter includes nanocapsules made of polymer multi-layers and a chemical part for the stabilization of the polymer multi-layer. Finally, there are also some preliminary results on the preparation of hybrid polymer silica shell nanocapsules always around nanoemulsions in the Appendix.

List of Figures

Chapter I

Chapter II

Apendix

List of Tables

Chapter II

Chapter III

Appendix

Table A.E.1. Primary emulsions at 10 and 20% wt of oil for the five different concentration of lecithin (L1÷L5) at the different processes cycles and cycles + steps.

Tab. A.E.2. Stability tests secondary emulsions reprocessed once (A, C, E, G, I), reprocessed twice (B, D, F, H, L) and no re-processed (M).

Table A.E.3. Fluorescence emission at 510nm for L4 secondary emulsions coated with chitosan-FITC and free chitosan at the same concentrations.

Table A.E.4. Summary of the different concentrations utilized and the molecular weights obtained.

Table A.E.5. DLS results on purification without dilution.

Table A.E.6. Summary of DLS and EDS analysis on purified L1 secondary emulsions.

Table A.E.7. Alginate functionalization: conditions of reaction and degree of functionalization.

List of Symbols

ABC: ATP-binding cassette;

APM: Auxiliary processing module;

APTS: 3-(aminopropyl)triethoxysilane

BBB: Blood brain barrier;

BSA: Bovine serum albumin;

CN: Carbon Nanotube;

DABCO: 1,4-diazabicyclo[2.2.2]octane;

DDS: Drug Delivery System;

DLS: Dynamic light scattering;

DMF: Dimethylformamide;

DMSO: Dimethylsulfoxide;

DTNB: 5,5′-Dithiobis(2-nitrobenzoic acid);

ECM: Extracellular matrix;

EDAC or EDC : N-Ethyl-N′-(3-dimethylaminopropyl)carbodiimide;

EDTA: Ethylenediaminetetraacetate;

EDX: Energy-dispersive X-ray;

EGFR: Epidermal growth factor receptor;

EPR: Enhanced Permeability and Retention;

FDA: Food and drug administration;

FITC: Fluorescein 5(6)-isothiocyanate;

GAG: Glycosaminoglycan;

GI: Grastrointestinal;

GRAS: Generally recognized as safe;

GUV: Giant unilamellar vesicle;

HDL: High density lipoproteins;

HOBt: 1-Hydroxybenzotriazole hydrate;

IFP: Interstitial Fluid Pressure;

LBL: Layer-by-layer;

LDL: low density lipoproteins;

LDV: Laser doppler velocimetry;

LMW: Low molecular weight;

LPC: Lyso-phosphatidylcholine;

LPE: Lyso-phosphatidylethanolamine;

LUV: Large unilamellar vesicle;

MCT: Medium chain triglyceride;

MF: Melamine formaldehyde;

MNP: Magnetic nanoparticle;

MPD: Myeloproliherative diseases;

MPS: Mononuclear phagocytic system;

MR: Magnetic resonance;

MRI: Magnetic resonance imaging;

MSN: Mesoporous silica;

NAC: N-Acetyl-L-cysteine;

NC: Nanocarrier;

NE: Nanoemulsion;

NIBS: Non-invasive backscatter;

NIR: Near Infrared;

NIRF: Near infrared fluorescence;

NIST: National Institute of Standards and Technology;

NMR: Nuclear magnetic resonance;

NP: Nanoparticle;

NR: Nile Red;

OCMTS: Octamethylcyclotetrasiloxane;

PAMAM: Poly(amido amine)

PAV: Prednisolone acetate valerate;

PC: Phosphatidyl choline;

PCL: Polycaprolactone;

PDI: Polydispersion index;

PE: Phosphatidylethanolamines;

PEEP: Poly(ethylethylene phosphate);

PEG: Polyethylenglycole;

PEI: Polyethylene imide;

PGA: Polyglycolic acid;

P-gp: Permeability-glycoproteins;

PHBHV: Poly(hydroxybuttyrate-co-hydroxyvalerate);

PIC: Phase inversion composition;

PIT: Phase inversion temperature;

PLA: Poly(lactic acid);

PLGA: Poly(lactic co-glycolic acid);

PLL: Poly-lysine;

PMPC: Poly(2-methacryloyloxyethyl phosphorylcholine);

PNIPAM: Poly(N-isopropylacrylamide);

PS: Polystirene,

PVA: Poly(vinyl alcohol);

PVP: Poly(vinylpyrrolidone);

QR: Quercetine;

RES: Reticulo Endothelial System;

RF: Radio frequency;

RGD: Arginine glicyne aspartic acid;

RME: Receptor mediated endocytosis;

ROS: Reactive oxygen species;

SEM: Scanning elctron microscopy;

SLN: Solid Lipid Nanoparticles;

SPH: Sphingomyelin;

SPR: Surface plasmon resonance;

STED: Stimulated emission depletion;

SUV: Small unilamellar vesicle;

TEM: Transmission electron microscopy;

Tf: Transferrin;

TMS: Tetramethylsilane;

USP: United States Pharmacopea;

UV: Ultraviolet;

UV-Vis: Ultraviolet Visible;

Vd: Volume of distribution;

ZnPc: Zinc (II) phthalocyanine;

Chapter I: Nano-bio-technologies

1.1. Introduction

Nano-bio-technologies represent today one of the most investigated and challenging topics of scientific research both at an academic and industrial level. This study involves a body of knowledge ranging from pharmaceutics, biology, chemistry and material science. It comprises several important fields such as nanomedicine, including drug delivery and diagnostics, nano-food, nutraceutics, cosmetics.

According to the National Nanotechnology Initiative (2006), "Nanotechnology is the understanding and control of matter at dimensions of roughly 1 to 100 nanometers, where unique phenomena enable novel applications. Encompassing nanoscale science, engineering and technology, nanotechnology involves imaging, measuring, modeling, and manipulating matter at this length scale." Consequently, interest and activities in this research area have greatly increased over the past years. The potential benefits of nanotechnology have been recognized by many industries, and commercial products are already being manufactured, such as in the microelectronics, aerospace, pharmaceutical industries, food industries, cosmetics and so on [1].

One of the possible contributions of nanotechnology, in the case of nanomedicine, would be in building biocompatible multifunctional nanocarriers (NCs) able to navigate within living organisms releasing their cargo at the site of interest by means of active or passive stimuli. Such carrier systems are used to improve cargo stability, to sustain and control their release rates, to increase the bioavailability of cargo substances, and to target them to specific sites within the body. A system which combines all these functionalities into one structure has still not been well developed. The requirements of such a system can be conceptually divided into several steps. First, the cargo (in general bioactive molecules) has to be encapsulated. This not only allows for high local concentration inside the carrier, but also for protection of the cargo molecules against cytotoxic damage and enzymatic degradation. Next, the cargo has to be delivered to the target cells while sparing the surrounding cells by exploiting an internal or an external trigger.

NCs should be limited in size to cross for example the pores of tumor capillaries. The upper limit for an ideal vehicle size should not exceed about 200 nm. Secondly, due to their nature, the capsules tend towards protein adsorption, potentially leading to capsule aggregation in the blood capillaries [2]. Of course NCs design will be depending on the kind of administration route, which is mostly via intraveneous injection but it can be also via oral, skin or other routes.

In contrast, applications of nanotechnology within the food industry are rather limited. However, achievements and discoveries in nanotechnology are beginning to impact the food industry and associated industries; this affects important aspects such as food safety, synthesis of new food products and ingredients, on demand and interactive food. Building on the concept of "on demand" food, for example, the idea of interactive food is to allow consumers to modify food depending on their own nutritional needs or tastes. The concept is that thousands of nanocapsules containing flavour or color enhancers or added nutritional elements (such as vitamins), would remain dormant in the food and only be released when triggered by the consumer. Moreover, food science and the food industry face the enormous challenge of making food both healthy and tasty. Because of the pressures of life in modern society, many consumers tend to choose food rich in fats and carbohydrates increasing the number of obesity and diabetes cases. The challenge for the food industry is to make healthy food a logical choice for the consumer. This logical choice can be realized by manipulating the complex structure and proprieties of food [3]. One way could be to reduce the volume in nanometer size preserving always, with the same surfaces, the same organoleptic proprieties. In general, when a functional food aids in the prevention and/or treatment of disease(s)/disorder(s) as well as deficiency conditions like anemia it is called a "nutraceutical" [4]. Examples of nutraceuticals include fortified dairy products (milk as such is a nutrient and its product casein is a pharmaceutical) and citrus fruits (orange juice is nutrient and its constituent ascorbic acid is a pharmaceutical). In this case, the use of nanotechnology for instance nanoemulsions and polymer micelles-based delivery systems can boost the bioavailability of nutrients such as phytochemicals [5].

Nanotechnology has also applications in the cosmetic industry. The functions of whitening, anti-aging and so on variously are expected for cosmetics. Therefore development of drug delivery systems (DDS) for cosmetics is highly desired, since a clearer effect can be obtained by delivering an active ingredient, for example, into the skin in this way. Examples of NCs for drug delivery, also used in cosmetic industry are nano-encapsulation vesicular delivery systems,

nanoemulsions and nanocrystals, liposomes and niosomes, micelles, polymeric nanocapsules, solid lipid NCs and nanostructured lipid carriers, carbon nanotubes and fullerenes, and dendrimers. The primary advantages of using nanoparticles (NPs)-based formulations in cosmetic products are to improve the stability of various cosmetic ingredients (like unsaturated fatty acids, vitamins), enhance penetration of certain ingredients (such as vitamins), increase the efficacy and tolerance of ultraviolet (UV) filters on the skin surface and make the product more aesthetically pleasing (e.g., in mineral sunscreens, making the particles of the active mineral smaller allows them to be applied without leaving a noticeable white cast). However, concerns have been raised regarding the potential dangers which may occur as a consequence of NPs contact with human skin. This has initiated an integrated approach including advanced physico-chemical characterization of different types of NCs to understand their stability and mechanisms by which they penetrate intact skin. Some physico-chemical characteristics which may be important in understanding how far a nanoparticle may penetrate the skin include particle morphology and size, size distribution, surface chemistry, surface coating, surface charge, specific surface area, pore density, porosity, water solubility, agglomeration and aggregation [**6, 7**]. The direction also in this case is towards completely biodegradable materials.

1.2. Drug delivery

1.2.1. Introduction to drug delivery

The effectiveness of most of the present drugs is limited by their poor solubility in water, strong side effects due to the combination of high drug toxicity and non controlled bio-distribution, and clearance by the extremely aggressive immune defense system of human body. Indeed, the host immune system is based on the reticulo-endothelial system (RES), which includes kidney, liver, spleen and lymph nodes causing clearance of external bodies [**8**]. Each of them acts in response to certain size range.

In the last three decades nanotechnology has attracted a huge interest in healthcare due to the possibility to vehicle whatever drug, carry and deliver it directly on the site of disease by means of biocompatible NCs [**9**]. NCs not only improve the solubility of drugs but also protect them

from the attack of the immune defenses. Indeed, NCs can be properly modified on their surface in order to strongly reduce clearance thus enhancing circulation time. Therefore, they can pave the way for a much more effective use of present drugs, instead of developing new drug molecules which is expensive and time consuming.

Moreover, NCs can improve drug bio-distribution allowing its delivery at the site of disease by both passive and active mechanisms. As a matter of fact, tumor vasculature is leaky therefore NCs circulating in the blood due to their small size can accumulate in the tumor tissue more than in the healthy tissue [10]. This Enhanced Permeability and Retention (EPR) mechanism require sizes below 200nm which are possible with NCs [11]. Shape also can play a role as it will be described later. Moreover, NCs can promote an active targeting by conjugating their surface with specific receptors again making drug delivery specific to the site of disease [12]. In the **Figure 1.1** it is reported a scheme of multifunctional nanocapsules while extravasating from blood vessel.
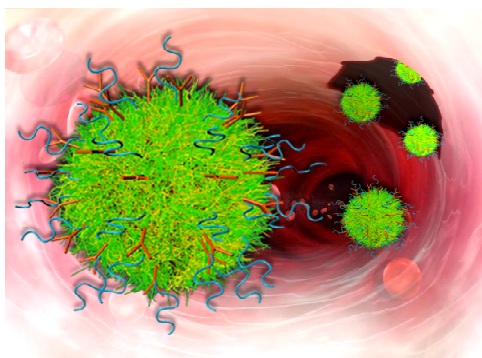
Figure 1.1. Scheme of engineered polymer nanocapsules while traveling and extravasating from blood vessel.

Another major obstacle to successfully treating malignant diseases is the tumor drug resistance [13-15]. Indeed, drug tend to be sequestrated in acidic endosomes of perivascular tumor cells producing an heterogeneous therapeutic treatment which enhances malignance of cancer cells exposed to under-lethal doses which become more resistant to the cytotoxic effects of chemotherapeutic [16]. In addition the enhanced interstitial fluid pressure (IFP) in the tumor tissues also prevents a uniform diffusion of the drug [17]. These and other adverse drug resistance phenomena contribute to treatment failure in over 90 % of patients but again, nanotechnology represents a promising route in this field [8]. Indeed, drugs that are encapsulated

in NCs depending on the physical and chemical properties of their reservoir can be delivered with desired pharmacokinetic profiles respect to the free drugs. Moreover, biomolecules acting as pro-drugs, for instance hyaluronidase [18] can be embedded into NCs to enhance drug penetration of physiological barriers [8].

1.2.2. Side effects in drug delivery

One major limitation in the use of the actual chemotherapeutics is their toxicity that indeed is needed to kill tumor cells but they reach and kill also healthy cells. This is due to the fact that actual chemotherapeutics are mainly delivered as free drugs therefore they can reach any tissue. Moreover, to be able to reach in a proper concentration target tissue they are needed high doses of them in the blood. Furthermore, many widely used conventional chemotherapeutics, such as taxanes, include synthetic solvents (for example, castor oil and polysorbate 80) that directly contribute to adverse effects [17]. Another example of powerful drug is the Doxorubicin, an anthracycline antibiotic used in the treatment of a wide range of cancers such as some leukemias and Hodgkin's lymphoma, as well as cancers of the bladder, breast, stomach, lung ovaries, thyroid, soft tissue sarcoma and others. Apart from inhibiting some essential activities for the life of the cell, leading it to death as for most of the drugs used for treatment of cancer diseases, Doxorubicin presents a severe cardiotoxicity [19]. Therefore there is an increasing need to design suitable DDS in order to guarantee not only the efficacy of pharmacological therapy but also avoid or minimize all the unpleasant side effects and indeed there are already some NCs based therapeutics, FDA (Food and Drug Administration) approved for clinical uses, such as pegylated liposomal doxorubicin, liposomal daunorubicin, albumin-bound paclitaxel [17]. For instance, a PEG-ylated (polyethylene glycol coated) liposome-encapsulated form of Doxorubicin (Doxil® or Caelyx®) was developed by Ben Venue Laboratories for Johnson & Johnson to treat some serious skin cancers such as Kaposi's sarcoma and other AIDS-related cancers. This particular drug delivery system and the utilization of PEG coating results in preferential concentration of Doxil® in skin, thus increasing the therapeutic effects of the drug and reducing the cardiotoxicity of the therapeutic agent compared to un-encapsulated doxorubicin. It was also approved for treatment of ovarian cancer and multiple myeloma [20, 21]. However, although less toxic than conventional therapies these agents are still associated with adverse effects, such as stomatitis

and palmar-plantar erythrodysesthesia for PEG-ylated liposomal doxorubicin and sensory neuropathy and nausea for albumin-bound paclitaxel. Moreover, despite the much higher cost than conventional drugs, the increase in overall survival is modest in many cases [**17**]. Therefore, a better understanding of the barriers that prevent efficacy and uniform delivery of DDS just into tumors is needed to develop strategies to really enhance no-side effects and effective treatments.

1.2.2. Clearance in drug delivery

The fate of a drug *in vivo* administration is determined by a combination of several processes: for example drugs administrated intravenously are subjected to distribution, metabolism, and elimination, while drugs administrated via the extravascular route are subjected to absorption, distribution, and metabolism as well as elimination. However, regardless of the administration rout involved, there is always a response from the body to drug clearance. The entity of this clearance depends on several features like drug chemical structure but also size and shape of DDS. During the last few decades, much work has been directed toward the development of delivery systems which will allow the fate of drugs within the patient to be controlled by modifying the above features.

One of the first attempts to modify the way a therapeutic is administered was the process of chemically bonding a drug molecule, a protein, a peptide or antibody fragments to PEG molecules through a particular chemical bond that is degradable in a physiological environment. The main advantage of the PEG-ylation is that PEG disguises the agent from the host's immune system (reduced immunogenicity) [**22**] and increases the hydrodynamic size of the agent prolonging its circulatory time by reducing renal clearance. The frequency of the drug intake can, therefore, be diminished, without lowering the efficiency and, potentially, the toxicity can be reduced [**23**]. Furthermore, PEG-ylation can provide water solubility to hydrophobic molecules and can alter the absorption and distribution patterns. Finally it can cause changes in binding affinity of the therapeutic moiety to the cell receptors [**24, 25**]. PEG is not biodegradable or resorbable by the body but has the advantage of being biocompatible and extremely hydrophilic [**26**]. Some successful examples of this application are already available and many others are being tested and put on the market [**27, 28**].

In the case of drugs loaded into NCs the advantage is that one strategy of enhanced circulation time can be applied to several kinds of drugs. Also in the case of NCs PEGylation is commonly used as strategy for this mean. For example PEG has first been used to improve circulation time of micelles and liposomes then serving as classic example during the development of any kind of NCs [12]. In particular, stabilization and protection induced by PEG is due to the minimization of the opsonization promoted by the immune defense system. Opsonization is a plasma protein deposition process that allows mononuclear phagocytic systems (MPS) present in the liver and spleen and to a lesser extent, in the bone marrow, to remove the carriers from circulation [11]. In other words there is a deposition of macromolecules called opsonins (fibronectins, immunoglobulins and complement proteins, circulating in blood vessels) onto the foreign bodies and opsonins are recognized by receptors expressed on the cell membrane of phagocytes [29].

There are cases of materials which do not need a PEG-ylation to survive in the blood for enough time; NCs made of hyaluronic acid is an example [10].

Size and particle surface features both play an importante role in the blood opsonization processes and clearance kinetics [29-31]. For example, Daunosome and Myocet are clinically used liposomes with sizes of 80-90 nm without PEG coating that have been reported to exhibit enhanced circulation times, although to a lesser degree than PEG-ylated liposomes such as Doxil/Caelyx [12]. Indeed, it has been seen that after administration of NCs of different sizes, myeloproliferative diseases (MPD) cells present in the liver (Kupffer cells) and the spleen contain NCs of 150-300 nm whereas MPD cells present in the bone marrow contain NCs of 30-150 nm. Therefore, at least to reduce the main clearance that is the one induced by the liver it is required a size below 150 nm. From the other side it has to be taken also into account that very small particles (<20-30nm) are instead eliminated by renal excretion.

Moreover, very small sizes (at least between 30 and 100 nm) means large surface area. This may pose problems in terms of interaction and aggregation of these nanoparticles in biological systems, which subsequently determines the increase of the final particle size and, hence, clearance. For instance, dendrimers with a size of approximately 10 nm are well known to flocculate in biological media [32].

Lipid based nanosystems, instead, can interact with lipoproteins, leading to a dramatic size change; this happens for examples with micelles. The size of the particle, therefore, is not the only important factor to consider, as anticipated; also the surface properties of the NCs, in

particular surface charge density play an important role. Charged NCs are ingested faster than uncharged ones, and positively charged NCs are found to be ingested more than negatively charged ones. Atomic force microscopy measurements of adhesive forces between NCs and cell membranes show that the uptake of polyelectrolyte NCs strongly correlates with the adhesion of capsules to the outer cell membrane [33]. Furthermore, the surface charge of the nanocapsules can affect the smooth execution of cell functions, interacting with the membrane potential. It is therefore necessary to consider the surface charge of the polyelectrolyte nanocapsules [2].Again, PEG-ylation can be a solution to allow surface charge density control and avoid fast clearance by opsonization [8]. It is worth noticing that PEG does not completely solve but slows the carrier recognition by the phagocitic cells and the second one is that PEG chains could hide, for example, some antibodies with which the carrier was functionalized for targeting. Therefore, there are strategies which allow PEG separation from NCs in presence of a certain environment like a specific pH.

  Another route to elude the RES could be based on the choice of certain NC shape [34]. Indeed, it has been demonstrated how the internalization process can depend on the shape of the NCs. The internalization process includes a variety of pathways: clathrin-dependent, independent and dipendent receptor-mediated endocytosis, pinocytosis. Among these, the most effective mechanism for the uptake of NCs is the receptor-mediated endocytosis (RME) where molecules (ligands) distribuited over the NCs surface bind to counter-molucules (receptors) expressed over the cell membrane, which eventually bends to invaginat the foreign carrier. The receptors together with the bond NCs enter the cell by membrane invagination (**Figure 1.2**).
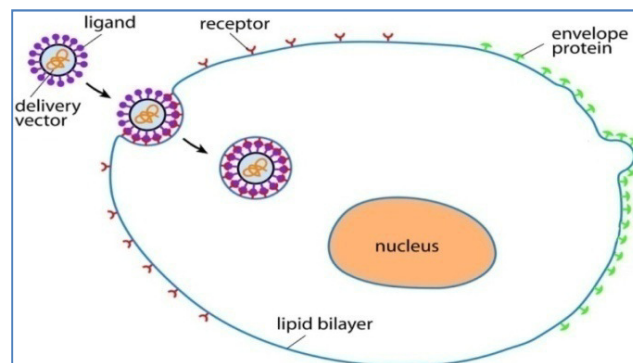
Figure 1.2. A schematic illustration of receptor-mediate endocytosis (RME).

Some experiments in vitro show how shapes different from spherical can induce even zero internalization based on the contact angle between particle and cell [**35**].

In the internalization process, also the elastic deformation of the cytoskeleton of the cell plays a role and can be considered as important as the specific ligand-receptor binding [**33**]. In addition, it is frequently observed that nanocapsules are deformed upon the incorporation process due to the mechanical stress caused in the intracellular space. Therefore, mechanical properties of the NCs can also impact the internalization mechanism. From the RES elusion point of view one could be interested in a rigid NC whereas from the internalization of NC into target cells it could be more interesting to have highly deformable NCs like nanocapsules.

1.2.4. Delivery at site of disease

Drug biodistribution plays a key role in treatment efficacy. Indeed, the ideal situation would imply the presence of drug just at the site of disease in order to be able to kill all the tumor cells and keep alive the healthy ones all around the body (**Figure 1.3**).

One of the major advantages offered by the use of NCs is the possibility to get closer and closer to that ideal case through passive targeting of drugs to the site of action or by active targeting of the drug [**9**].
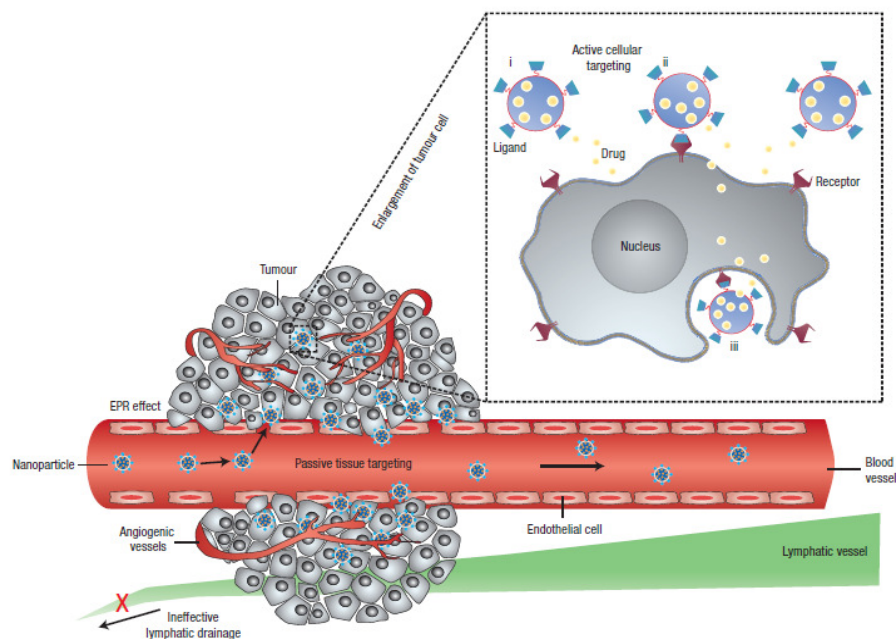
Figure 1.3. Schematic representation of different mechanisms by which NCs can deliver drugs to tumors.

Passive targeting exploits the anatomical differences between normal and diseased tissues to deliver the drugs to the required site due to EPR effect. Indeed, the integrity of the endothelial barrier in tumor tissue is perturbed by inflammatory processes or by tumor growth, the latter being a consequence of dysregulated angiogenesis [29]. The explanation here is that tumor tissues, in order to grow quickly, stimulate more the production of blood vessels that are abnormal in form and architecture because they are made of poorly-aligned defective endothelial cells with wide fenestrations, lacking a smooth muscle layer or innervation with a wide lumen and other heavily impaired functionalities. Therefore, circulating NPs can accumulate more in the tumor tissue than in the normal one. Actually even in lesser extent this effect is also observed at the site on inflammation. The only difference between them is the duration of retention period; in the case of inflammation retention time is shorter because the lymphatic drainage system is still operative differently from cancer. Retention time in cancer can last a few weeks whereas in inflamed tissue the retention can last few days. Blood vessels fenestrations which allow EPR depend on the kind of tumor and stadium and they are typically in the range of 200-780 nm [11]. Therefore in terms of EPR NCs size should not exceed 200 nm, preferable below 150 nm to better escape MPD cells and higher than 30 nm to avoid renal excretion. EPR is a universal phenomenon in solid tumors with the exception of hypovascular tumors, such as prostate or pancreatic cancers [8]. Although the EPR effect helps retain NCs in the tumor, NCs must first remain in circulation long enough to reach and extravasate the site of a tumor following one of the routes described in the previous paragraph about clearance. One of the examples is Doxil which has shown good drug retention resulting 6 times more effective than free doxorubicin [9]. Another example is the cisplatin loaded glycol chitosan NCs successfully accumulated by tumor tissues in tumor-bearing mice because of the prolonged circulation, this time induced by the hydrophilicity of the glycol groups, and EPR effect.

Combined with the above described EPR effect - passive mechanism exploiting tumor fenestrations - it is possible to enhance the specificity of the treatment by mean of an active targeting of the drug or the NCs loading drug. Active targeting requires the conjugation of receptor specific ligands that can promote site specific targeting and it is also size dependent [36]. The success of drug targeting depends on the selection of the targeting moiety, which should be abundant have high affinity and specificity of binding to cell surface receptors. The active targeting can be achieved by molecular recognition of the diseased cells by various

signature molecules over-expressed at the diseased site either via the ligand-receptor, antigen-antibody interactions or by targeting through aptamers. In this way the therapeutic agent can be actively targeted by conjugating the carrier with a cell or tissue specific ligand, thereby allowing a preferential accumulation of the drug at the diseased site. Examples of active targeting include ligands, such as the arginine-glycine-aspartic acod (RGD) peptide, epidermal growth factor receptor (EGFR), biotin, folate, transferrin (Tf) [8]. For instance, PEG-ylated gold NCs have been decorated with various amounts of Tf and the results suggest that targeted NCs can provide greater intracellular delivery of therapeutic agents to the cancer cells within solid tumors than their non-targeted analogs [9]. Other examples as said are the aptamers, which are DNA or RNA oligonucleotide sequences that selectively bind to their target with high affinity and specificity. They can target tissues and have an accumulation and a therapeutic effect by their own as shown by injecting in vivo an RNA TTA1 aptamer [37] or by modifying NCs like shown with paclitaxel-polylactide nanoconjugates which showed an enhanced targeting to cancer cells [9].

1.2.3. Drug resistance in drug delivery

Drug behavior is described by parameters such as volume of distribution (V_d), half-lives from plasma and clearance from the body [13]. These parameters are important to determine overall drug disposition which might relate to toxicity towards certain body organs but they give limited information about access to target tumor cells. An average concentration of drug that is higher in the tumor than in normal tissues is not enough if tissue penetration is poor. To be effective anticancer drugs must penetrate tissue efficiently, reaching all the cancer cells and in a concentration sufficient to exert a therapeutic effect as the survival of one cell could form the focus of tumor recurrence, at distances as far as 200µm [14]. In the reality the distribution of many anticancer drugs in tumor tissue is incomplete for several reasons [13]. For examples in the case of basic drugs like doxorubicin, epirubicin, mitoxantrone, they are sequestered in acidic endosomes of cells that are proximal to the vasculature and this retention does not allow drug to move from one cell to another following the typical penetration mechanism of lipid soluble drugs (**Figure 1.4**) [**13, 14**].
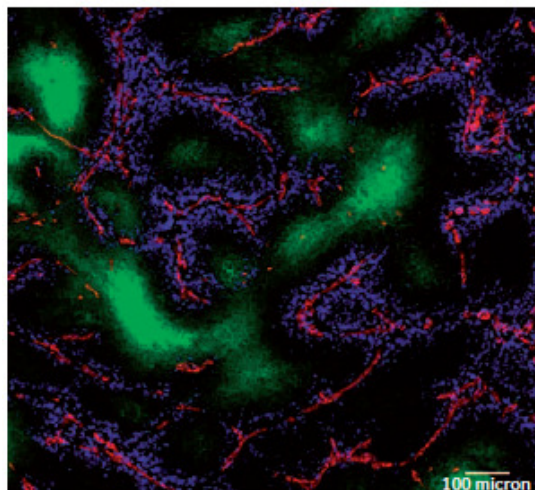
Figure 1.4. Distribution of doxorubicin in vivo (blue) in relation to tumor blood vessels (red) and inner part of tumor (green).

Moreover, in tumor one reason for ineffective drug penetration are the disorganized vascular network and the absence of functional limphatics causing an increased IFP which reduces drug convection towards the tissue and thereby inhibits drug distribution. Moreover, the composition and the structure of the extracellular matrix (ECM) of the tumor tissue is different typically more adhesive thus slowing down the movement of molecules within tumor. Furthermore, poor vascular organization leads to low concentration of oxygen in the inner part of the tumor (almost 0 at around 100µm from blood vessels) with the increase of metabolism and its products such as lactic and carbonic acids which lower the extracellular pH [**14**]. Hypoxic cells leaving in this part of the tumor behave completely different from peri-vascular cells and they are more resistant to conventional chemotherapy [**13**]. For these kinds of cells they have been developed new drugs so-called pro-drugs which are reduced under hypoxic conditions to an active form that is cytotoxic. The design of an effective pro-drug is complicated because as it diffuses from blood vessels to the hypoxic region the decrease of O_2 determines an increase of the metabolism of such molecule and there is a risk that no drug will remain to further diffuse in the tissue. On the other hand too little metabolism could reduce the efficacy of drug itself in killing tumor cells while traveling distal from blood vessels.

The resistance to drugs from cells is a major obstacle in successfully treating malignant diseases [**8**]. This phenomenon contributes to treatment failure in over 90% of patients with metastatic disease. Drug resistance can be intrinsic (gene mutation, gene amplification or

epigenetic) or acquired through exposure to chemotherapeutic agents. Tumor microenvironment can lead to drug resistance like in the case of hypoxic cells. One of the main modalities for drug resistance is that cells present a high expression of the ATP-binding cassette (ABC) transporters such as permeability-glycoproteins (P-gp) leading to a subsequent efflux of anticancer drugs from the cancer cell cytoplasm. Indeed, tumor cells often use glycolysis – the conversion of glucose into lactate to produce ATP- to obtain the energy they need to survive and proliferate rather than oxidative metabolism that leads to the production of CO_2 and carbonic acid [14]. Nanotechnology provides an innovative and promising alternative to conventional small-molecule chemotherapeutics like drugs or pro-drugs [8]. Indeed, NCs can be taken up by non-specific endocytosis and cross the cellular membrane in an 'invisible' form that prevents drugs from being recognized by efflux pumps (**Figure 1.5**).
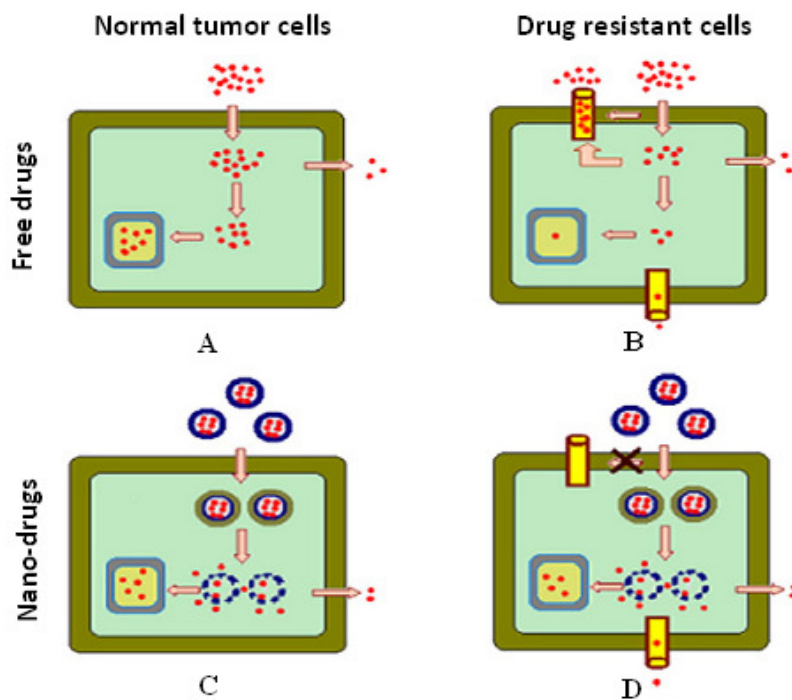
Figure 1.5. Model of the internalization process for free drugs and drugs in NCs.

Free drugs can be internalized by normal cells and just a small amount can diffuse out of the cell (**Figure 1.5.A**). In the case of drug resistant cells for free drugs, due to the P-gp present on the cell membrane, there is a more difficult internalization and an efflux of the drug from the cytoplasm towards the outside (**Figure 1.5.B**). When drug is vehicled by NCs these DDS can

enter eluding P-gp and after degradation release all drug in the cell (**Figure 1.5.D**). Of course compared to the case of normal tumor cells (**Figure 1.5.C**), some drug will diffuse from the cytoplasm out of the cell membrane through the usual efflux mechanism but the amount of drug reaching nucleus can be significantly high and enough to kill cell.

Also the issue of some drugs to be sequestered in acidic organelles of cells that are proximal to the vasculature can be faced by the use of NCs [**16**]. However, once using NCs it has to be considered that they should be small enough to deeply penetrate tumor tissue, possibly not higher than 10nm, as well as properly modified on the surface to move freely in the ECM without binding with it. At the same time it is known how such a small size is not optimal in terms of clearance due to the excretion from the kidney. Therefore a multistage DDS is maybe the optimal strategy as shown just as model by using PEGylated quantum dots of 10nm in size embedded in a gelatin NCs of 100nm also PEGylated on their surface.

Another important consideration regarding NCs penetration is that neutral and hydrophilic NCs [**16, 17**] diffuse faster and distribute more homogeneously inside the tumor interstitial space than cationic and anionic NCs because the latter form aggregates with negatively (for example, hyaluronan) and positively (for example, collagen) matrix molecules [**17**]. Of course the enzymatic activity in the ECM environment sooner or later can rescue the mobility of the NCs but the penetration and delivery time is a key parameter to avoid the exposure of cells to sublethal concentration of drug. Indeed, in these conditions they can develop drug resistance as it was shown. Another determinant of interstitial transport is the sulfated glycosaminoglycan content. These thin and elongated fibers not only carry a highly negative charge but they also significantly increase the viscosity of the interstitial fluid. For what concern the binding with the ECM particularly collagen and glycosaminoglycanit, to degrade these components the use of co-drugs like degrading bacteria, enzymes or even hormones like relaxin which modify the structure of collagen fibers has been proposed. However, agents that modify the ECM or its interaction with tumor cells might increase the probability of metastatic spread, so that their clinical applicability is unclear [**14**].

As far as concerns the shape, studies have shown that macromolecules with linear and semi-flexible configurations diffuse more efficiently than rigid spherical NCs [**17**].

Another strategy which could be implemented independently on the kind of DDS is based on the normalization of the tumor vasculature by using antiangiogenic agents which can restore the

balance between proa-angiogenic and antiangiogenic factors and reverse the vasculature to a more normal phenotype (**Figure 1.6**).
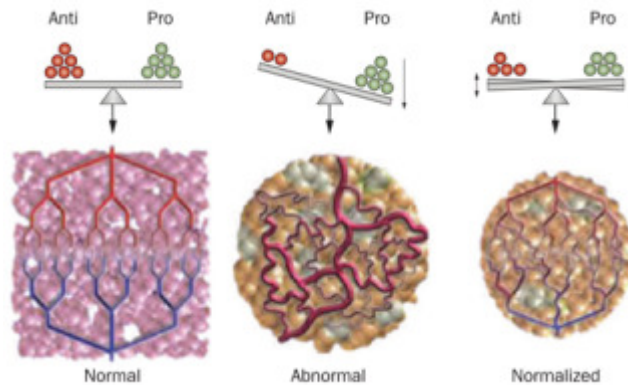
Figure 1.6. Model of normalization.

However, vessel normalization is transient, and thus, anticancer agents or NCs containing drugs should be given during the normalization window or just before normalization in order to exploit the EPR especially in the case of DDS based on the use of NCs.

1.2.4. NCs in nanomedicine

Despite the numerous strengths, discoveries and results cancer continues to be one of the biggest plagues of our time. Only in Europe there are predictions of deaths due to cancer for the 2013 approaching 1.5 million of people [**38**]. The hope is in the nanotechnologies applied to drug delivery but also to the diagnostics. Indeed, the EPR effect is observed even during the early stages of carcinogenesis (for example dyspasia and hyperplasia), thus NCs could be also used to detect very small lesions for surgical removal [**17**].

In terms of drug delivery, as already said the use of NCs to vehicle and deliver drugs is opening new therapeutic opportunities thanks to a series of advantages [**9**] like increase the aqueous solubility of drugs, protect drug from degradation, produce a prolonged release of the drug, improve the bioavailability of the drug, provide a targeted delivery of the drug, decrease the toxic side effects of the drug, offer appropriate form for all routes of administration, allow rapid-formulation development. Moreover, in terms of bioavailability as already described in the

previous paragraph it can allow internalizing drugs in drug resistant cells [**8**]. Moreover, they can carry multiple drugs and/or imaging agents and owing to their high surface area to volume ratio it is possible to achieve high ligand density on the surface for targeting purposes [**12**]. Several kinds of NCs have been developed up to now belonging to different classes like lipid lased nanocarriers (for example, liposomes, micelles, oil in water emulsions, solid lipid nanoparticles), organic NCs (for example, dendrimers, carbon based nanomaterials, viral capsides, nanostructures made of biological building blocks like proteins), polymer NCs (for examples, nanoparticles, nanocapsules, polymersomes, polymer micelles), inorganic NCs (for example, ceramic, magnetic and metal based nanoparticles as well as nanoshells).

1.2.4.1. Lipid based carriers:

Lipid-based carriers have attractive biological properties, including biocompatibility, biodegradability, isolation of drugs from the surrounding environment, and the ability to entrap both hydrophobic and hydrophilic drugs. Main kinds of lipid based carriers are liposomes, phospholipids micelles, oil in water emulsions and solid lipid NPs (**Figure 1.7**).

Liposomes: Liposomes are concentric bilayered structures made of amphipathic phospholipids. Their diameters range between a few and thousand nanometers. Depending on the number of bilayers, three main kinds of liposomes are distinguished: small unilamellar vesicles (SUVs; 20-100 nm), large unilamellar vesicles (LUVs; 100-500 nm), both usually used as protective capsules and giant unilamellar vesicles (GUVs; 0.5-100 μm), generally studied as oversimplified models of biological cells. Liposome formulations are particularly attractive, as they may carry lipid-soluble drugs intercalated in the lipid bilayer and, at the same time, water-soluble drugs in the aqueous core [**39**]. The liposome surface is amenable to modification with targeting ligands and polymers [**40**]. There are several examples of drugs already available on the market made in liposomial forms, among all the already cited liposomial doxorubicin Doxil®, but also AmBisome® (liposomial Amphotericin B used for fungal infections). Main limitations in the use of liposomes include the high production cost (PEG-ylation, optimization of drug encapsulation and so on), fast oxidation of some phospholipids and side effects like in the case of the palmar plantar erythrodysestesia due to uncontrolled extravasation [**12**].

Lipid Micelles: These drug carriers are formed in solution as aggregates in which the amphiphilic component molecules are generally arranged in a spheroidal structure with hydrophobic cores shielded from the water by a mantle of hydrophilic groups. Micelles are widely used to increase solubility and bioavailability of poorly soluble drugs [41]. For instance they have shown improved bioavailability of protopanaxadiol by mixing phospholipid micelles with Labrasol® in rats. Moreover, phospholipid micelles can be used to vehicle peptide based drugs as an important class of therapeutic agents which development into commercial products is often hampered due to their inherent physico-chemical and biological instabilities [42]. Despite their simplicity, this feature represent also the main limitation in being really effective for the tumor which requires the development of more and more complex and multifunctional systems. Moreover, for what concernes the administration route, the experience with micelles as well as with liposomes is that they can never be administered orally because they are readily disrupted by intestinal detergents such as bile salts and are subject to degradation by intestinal phospholipases, releasing prematurely the carrier-entrapped drug in the gastro intestinal (GI) fluid [43].

Oil in water Nanoemulsions: Nanoemulsions (NEs) are biodegradable, biocompatible, easy to produce and used as carriers for lipophilic drugs which are prone to hydrolysis [45]. They are employed as a sustained release delivery system for depot formation via subcutaneous injection. They enhance gastrointestinal absorption and reduce inter- and intra-subject variability for various drugs. Due to their very large interfacial area, they exhibit excellent drug release profile. NEs have been studied and developed for parenteral, oral, ocular, pulmonary and dermal deliveries. They have also been tested as multifunctional platform for both imaging and anticancer therapy. [46]. Stability against sedimentation is attained based on the nano size of the droplets because the sedimentation rate due to gravity is less than Brownian movement and diffusion. NEs are metastable and can be destabilized by Ostwald ripening whereby the small droplets dissolve and their mass is taken up by the large droplets. When this happens, the nanoemulsion becomes opaque and creaming will occur. There are some methods to improve emulsions stabilities which will be described in the following chapter as well as their applications in more detail.

Solid Lipid Nanoparticles (SLN): SLN are a new pharmaceutical delivery system developed at the beginning of the 1990, made of solid lipids which remain solid at room temperature [47]. The use of physiological lipids, the avoidance of organic solvents and the high pressure homogenization as an established production method represent some of the advantages of these systems. SLNs have good tolerability as they are prepared from physiological lipids and are especially useful in ocular drug delivery as they can enhance the corneal absorption and improve the ocular bioavailability of drugs. They also allowed a targeting effect on the brain [9]. Moreover, DNA modified SLNs have shown a high gene expression especially in vivo, thus representing great potential for targeted gene delivery. Furthermore, they have been developed and investigated for parenteral, pulmonary and dermal application routes. To avoid clearance from the RES also in this case it has been proposed to obtain stealth NCs by PEG-ylation. SLNs have another advantage of allowing autoclave sterilization, a necessary step towards formulation of ocular preparations [47].
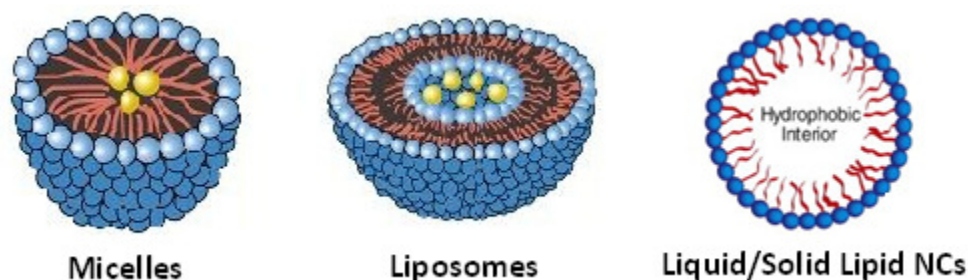
Figure 1.7. Schemes of the main lipid based NCs like micelles, liposomes, and liquid or solid lipid NCs.

1.2.4.2. Organic NPs

Organic NPs include dendrimers, viral capsids, carbon-based nanomaterials, like fullerenes and carbon nanotubes, and nanostructures made from biological building blocks such as proteins like Abraxane which is an FDA approved albumin-bound paclitaxel nanoparticle formulation [12] (**Figure 1.8**).

Dendrimers: Dendrimers derive their name from the Greek word dendra, meaning reminiscent of a tree [9]. These are highly branched macromolecules with controlled near monodisperse

three-dimensional architecture emanating from a central core [**40**]. Macromolecule's growth starts from a central core molecule and growth occurs in an outward direction by a series of sequential reactions. Hence, precise control over size can be achieved by the extent of sequential reactions, starting from a few nanometers up to 100 nm. This class of compounds is interesting because the number of branching increases in a geometric progression with each unit step of growth. As a result, the shape and molecular rigidity changes as the molecular weight of such compounds increases. As a rule, this is accompanied by a change of physicochemical properties of the dendrimers such as the characteristic viscosity, solubility, density, etc. Cavities in the core structure and folding of the branches create cages and channels. The surface groups of dendrimers are amenable to modification and can be tailored for specific applications. Therapeutic and diagnostic agents are usually attached to surface groups on dendrimers by covalent bonding [**40, 9**] or through reversible ionic interactions [**48**]. Promising results in vivo by using dendrimer methotrexate conjugates on animal tumor reduction have been the motivation for further pre-clinical development, thus a variety of dendrimers are now under investigation for cancer treatments [**12**]. In addition, low solution viscosities make them useful as injectable sealants for corneal wounds [**9**]. Dendrimers have also revealed their potential in transdermal drug delivery enhancing bioavailability of indomethacin by using poly(amido amine) (PAMAM) as dendrimer. Furthermore the use of dendrimers as potential gene-delivery is also currently under investigation. One limitation is the need of many repetitive steps for synthesis and therefore the high cost which poses a challenge for large-scale production [**12**].

Fullerenes and Carbon Nanotubes: Fullerenes are particular molecules composed entirely of carbon in the form of a hollow sphere or ellipsoid with the wall composed of one atom thick sheets of carbon and diameter of few nanometers. Recent studies have demonstrated that they can be drug carriers by bounding the surface to a drug with covalent or non covalent bonds [**49**]. Furthermore, because fullerenes are strong anti-oxidants, they have been used as neuroprotective and anti-inflammatory agents. Therefore, they could be used to treat various diseases. However, one limitation is in their manipulation difficulty.

Carbon nanotubes (CNs) belong to the same structural family as fullerenes and consist of graphite sheets rolled up into a tubular form. These structures can be obtained either as single or multi-walled nanotubes. The diameter and the length of single-walled nanotubes may vary

between 0.5–3.0 nm and 20–1000 nm, respectively. The corresponding lengths are 1.5–100 nm and 1–50 µm, respectively. CNs can apparently cross the cell membrane as 'nanoneedles', without perturbing or disrupting the membrane and localize into cytosol and mitochondria even though the mechanisms are purely understood. A number of CN derivatives, are under trial for the treatment of Parkinson's diseases and nervous system ischemia and, in many cases, it has been shown that structure and features of the carrier can be involved by their own in disease treatment [**50**]. They have been tested in vivo on animal model as anticancer drug carrier as well as carriers of immunoactive compounds, proteins, and genes and finally for photothermal cancer therapy considering their capability to be heated by near infrared (NIR) [**51**].

However, detailed understanding of the pharmacological and toxicological properties of carbon nanomaterials, as well as a balanced evaluation of their risks and benefits to human health, is required before they can be recommended for routine clinical use [**52**]. Factors that influence the safety of and kinetics of drug release from nanomaterials include their shape, length, and dispersability, as well as the presence of metal contaminants.
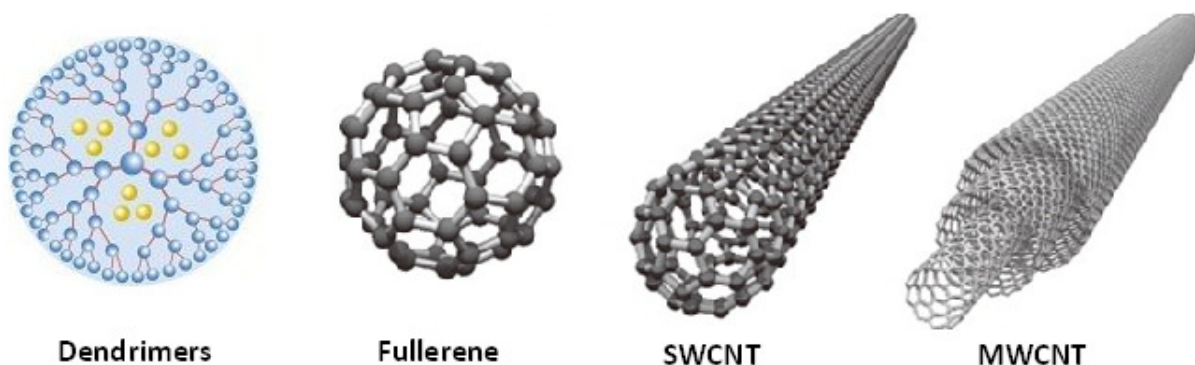
Figure 1.8. Schemes of the main organic NCs like dendrimers, fullerene, single and multiwalled carbon nanotubes.

1.2.4.3. Polymer NCs

Polymers are the most commonly explored materials for constructing NPs-based drug carriers [**12**]; one of the earliest reports of their use for cancer therapy dates back to 1979. Then, over the past few decades, researchers have had considerable interest in developing biodegradable polymer NCs [**9**]. They can be mainly divided in nanospheres, nanocapsules, micelles and polymersomes (**Figure 1.9**).

Nanosphere: They have a matrix like structure, where active compounds can be absorbed on their surface, entrapped or dissolved in the matrix [**9**]. They can be made from synthetic polymers, including poly(lactic acid) (PLA), and poly(lactic co-glycolic acid) (PLGA) or from natural polymers such as chitosan, collagen and so on [**12**] and they can be used to encapsulate drugs without chemical modification differently from polymer-drugs conjugates. The drug can be released in a controlled manner through surface or bulk erosion, diffusion through the polymer matrix, swelling followed by diffusion or in response to the local environment. As with liposomes, technology also allows precision surface modification of nanospheres with polymeric and biological materials for specific applications or targeting to the desired locations in the body [**40**]. Recently, NPs formulated from PLGA were investigated as drug delivery system for photodynamic therapy by carrying zinc (II) phthalocyanine (ZnPc) showing tumor regression in vivo compared to animal treatment with free ZnPc. PLGA NPs have also been tested in vivo loaded with drug and chemosensitizer as treatment against drug resistance [**9**]. Other examples involving chitosan conjugated with folic acid showed capability to reduce production of P-gp as a way to overcome tumor drug resistance. PLGA NPs modified in surface with chitosan have been used as drug carrier for brain delivery. Several multifunctional NPs are now in various stages of pre-clinical and clinical development. There are, however, a few examples of polymeric NPs that show near-homogeneous size distribution.

Nanocapsules: Nanocapsules have a polymeric shell and an inner core with the active substance usually dissolved in the core but it can also be adsorbed on the shell [**9**]. The cavity can contain the active substance in liquid or solid or as a molecular dispersion [**26**]. Moreover, the reservoir can be lipophilic or hydrophilic according to the preparation methods. In the case of nanocapsules the polymeric shell plays a predominant role in protecting the active substances incorporated and probably in the release profile. Shell thickness value can vary from a few to tens of nanometers, depending on the production method. Nanocapsules can be employed as confined protective shell for enzymes, as transfection vectors in gene therapy, as dye dispersants, as carriers in heterogenous catalysis, imaging and most of all as drug carriers [**45**]. They can protect drugs from degradation, reduce systemic toxicity, provide controlled release and mask unpleasant taste. In particular, biodegradable materials allow sustained release within the target site over a period of days or even weeks whereas just biocompatible polymers can be destroyed

by external stimuli allowing a fast drug release. Loading capability depends on the preparation method but is usually very high considering the entire inner compartment involved [**26**]. Therefore, nanocapsules, prepared with biodegradable polymers, have received more and more attention and have been regarded as one of the most promising drug delivery systems. Main limitations are related to the preparation procedures which can be time consuming, not consolidated, not optimized to control size and shell thickness, not capabille to embed drug at very high efficiencies or not suitable to use really natural polymers. Main topic of this thesis was to afford most of the general issues and build up nanocapsules controlled in size, polydispersion index (PDI), shell thickness and made of natural polymers with vegetal oil as core to allow high loading capabilities for lipophilic active substances.

Polymer micelles: Polymer micelles represent a class of micelles that are formed of block copolymers consisting of hydrophilic and hydrophobic blocks [**9, 40, 43**]. Like other micelles they are composed of a core of hydrophobic blocks stabilized by a corona of hydrophilic polymer chains. The hydrophilic block is typically PEG with a molecular weight from 1 to 15 kDa. These NCs provides a set of advantages like high drug-loading capacity and long circulation times due to the hydrophilic corona and small size under 100 nm in diameter. In addition they can be made target specific by the chemical attachment of a targeting moiety to their surface. Hydrophobic drugs or contrast agents may be trapped physically within the hydrophobic cores or can be linked covalently to component molecules of the micelle. The polymer used are biodegradable, bioresorbable and biocompatible. Among the polymer used to construct copolymers there are polyglycolic acid (PGA), polycaprolactone (PCL), PLA and many others. There are some promising in vivo tests for polymeric micelles loading doxorubicin towards drug resistant ovarian cancer [**44**]. They can incorporate paclitaxel, tamoxifen, camphothesin, porphyrine and vitamins [**9**]. They can be made thermo or pH sensitive by using poly(N-isopropylacrylamide) (PNIPAM) and functionalized for active targeting. However, the targeting ability of polymer micelles is limited due low drug incorporation stability which cause the loaded drug to be released before getting to the site of action [**45**]. Consequently, manipulation of the production parameters and the design of the inner core are under investigation to improve drug loading and drug incorporation stability.

Polymersomes: Tri-block copolymers made of a hydrophobic center block and two hydrophilic end block blocks under proper condition can form unilamellar polymer vesicles named polymersomes [**53, 12**]. During the self-assembly process in aqueous solution, the hydrophobic components of amphiphilic copolymers attract each other to form a membrane to minimize the contact with water and tend to enclose into a hollow structure, while the hydrophilic parts are expressed on both the inside and outside of the membrane, forming the hydrophilic shells. Therefore, polymersomes have architecture similar to that of liposomes, but being composed of synthetic polymer amphiphiles which make them more robust. Like liposomes they are able to stably load a broad range of active molecules (e.g. fluorescent molecules, anti-cancer drugs, genes or proteins etc.) into either hydrophilic or hydrophobic compartments. Typically, the membrane of this polymersome is composed of aliphatic biodegradable polyester such as PLA or PCL, whereas the corona is a hydrophilic block, such as PEG. In addition to PEG, hydrophilic block polymers such as poly(2-methacryloyloxyethyl phosphorylcholine) (PMPC) and poly(ethylethylene phosphate) (PEEP), which impart excellent biocompatibility, have also been combined with PLA or PCL to form biocompatible and degradable polymersomes. In vivo tests show promising results for these kinds of drug delivery systems. They have also been tested as theranostic NCs for magnetic resonance (MR) Imaging and magneto-chemotherapy [**54**]. Specific disadvantages of polymersomes like of polymer micelles are the difficulty of polymer synthesis, the immature drug-incorporation technology, slow extravasation and possible chronic liver toxicity due to slow metabolic process which is indeed also related to other synthetic polymer NPs at least the ones not made of natural polymers [**55**]. However, by working on the biodegradability of the synthetic polymers used a widespread of polymeric micelles and polymersomes could be expected in the field of drug delivery.
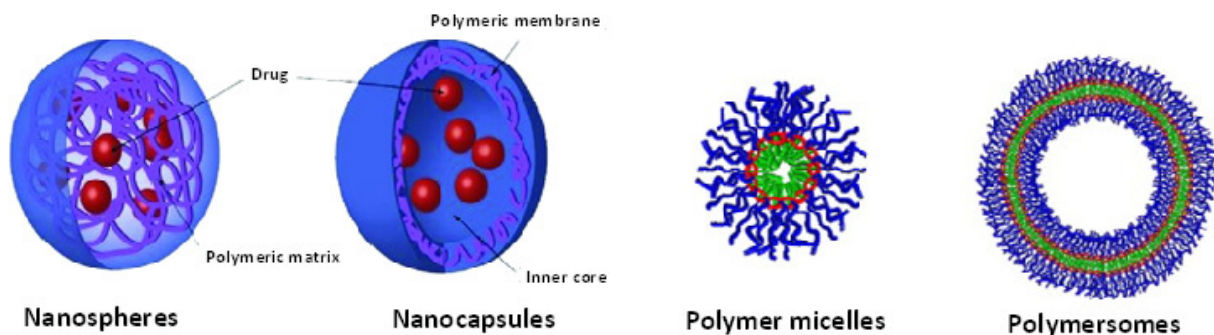
Figure 1.9. Schemes of the main polymer NCs like nanospheres, nanocapsules, polymer micelles, polymersomes.

1.2.4.4. Inorganic NPs

Inorganic NPs are useful for drug delivery as well as gene therapy by carrying a huge amount of molecules on their high developed surface, due to the small size. They can also be used by their own to care tumor by hyperthermia through local heating by external stimuli mainly photo but also radio frequency (RF) in some cases. Moreover, they usually are exploited as tracers for imaging allowing a theranostic approach and they can be combined with some of the previous systems especially the polymer ones to combine their properties with the ones of the other NCs.

Ceramic NPs and nanocapsules: The use of ceramic particles for drug delivery, especially biomacromolecular therapeutics, is emerging as a new area [**9**]. Silica, alumina and titania are examples of highly biocompatible ceramic NPs. Because of their possible ultra-low size (down to 50 nm) and porous nature they are becoming important drug delivery vehicles. Indeed, this size makes them more effective in evading the uptake by the RES, as already described. In addition they do not show swelling or changes in porosity with pH. Therefore, they can protect different bio-macromolecules, such as enzymes, against denaturation induced by changes in the external pH and temperature. Further their surfaces can be easily functionalized for conjugation to target-specific ligands such as monoclonal antibodies. Most of the studie regard silica, showing how, properly doped, can be used for drug or gene delivery. Other oxides like ceria (CeO_2) and yttria (Y_2O_3) have shown that they may act as antioxidant, block reactive oxygen species (ROS) production and cause a low level of ROS production. In this way they can promote survival of cells under oxidative stress leading to protection of cells from death. Inorganic nanocapsules especially the ones made of silica are also gaining a huge interest both in the field of diagnostic and theranostic as it will be described in the Appendix.

Magnetic NPs: Magnetic NPs (MNPs) are being widely used for biotechnological and biomedical applications [**9**]. Magnetic iron oxides are the most used but they have hydrophobic surfaces, therefore, they have to be coated by synthetic and natural polymers like dextran, PEG, poly(vinylpyrrolidone) (PVP) streptavidin, poly-lysine (PLL), polyethylene imide (PEI) and so on to avoid aggregation. MNPs with surface bound drugs can be injected into the vascular system and captured at the tumor site via a locally applied magnetic field. Drug is then released

typically by means of a change of the pH. Magnetite (Fe_3O_4) is generally preferred to maghemite (Fe_2O_3) because they are highly biocompatible and they are super-paramagnetic therefore no permanent magnetization there exist each other inducing aggregation. They can be used not only for guided drug delivery but also for magnetic resonance imaging (MRI). For instance they were combined with fluorescence labeled dendrimers to track - in a precise way by multimodal imaging - the fate of these dendrimers once injected in vivo showing capability of dendrimers smaller than 11.7-11.9 nm to cross blood brain barriers (BBB) and reach malignant glioma cells. Various magnetizable nanophases (magnetite, maghemite, Co, etc.) can be incorporated into different biocompatible and nontoxic polymers, such as PLGA, PLA, dextran, chitosan. Then they can carry therapeutic agents in the bulk of the polymer and be guided by external magnetic field. Recently, PEI modified MNPs have been used as a potential vascular drug/gene carrier to brain tumors. MNPs are also promising for multi-functional chemotherapeutic application that combines drug release and magnetic hyperthermia therapy.

Metal based NPs: Metal NPs have the advantage to be extremely small, down to 50nm and thus the large surface area provides the ability to carry a relatively high dose of drugs. Gold NPs are the most commonly used [**9**]. Indeed, it is easy to synthesize them in a range of sizes, in a cheap and reproducible way. Moreover, due to their negative charge they can be easily functionalized by various biomolecules and they are considered biocompatible and nontoxic. Gold NPs have a variety of drug-delivery applications. For instance, they have been used to deliver insulin via efficient transmucosal delivery. They have been useful in improving anticancer delivery in vitro of oxaliplatin. They have shown an important role in efficient drug delivery and biomarking of drug-resistant tumor cells. In addition, they present a surface plasmon resonance (SPR) effect which can be used for imaging as well as for photothermal therapy. Indeed, they can be heated by NIR light destroying targeted tumor cells by hyperthermia [**12**]. Silver NPs have also been considered and used in drug delivery for their positive effects through their antimicrobial properties, reduction in wound inflammation and modulation of fibrogenic cytokines [**9**].

Nanoshell: These systems with sizes typically ranging from 100 to 200nm are typically composed by a silica core and a metallic outer layer mainly made of gold [**12**]. They can be used

for theranostic. Indeed, their absorbing nanoshells are suitable for hyperthermia-based therapeutics by heating up the surrounding cancer tissue, whereas the scattering properties of the nanoshells make them useful as contrast agents for imaging applications. The advantage to use nanoshells is that by adjusting the core and shell thickness, nanoshells can be designed to absorb and scatter light at a desired wavelength [**56**].

Despite the advantages of inorganic NPs full attention must be given to safety and toxicological issues by studying empty non-drug-loaded NPs to understand possible side effects induced by the carrier itself. For instance cationic NPs including Au have been shown to cause hemolysis and blood clotting and usually anionic particles are rather non-toxic. Moreover, metal NPs like gold, once entrapped in acidic environment of cell organelles, can deliver high concentrations of ions which can induce gene-toxicity [**57**]. For silica NPs it has been found an increasing toxicity with doses and exposure times due to higher and higher ROS levels and glutathione levels corresponding to an increased oxidative stress [**9**]. Even in the case of Fe_3O_4, which is the only clinical approved metal oxide NPs, considered biocompatible and biodegradable, there are some concerns about its possible side effects especially to high doses such as inflammation, generation of reactive oxygen species (ROS), genotoxicity, and so on [**58**].

1.2.5. Evolution of NCs over the last decades

To face the complexity of the tumor there has been a continuous evolution of the NCs adding more and more complex features. The easiest NCs are the ones that just exploit the localization at the tumor site by escaping the vascular compartment through EPR mechanism. Of course even in this case they need at least one modification in most of the cases to guaranty a long circulation time.

However, much interest has been expressed over the last two decades in adding biological targeting capabilities to liposomes and many other NCs. Therefore, NCs surface can be conjugated with targeting moieties, including antibodies, ligands, aptamers and small peptides. Targeting has been directed to tumor cell surface markers and to molecules expressed in the tumor microenvironment and on the tumor-associated vascular endothelium. A major difficulty encountered with surface-bound biorecognition moieties is that they are typically much shorter than the polymer molecules used to elude the RES. Thus, they tend to be hidden inside the highly

flexible polymer shield, resulting in a decrease in targeting efficacy. To avoid this problem, the targeting moiety can be attached at the distal end of the polymer chain. Actually, two or more different moieties can be attached on the same NC for a more effective active targeting. Then NCs can embed different drugs providing local co-concentrations of synergistic therapeutic agents, or a combination of therapeutic and imaging moieties, in order to visualize the biodistribution of the active principle and to potentially monitor or alter the therapeutic course in real time.

Apart from the functionalization for a specific target there was also the need to have a system such that it could respond to the stimuli from the environment surrounding (such as pH or temperature of the pathological area) or applied from the outside of the body (such as magnetic field, ultrasound, laser irradiation). In response to these requirements, more evolved NCs have been provided. For instance NCs whose outer layer is composed of a pH-sensitive polymer that will swell or degrade and release drugs preferentially in the acidic environments of tumor lesions have been developed. Another possibility involves the activation of nanoparticles conteined in the shells of nanocarriers by, for example, NIR. This radiation penetrates deeply into the tissue and irradiates the nanoparpicles causing their heating, leading to the rupture of the carrier and then the following release of the carrier entrapped-drug. A further approach involves excitation of iron oxide NPs by rapidly switching magnetic fields so that it is possible to provide information on their distribution and on the location and extent of the target lesion as well as to create over-heating for hypothermia treatment [**8**].

Even more complex are the "multistage systems" NCs, where in a first stage (A) there is the injection of NCs landing on the inner wall of tumor-associated blood vessel, in a second stage (B) the release of "nanoshuttles" of the carrier that penetrate both the blood vessel wall and the tumor cell membrane and in the last stage (C) the delivery to the tumor of doses of a therapeutic agent [**59**] (**Figure 1.10**).
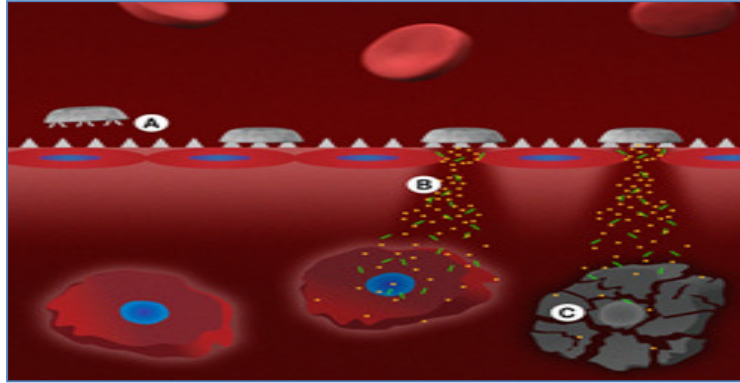
Figure 1.10. Scheme of a multistage DDS with bigger NCs targeting vessel walls and smaller NCs delivered in the tumor and releasing drug in tumor cells.

An alternative is a multistage approach in which NCs change their size to facilitate transport by adapting to each physiological barrier. The "original" NCs preferentially extravasate from the leaky regions of the tumor vasculature. After extravasation into tumor tissue, they are triggered to release smaller particles in to the tumor via an external stimulus (light, heat, ultrasound, magnetic field) significantly lowering their diffusion hindrance in the interstitial matrix and allowing penetration into the tumor parenchyma [**16**]. These smaller NCs can carry therapeutics released as the particles penetrate deep into the tumor (**Figure 1.11**).
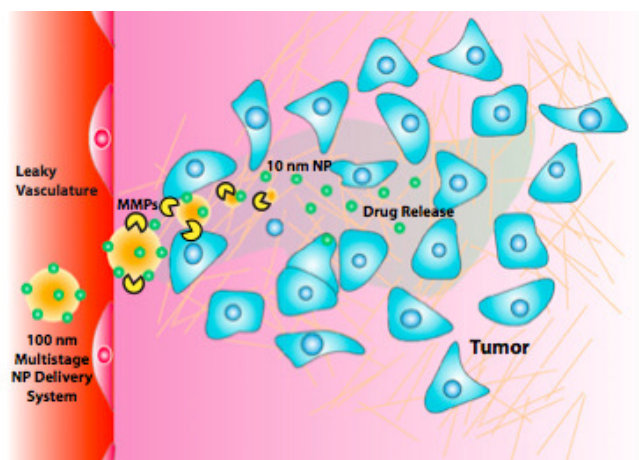
Figure 1.11. Scheme of a multistage DDS with NCs extravasating from blood vessel and reducing size in tumor tissue to deeply penetrate inside and reach all tumor cells.

In the most evolved context a novel type of polyelectrolyte multilayer capsules (e.g. polymer walls around cavities) with given size in the nanometer range and tunable wall properties has been recently introduced as an interesting platform for the assembly of simply multifunctional carrier systems for several reasons [60]. Firstly, they can be synthesized under mild conditions by using numerous different materials. Secondly, their functional properties can be well-defined by embedding different nanoscale building blocks (as colloidal inorganic nanoparticles or biomolecules) within and on top of their wall. Thirdly, they can efficiently host biological macromolecules within their cavity for numerous biomedical applications. Finally, they can be composed of biocompatible materials for the delivery of encapsulated materials into cells. The distinct advantage of using these systems lies in the potential of combining a variety of substances with different functionalities in one unique system by proper functionalizion of its layers together with possible cargo molecules into their cavities.

1.2.6. Administration routes

The administration route is another important aspect to consider. Oral administration represents by far the easiest and most convenient route of drug delivery, especially in the case of chronic therapies [43]. In comparison with other possible routes of administration, it has many advantages. Not only it is non-invasive and relatively free from complications arising from the need for sterile techniques that usually occurs with parenteral formulations, but it is also easily dosed with low preparation costs, all of which should encourage patient compliance. Although oral drug formulation is convenient from the patient's perspective, it presents some problems including the stability of the DDS in the GI tract. The GI tract presents a variety of hurdles for a drug, from morphological barriers (mucus layer, microvilli, etc.) to stringent physiological factors (a wide range of pH, enzymatic activities, specific transport mechanisms, etc.), which all conspire to limit intestinal absorption of drug. The transport of a drug across the intestinal membrane is a complex transfer process involving several mechanisms. Based on the physiology of the intestinal epithelium, three potential routes for drug transport across intestinal barriers have been considered (**Figure 1.12**): (A) the paracellular route, a passive, diffusional transport pathway taken by small, hydrophilic molecules (e.g., mannitol) which can pass through the tight junction channels between adjacent epithelial cells; (B) transcellular passive diffusion of

lipophilic molecules through the lipid bilayer and the membrane-bound protein regions of the cell membrane; and (C) transcellular receptor-mediated transcytosis through specific surfacebound ligands.
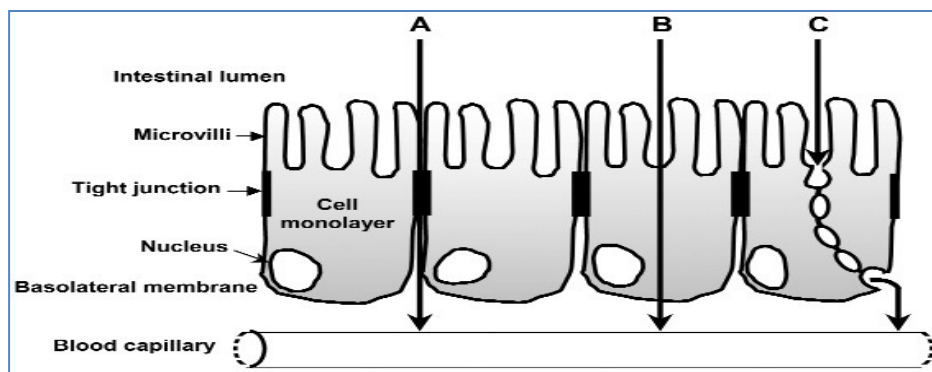
Figure 1.12. Schematic representation of intestinal epithelial cells showing potential transepithelial pathways: (A) paracellular route; (B) transcellular passive diffusion; and (C) transcellular receptor-mediated transcytosis.

To be absorbed a specific drug must cross the barrier, which comprises an unstirred water layer, mucus layer, apical and basal cell membranes and cell contents, tight junctions, basement membrane, the walls of lymph and blood capillaries. Structure, composition, thickness, surface area, and pH of this barrier are then important considerations in drug delivery systems. Another method to administer drug is by parenteral route. This is a method of choice due to the network of blood and lymphatic vessels in the body that provide natural routes for the distribution of nutrients and delivery of therapeutic agents [40]. It allows avoiding the hostile gastro-intestinal environment which prevents the use of many drug and DDS systems. However, this is an invasive route, which can lead to a reduced acceptance by patients and, consequently, increased costs of therapy, especially when a prolonged or chronic treatment is required [61]. Anyway most of the treatments are made with this kind of administration because it remains the most effective as it allows exploiting all the different generations of drug loaded NCs.

Another administration route is through the skin [62]. The cutaneous administration could avoid a variety of disadvantages compared with the oral administration including drastic pH changes, deleterious presence of food and enzymes and first-pass effect of the liver. It also avoids injection inconvenience and needle phobia. In addition, it is no invasive with the minimization of side-effects in the traditionally drug therapy. However, so few applications

using this kind of administration are present in the market because few molecules yielded skin permeability coefficients sufficiently high to meet the clinical therapeutic needs and because of their very low skin permeation rates. The continuous stratum corneum (the outer layer of skin) provided a major barricade for drug penetration to the deeper skin layers and was therefore the usual target for attempts to strength drug permeation ability. Nevertheless, some applications are designed for treating of skin diseases. One of these is the Dermosome Technology for topical treatment of psoriasis with a formulation of cyclosporine. The Dermosome Technology is a product developed by Advancell [63] made up of chitosan nanocapsules for topical administration of active ingredients. These nanocapsules are formed by an oily core, which houses the active ingredient. The technology adheres to the skin, allowing a longer time of contact, combined with its tiny size, increases the contact area between skin and structure, causing the active to accumulate significantly at the level of the epidermis.

1.3. Nanotechnology in food

Functional foods contain larger profit margins than conventional foods (30 to 500 percent higher) [4]. The global market size was estimated in 2008 between 30 and 60 billion US$, with Japan, USA, and Europe occupying the biggest share and is increasing at high rate. In many cases the difference between pharmaceuticals and nutraceuticals is identified in the diseases treating in the first case and diseases prevention in the second case. Actually, this distintion is cute but superficial and erroneous. Indeed, pharmaceuticals are substances which have (or have had) patent protection as a result of expensive testing to conform to the specifications of respective Governments. Whereas, many nutrients may never receive government approval since no one could justify the expense of testing requirements for substances that in principle cannot be protected by patent laws. Both pharmaceuticals and nutrients can cure and prevent diseases but only pharmaceuticals have governmental sanction. Many pharmaceuticals have their origin in plants and animals and are no less "natural" than nutrients. Classic example of nutrients is synthetic vitamins. When functional food aids in the prevention and/or treatment of diseases and or disorders it is called a "nutraceutical". Examples of nutraceuticals include fortified dairy products (milk as such is a nutrient and its product casein is a pharmaceutical) and citrus fruits (orange juice is nutrient and its constituent ascorbic acid is a pharmaceutical). In practice,

nutraceuticals have been claimed to have a physiological benefit or provide diseases protection as cardiovascular, antiobese, antidiabetics, anticancer agents, as immune boosters and for chronic inflammatory disorders and degenerative diseases. Therefore, the interest towards nutraceuticals is increasing and a nutraceutical research community is absolutely necessary to convert the majority of potentiality of nutraceuticals in established ones.

The field of nanotechnology is experiencing significant growth in the nutraceutical delivery due to the confluence of interests of industry, government and academia [**5**]. Indeed, there have been important advances made in NPs formulations designed to improve the bioavailability of poorly water-soluble ingredients. Fundamental thermodynamic and mass transfer equations reveal that, in order to generate a broad spectrum delivery system, NPs with 100 nm diameter (or less) should be produced. However, experimental data reveal that, in some cases, even NPs in the 100–1000 nm range are capable of producing substantial improvement in the bioavailability of the active ingredients. In most cases, this improvement in bioavailability seems to be linked to the direct uptake of the NP. Furthermore, direct NP uptake is controlled by the size and surface chemistry of the NP system.

The confluence of pharmaceutical, nutrition, and colloid sciences with food engineering will be the key to unlock the full potential of NP delivery systems in food applications. In addition to the potential technological impact of nanoparticle delivery systems in the food industry, there are also concerns about unforeseen side effects of the technology. The fact that these carriers are designed with food-grade ingredients does not mean that they might not cause undesired effects such as transporting or depositing active ingredients or excipients in tissue that they are not supposed to, or enhancing the absorption of substances that they are not meant to transport but that are present in the food matrix. Regulations on food nanotechnology are a likely development in the near future that may have a significant impact on the methods of preparations, dosages, and ingredients used in these systems.

1.4. Nanotechnology in cosmetics

The applications of nanotechnology and nanomaterials can be found in many cosmetic products including moisturisers, hair care products, make up and sunscreen. Almost all of major cosmetic manufacturers use nanomaterials in their products. L'Oréal has a number of nanotechnology-

related products in the market and ranks 6th in US in the number of nanotech related patents in US. The European Commission estimated in 2006, that 5 % of cosmetic products contained nanoparticles. The application of nanomaterials in cosmetic products has been the subject of continuous discussion in the media, scientific circles and among policy makers for the past few years. Toxicity issues have been raised due to conflicting research papers about the safety of nanomaterials and lack of agreement between researchers on whether the nanomaterials are safe for dermal use. There are a number of classes of nanoparticles used, or proposed for use, in cosmetic applications. In cosmetics there are currently two main uses for nanotechnology. The first of these is the use of nanoparticles as UV filters. Titanium dioxide (TiO_2) and zinc oxide (ZnO) are the main compounds used in these applications. Organic alternatives to these have also been developed [6].

The second use is nanotechnology for delivery of active substances. Like for the nutraceutical also in this case there is a field so called cosmeceutical which is a combination of the two words cosmetics and pharmaceutical. And again it has to be pointed out that even if cosmeceutics can have therapeutic effects cosmetics products are not approved by FDA therefore they cannot be defined as drug. On the contrary if they are defined drugs that means they are pharmaceutical products. Lipid based nanocarriers like liposomes [64], SLN [65] and emulsions [66] are examples of effective NCs through skin. In particular, for the latter case it is worth noticing that NEs have a number of advantages over larger size emulsions. They can be stabilized to increase the time before creaming occurs, therefore increasing the shelf life of products containing them. They are transparent or translucent, and have a larger surface area due to the small particle size. It has been found that the smaller the size of the emulsion, the higher the stability and better suitability to carry active ingredients.

Polymer NPs, such as nanospheres and nanocapsules [67] have also been identified as potential cosmetic NCs. The trend in the skincare applications of polymers is moving from self repair (those that repair the skin damage according to changes in the environment using nanoencapsulation, controlled release etc.) to self predicting polymers that can predict future changes and change their properties accordingly to prevent the damage. An example of this is a hydrogel which can respond to temperature and be used as a facial mask. The patented technology called Facial Switch™ shrinks the hydrogel by increasing the temperature, thus allowing release of nutrients.

1.5. Thesis objective: new solutions to Nano-Bio-technologies

In this thesis we focused the attention on the use of nanocapsules like carriers for their capability to embed high payloads of active substances. Moreover we just used natural materials like vegetal oils and natural polysaccharides to avoid side effects from the preparations of such NCs. In particular, we chose to start from an oil core template for the preparation of NCs to be used in bio-nano-technology fields.

Indeed, oil in water emulsions can easily reach sizes down to 100nm making these systems very interesting from a nanotechnology point of view. Then, there is strong need to load and vehicle lipophilic active substances and drugs in order to face their scarce solubility in water which typically prevents an effective bio-distribution of such molecules. Moreover, it is possible to use vegetal oils and natural surfactants like the soybean and the Lipoid E80 used in this work. However, the widespread use of oil carriers in the above said fields is generally limited or prevented by the intrinsic instability of immiscible systems like an emulsion. Herein we have focused on the stabilization of oil in water emulsions of sizes below 200 nm by decorating them with a biodegradable polymer and trying to find out optimal process conditions. The objective was then to develop nanoemulsions based product monodisperse and stable over time to be used by their own and as liquid template for the layer-bylayer preparation of biodegradable polymer nanocapsules. Biodegradable polymer nanocapsules can indeed have a huge impact on the development of new carriers for cancer treatment for a series of advantages such as high payload of lipophilic drugs, possibility to easily functionalize them for active targeting, long circulation in the blood, penetration capability, embed tracers for imaging and so on. Moreover, looking at the possible use of these nanocapsules as carriers to be injected in the blood, polymers have been successfully modified in order to be cross-linked once coupled in the multilayer to provide stability against the physiological environment to be explored during their use. Finally it was also tried to prepare monodisperse inorganic nanocapsules made of silica to demonstrate the potentiality of nanoemulsions template once optimized its preparation. Silica is a very interesting bio-interface recognized for its biocompatibility, capability to be functionalized like polymeric capsules. Moreover, by tuning the thickness and porosity it is possible to obtain completely impermeable systems or permeable and more degradable systems. These systems can have a huge impact for diagnostics in vivo both for single and multimodal imaging. Specifically, the use

of an oil core, like in our case, allows high payloads of drugs for a possible theranostic approach where silica nanocapsules are not only meant to make diagnostics but also to deliver drug in certain conditions.

During this thesis one of the main objective was to assess the capability to use nano-emulsions stable over time for times comparable to the stable inorganic templates, opening a fascinating scenario in the templating synthesis. Indeed oil template does not need to be removed, which is risky for the capsule, especially in the case of small sizes and natural polymers, and time consuming; capsules can be pre-loaded with high payloads of scarcely or no soluble bio-molecules, drugs, tracers and so on.

Chapter II: Monodisperse and biodegradable oil in water emulsions with tunable stability

2.1. Introduction on NEs

2.1.1. Applications

NEs are oil-in-water emulsions with mean droplet diameters usually ranging from 100 and 500nm [66]. They can be made from surfactants approved for human consumption and common food substances that are "generally recognized as safe" (GRAS) by the FDA. Differently from microemulsions, which are systems thermodynamically stable, they present a reasonable low concentration of surfactant (typically less than 10%). Their small size allows improved stability over time, due to the low gravity and the acquired elasticity, confers certain transparency to the product, as well as capability to reach and target tumor area. In general NEs show a great promise for the future of food, cosmetics, diagnostics, drug therapies, and so on. [68].

Their capacity to dissolve large quantities of hydrophobics, along with their mutual compatibility and ability to protect the drugs from hydrolysis and enzymatic degradation make them ideal vehicles for the purpose of parenteral transport [47]. In this case, frequency and dosage of injections can be reduced as these systems guarantee the release of drugs in a sustained and controlled mode over long periods of time. For instance, NEs loaded with thalidomide did lead to therapeutic plasma concentrations with a starting dose as low as 25 mg. Moreover, treatment of colon adenocarcinoma in the mouse with NEs brought to higher tumor suppression rate compared to plain drug solution treatment. NEs were also used as theranostic platform for instance by using prednisolone acetate valerate (PAV) for therapeutic purposes and iron oxide NPs for MRI imaging as well as die Cy7 for near infrared fluorescence (NIRF) imaging with promising results in terms of animal tumor inhibition.

One interesting administration route of NEs is the nasal mucosa which is interesting for its reduced enzymatic activity, the moderately permeable epithelium, its direct connection with the brain and non-invasiveness. For instance Alzheimer, Parkinson's diseases, meningitis, depression, and schizophrenia can be treated by this route.

Moreover, NEs are able to easily penetrate the pores of the skin and reach the systemic circulation thus getting channelized for effective delivery. For instance, they improved transdermal permeation of many drugs over the conventional topical formulations such as emulsions and gels. The main advantage of this route is the absence of gastrointestinal side effects associated with oral delivery. At the same time, NEs have recently become increasingly important as potential vehicles for the controlled delivery of cosmetics and for the optimized dispersion of active ingredients [68]. In general they are acceptable both in skin care (cosmetics) and in care through skin (transdermal pharmaceutical) also because they are quite stable products and the incorporation of potentially irritating surfactants can usually be avoided by using high-energy equipments during manufacturing to obtain reduced size. Then, they possess good sensorial properties (rapid penetration, merging textures) and biophysical properties (especially, hydrating power) [69]. An example of skin care is the treatment of dry hair aspect; significant improvement and a prolonged effect was obtained after exposure to a cationic NE with hair more fluid and shiny, less brittle and non-greasy [70].

Further, due to the renewed interest in herbal drug formulations, NEs may be the ideal delivery platform for these phytopharmaceuticals, generally difficult to formulate, with expected high businesses for the pharmaceutical industries [47]. NEs could also be exploited to overcome the poor absorption of flavonoid nutrients - a group of antioxidant compounds found primarily in plants - and poor miscibility of these compounds. An example is the breviscapine, flavones glucuronide, which is a medicine extracted from a Chinese herb so called Erigeron breviscapinus [71]. It was observed how loading breviscapine into lipid emulsions produced a significant change in pharmacokinetic parameters with a much higher breviscapine concentration in plasma over time compared with free substance. All NEs used for nutraceuticals and pharmaceuticals, can also be engineered to further improve their efficacy [72]. This can be made possible by covering NEs with multilayer polymer shell so that a functional component trapped within the core could be released in response to a specific environmental trigger by designing the response of the shell to the environment. Then, as already described in Chapter I NEs have a huge

applicability in the field of functional foods like "healthy food". Especially in this case to make possible the exploitation of such products it is necessary to find a way to reduce the high production cost due to the high energy utilized for production of NEs.

NEs have an antimicrobial behavior against bacteria (e.g. E. coil, Salmonella, S. aureus), enveloped viruses (e.g. HIV, Herpes simplex), fungi (e.g. Candida, dermatophytes) and spores (e.g. anthrax) [68]. Indeed, they are thermodynamically driven to fuse with lipid-containing organisms and when enough nanoparticles fuse with pathogens, they release part of the energy trapped within the emulsion destabilizing pathogen lipid membrane and producing their lysis and death. In the case of spores, additional germination enhancers are incorporated into the emulsion.

NEs can be applied for delivery of fragrant, which may be incorporated in many personal care products. This could also be applied in perfumes, which are desirable to be formulated alcohol free [47].

2.1.2. Preparation methods

As said, NEs are heterogeneous system consisting of at least two immiscible liquid phases. Consequently, they do not form spontaneously and their properties depend not only on the thermodynamic conditions such as composition, temperature or pressure, but also on the preparation method and the order of addition of components. The structure of an emulsion generally consists of droplets of the dispersed phase (or internal) in a continuous phase (or external), stabilized by a surfactant, as illustrated in **Figure 2.1**. This structure decisively determines the physical properties and, thus, the functionality and quality of the emulsion. In the preparation of emulsions, from both fundamental and technological point of view, it is fundamental to obtain a desired droplet size and a narrow size distribution [73].
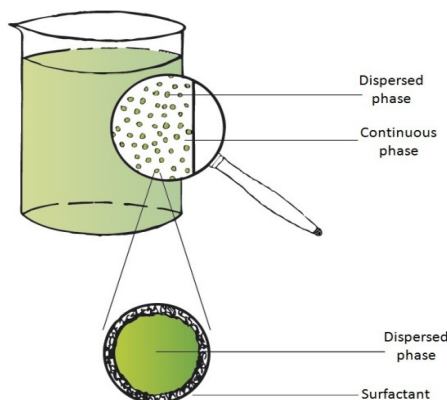
Figure 2.1. Typical structure of an emulsion.

Being non-equilibrium systems of structured liquids, NEs preparation typically involves the input of a large amount of either energy or surfactants [**66**].

The high-energy method utilizes mechanical equipments, such as ultrasonicators, microfluidizer and high pressure homogenisers, to create intensely disruptive forces which break up the oil and water phases to form nano-sized droplets. Final particle size here will depend on the type of instruments employed and their operating conditions like time and temperature along with sample properties and composition. This method allows for a great control of particle size and a large choice of composition, which in turn controls the stability, rheology and colour of the emulsion.

NEs can also be prepared by a low-energy emulsification method, which has been recently developed according to the phase behavior and properties of the constituents, to promote the formation of ultra-small droplets. These low-energy techniques include phase inversion temperature (PIT) technique, solvent displacement methods and phase inversion composition (PIC) method. This emulsification can be brought about by changing the parameters which would affect the hydrophilic lipophilic balance of the system like temperature (in the case of PIT), composition, etc.. The low energy method is interesting because it utilizes the stored energy of the system to form small droplets. Moreover, in the case of solvent displacement method and PIC, emulsification conditions are quite gentle making possible the use of thermolabile drugs such as retinoids and macromolecules, including proteins, enzymes and nucleic acids. However, also in the high energy process temperature can be controlled.

2.1.2.1. Low energy emulsification

PIT method employs temperature dependent solubility of non ionic surfactants like polyethoxylated, which become hydrophobic above certain temperature allowing therefore a formation of water in oil emulsion due to the acquired solubility of the surfactant in the oil. However, it typically uses high temperature to create the phase inversion.

In the case of solvent displacement, the oily phase is dissolved in water-miscible organic solvents, such as acetone, ethanol and ethyl methyl ketone and it is poured into an aqueous phase containing surfactant to yield spontaneous NE by rapid diffusion of organic solvent. The organic solvent is removed from the NE by a suitable means, such as vacuum evaporation. Spontaneous nanoemulsification were also reported when solution of organic solvents containing a small percentage of oil is poured into aqueous phase without any surfactant. A major drawback of this method is the use of organic solvents, such as acetone, which require additional inputs for their removal from NE. In particular, a high ratio of solvent to oil is required to obtain NEs with a desirable droplet size.

PIC method has drawn a great deal of attention from scientists in various fields (including pharmaceutical sciences) as it generates NEs at room temperature without use of any organic solvent. Kinetically stable nanoemulsions with small droplet size (~50 nm) were generated by the stepwise addition of water into solution of surfactant in oil, with gentle stirring and at constant temperature. The spontaneous nanoemulsification was related to the phase inversion.

The main limitation of low energy techniques is that they pose several difficulties during scale-up. It has been demonstrated this capability in the case of PIC even though more experimentation should be done at higher scales in order to prove it [**74**].

2.1.2.2. High energy emulsification

One technique for producing NEs is based on the use of an immersion sonicator. The emulsification power of ultrasound has been known and applied for long. The ultrasonic power is adjustable and can be adapted to particular products and emulsification requirements. Highly intensive ultrasound provided by a vibrating metal probe supplies the power needed to disperse a liquid phase in small droplets in a second phase continuous phase. In the dispersing zone, imploding cavitation bubbles cause intensive shock waves in the surrounding liquid and result in

the formation of liquid jets of high liquid velocity. The most important aspect is to stabilize the newly formed droplets of the dispersed phase against, for example, coalescence in order to maintain the final droplet size distribution at a level that is equal to the distribution immediately after the droplet disruption in the ultrasonic dispersing zone (coalescence of the droplets after disruption influences the final droplet size distribution). Studies on emulsions have shown correlation between the energy density and droplet size. There is a clear tendency for smaller droplet size at increasing energy density. At appropriate energy density levels, ultrasound can well achieve a mean droplet size below micrometer scale. However, this method presents several limitations mainly due to the polydispersion, the difficulty to scale up to large volumes and also in terms of minimum size of the dispersion which can be reached. To make possible NE preparation at industrial scale high pressure homogenization techniques are needed.

High pressure homogenization allows producing extremely low particle sizes due to several forces, such as hydraulic shear, intense turbulence and cavitation [66]. The resultant product can be re-subjected to high-pressure homogenization until nanoemulsion with desired droplet size and polydispersity index is obtained. The smaller droplet size the higher the energy thus the pressure required. The emulsion is preferably prepared at high volume fraction of the disperse phase and diluted afterwards. However, very high phase volume ratios may result in coalescence during emulsification, even though more surfactant could be added to create a smaller reduction in effective surface tension and possibly diminishing recoalescence. If possible the surfactant is dissolved in the disperse phase rather than the continuous phase; this often leads to smaller droplets. It may be useful to emulsify in steps of increasing intensity, particularly with emulsions having highly viscous disperse phase.

To the field of high pressure homogenizer it belongs also a patented mixing technology called microfluidization, which makes use of a device called microfluidizer. This device uses a high-pressure positive displacement pump (500 - 20,000 psi), which forces the product through the interaction chamber, consisting of small channels called "microchannels". The principle of the technology consists of a liquid that is divided into two microchannels and then is recombined later in a reacting chamber where the jets of liquid collide together. This allows for reducing of the size of suspended particles, resulting in stable, uniform and consistent mixtures of product. The emulsion can be passed through the interaction chamber of the microfluidizer repeatedly until the desired particle size is obtained.

2.1.3. NE stability

As said emulsions are thermodynamically unstable due to the unfavorable contact between the two phases, by their different densities, and they need an emulsifier to reduce destabilization mechanisms over time. Emulsion destabilization is generally due to creaming and sedimentation as a consequence of the different densities of oil and water, coalescence due to an irreversible fusion of emulsion droplets, flocculation with following creaming due to an aggregation sometimes reversible, and finally by Ostwald ripening. In this case, residual solubility of oil in water is further increased with decreasing drop size. Single oil molecules leave the smaller droplets into the water phase and they can diffuse around and condense in a larger droplet so the larger droplets grow at the cost of the smaller ones. The driving force of the process is the decrease of interfacial area and, thus, interfacial energy [**75**]. These mechanisms are summarized in **Figure. 2.2**.
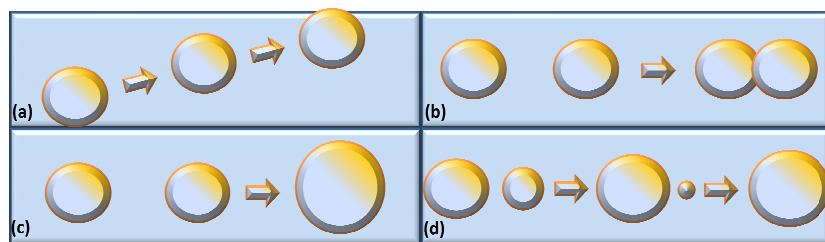
Figure 2.2. Breakdown mechanisms of emulsions (from a to d: creaming, flocculation, coalescence and Ostwald ripening).

The smaller the droplet size the more stable is the emulsions against sedimentation and creaming. Indeed, small sizes cause a large reduction in the force of gravity, and Brownian motion may be sufficient for overcoming it [**7**].

One of the most important and perhaps the most widely used methods to stabilize emulsions is the use of an emulsifier [**66**]. The latter adsorb to the surface of freshly formed oil droplets during homogenization and facilitate further droplet disruption by lowering the interfacial tension, thereby reducing the size of the droplets produced during homogenization [**76**]. Emulsifiers also reduce the tendency for droplets to aggregate by forming protective membranes and/or by generating repulsive forces between the droplets. A good emulsifier should rapidly adsorb to the surface of the lipid droplets formed during homogenization, rapidly lower the interfacial tension by a significant amount, and protect the droplets against aggregation during

emulsion processing, storage, and utilization. A wide variety of different kinds of synthetic and natural emulsifiers can be legally used in food emulsions, including low-molecular mass surfactants (leader groups are fatty alcohols, glycolipids and fatty acids) and macromolecular (high-molecular-mass) emulsifiers extracted from naturally occurring materials, polysaccharides and proteins [77]. Emulsifiers vary considerably in their ability to form and stabilize emulsions, as well as in their cost, ease of utilization, ingredient compatibility, and environmental sensitivity [76]. Consequently, there is not a single emulsifier that is ideal for use in every food product. Instead, the development of each new food product depends on the rational selection of the most appropriate emulsifier for that particular system. This selection depends on the composition and structure of the food matrix, as well as on the changes in environmental conditions that the emulsifier experiences during processing, storage, and utilization, such as mechanical agitation, temperature, and pressure. Each type of emulsifier has its own particular advantages and disadvantages. For example, some emulsifiers are highly effective at generating small emulsion droplets during homogenization because of their rapid adsorption rates, but are poor at providing long-term stability against droplet aggregation because they do not provide strong enough droplet-droplet repulsive interactions, e.g., some small molecule surfactants. On the other hand, some emulsifiers are highly effective at imparting long-term stability to emulsions, but are inefficient at creating emulsions with small droplet sizes during homogenization, e.g., some polysaccharides and proteins.

A strategy to improve emulsion stability which combines both kinds of emulsifier was proposed by MacClements and his group [76, 78, 79]. It consisted in producing secondary emulsions obtained with a polyelectrolyte thin layer, adsorbed through the interaction with an ionic emulsifier of opposite charge standing on the surface of oil droplets. One example is the use of lecithin, an anionic emulsifier, which rapidly adsorbs to the surface of lipid droplets during homogenization, producing a primary emulsion with small droplet sizes and then the addition of chitosan, a cationic biopolymer, to produce secondary emulsions containing droplets coated with a lecithin-chitosan membrane (**Figure 2.3**).
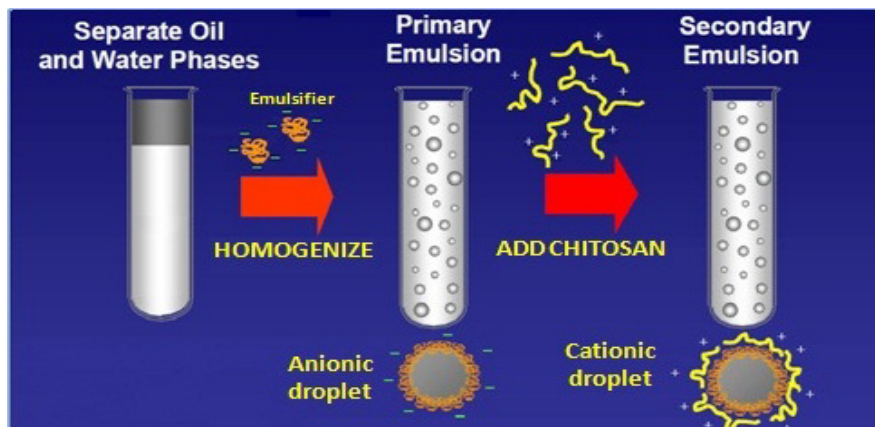
Figure 2.3. Two-stage mechanism for producing emulsion droplets coated by a two-layer interfacial membrane.

At low concentrations of chitosan, the emulsions become unstable to flocculation due to charge neutralization and bridging flocculation. Instead, at high concentration there is typically a depletion flocculation which can bring to creaming. However, at the right chitosan concentration, the net droplet charge switches from negative to positive, and kinetically stable emulsions can be produced. It was also reported in literature the possibility to re-disperse secondary emulsion by using sonication or stronger sources like a high pressure homogenizer even though in terms of size and monodispersion results were still scarce [**80, 81**].

Starting from this approach, herein we implemented a new post-processing method on secondary emulsions, which allowed us to improve emulsion homogeneity and therefore stability. In particular, emulsion behavior was monitored in terms of stability over time. It was possible to find the proper conditions - in terms of formulation and process - to obtain unprecedented, ultra-stable emulsions. Stability over time depending on polymer concentration is schematically represented in **Figure 2.4**. The absence of flocculation at high polymer concentrations was possible due to the innovative multiple re-dispersion process here developed.
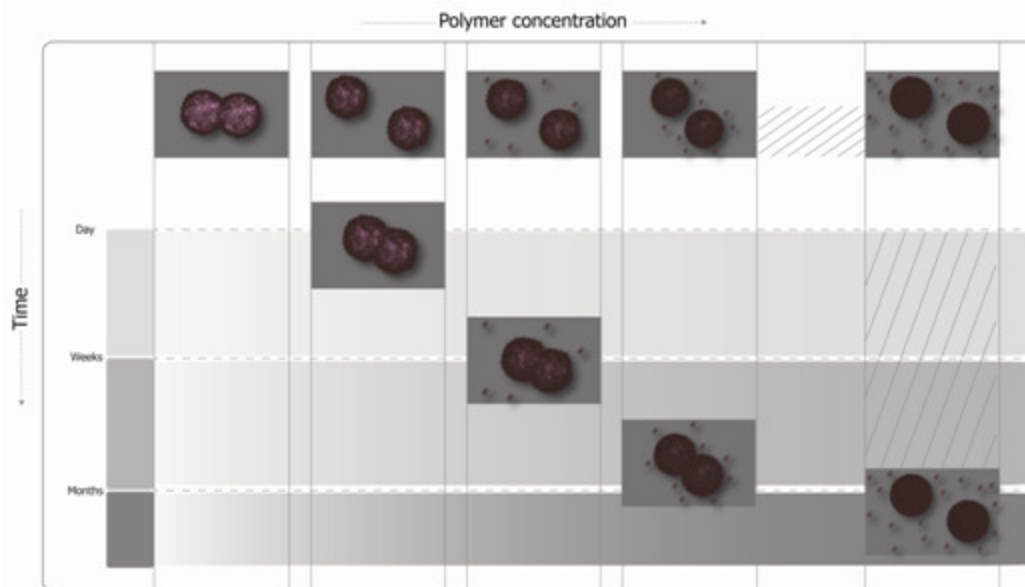
Figure 2.4. Stability scheme for multiple re-dispersed secondary emulsions at different polymer concentrations.

2.2. Materials and Methods

2.2.1. Materials

For the preparation of nano-sized O/W emulsions, Lipoid E80 an egg lecithin powder enriched of phosphatidyl choline (PC 80%; phosphatidylethanolamines (PE) 7,8%; lyso-phosphatidylcholine (LPC), lyso-phosphatidylethanolamine (LPE), sphingomyelin (SPH) in traces), as surfactant, and soybean oil (Medium chain triglyceride (MCT) oil; density at 20 °C of 0,0922 g/ml), both purcheased from Lipoid, have been used. For water phase MilliQ® water was used. In some preparations, oil phase was loaded with a lipophilic fluorophore like Nile Red (NR) (m.w.=318.37 g/mol) purchased from Sigma Aldrich. All these reagents were used without further purification. Then, NEs were further treated by depositing a layer of chitosan (polycation, low molecular weight (LMW) 90-150 kDa, DDA 84%) purchased from Sigma Aldrich and subjected to purification as well as dehydration as it will be described. Chitosan was also functionalized with Fluorescein 5(6)-isothiocyanate (FITC) (m.w.=389.38 g/mol), as it will be described later, always purchased from Sigma Aldrich. 1,4-diazabicyclo[2.2.2]octane (dabco) (m.w.=112.17 g/mol) antifade, also purchased from Sigma Aldrich, was used to avoid the bleaching phenomenon of FITC while analyzing samples by confocal and STED.

Lecithin Lipoid E80 has been chosen to be perfectly biocompatible, perfectly biodegradable and anionic which imparts a negatively charged surface on emulsion drops. It has been stored in a fridge at a temperature of about – 20 °C, preferably under vacuum and in a nitrogen atmosphere before its use. Vacuum is used to prevent its water absorbing and therefore difficulties in mixing with soy oil. As underlined in chapter II, lecithin acts as a stabilizing agent (for the reasons already described). Lecithin contains phosphatidyl choline (PC) which is an important precursor for many biochemical functions (**Figure 2.5**).
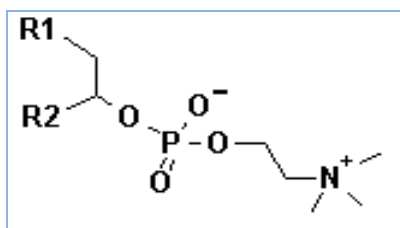
Figure 2.5. Phospatidyl choline chemical structure.

Choline provides structure and fluidity in cell membranes, improves transfer of nerve impulses to the brain and circulatory system, and aids in lipid and cholesterol transport and metabolism. The consumption of an adequate daily intake of choline supports brain, liver, and heart health.

Soybean oil is a popular vegetable oil that is valued for its affordability, high smoke point and health benefits. It often has a dark yellow or faint green color. Standard vegetable oil is often composed of soybean oil. Soybean oil accounts for 80% of all commercial oil used in the United States. This is a good all around oil that can be used for baking, cooking and frying. Soybean oil is made by extracting oils from the soybean. This is done by cracking the beans and then heating the beans to remove any unnecessary moisture. Next, the beans are sliced and then rolled to extract the oil with hexanes. Often, commercial brands mix soybean oil with other cheaper oils to make it more affordable. You can also find unrefined soybean oil, which is cold-pressed and expeller-pressed. Often unrefined oils have a stronger flavor, but usually retain a higher nutritional value than refined oils.

Soybean oil contains no cholesterol, which makes it a perfect choice for individuals with heart disease or high cholesterol. The fats in soybean oil are polyunsaturated which have shown to

help reduce total cholesterol, lower low density lipoproteins (LDL) or bad cholesterol levels and increase high density lipoproteins (HDL) or good cholesterol levels. Soybean oil has omega-3 fatty acids, which have shown to reduce the risk of cardiovascular disease, slow the growth of atherosclerotic plaque, slow the risk of arrhythmias or abnormal heartbeats and decrease triglyceride levels. Soybeans naturally contain antioxidants, which remain in the oil even after it is pressed. These antioxidants help prevent the damage caused by free radicals, which may help prevent certain cancers.

Figure 2.6. Picture of the soybean from which it is extracted the soybean oil.

Chitosan is a heterogeneous polysaccharide that consists primarily of acetylglucosamine (uncharged) and glucosamine (pKa ≈ 6,3-7) subunits (**Figure 2.7**).
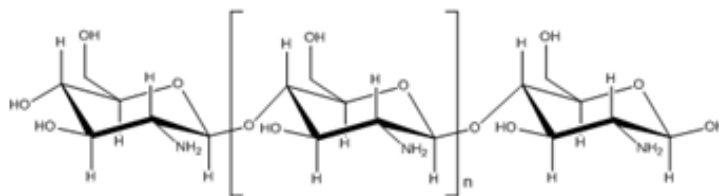
Figure 2.7. Chemical structure of the chitosan.

Although present in biomass, this polysaccharide is preferentially obtained by alkaline N-deacetylation of chitin, a structural polysaccharide, more highly acetylated and insoluble of chitosan, present in exoskeleton of crustaceans and many insects as well as the cell-wall of many fungal species. [**82, 83**]. At relatively low pH (< 6.5), chitosan is positively charged and tends to be soluble in dilute aqueous solutions, but at higher pH, it tends to lose its charge and may precipitate from solution due to deprotonation of the amino groups.

This biopolymer possesses a variety of biological and physiological properties, including biocompatibility, biodegradability and low toxicity [**84**]. All these important characteristics have led to the development of numerous application of chitosan in food, agriculture, and in particular in medicine and drug delivery. Indeed, chitosan was used for surgical suture, biodegradable sponges and bandages, matrices in microspheres and/or microcapsules, and in the delivery of drugs. Chitosan can also be used for heavy metal chelation, wastewater treatment, cholesterol lowering, texture modification, emulsion stabilization and so on. Many of these applications depend on interactions with surface-active materials, e.g., phospholipids, small molecule surfactants or bile acids. Chitosan has also been shown to be capable of adsorbing to the surfaces of lipid droplets and indeed it was used in this work to stabilize primary emulsions.

Flurescein isothiocyanate is a yellow coloured low molecular weight (m. w. 389,38 g / mol) dye whose chemical structure is illustred in the following **Figure 2.8**.
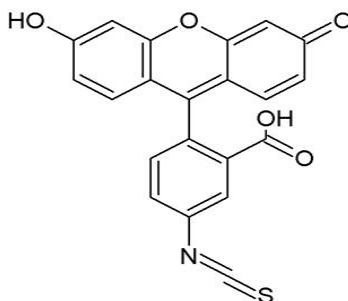
Figure 2.8. FITC chemical structure.

FITC is excitable at a wavelenght of 494 nm and produces maximum fluorescence emission at around 520 nm. This emission also depends on pH. In particular FITC has a small and steady increase of the fluorescence intensity between a pH of 3 and 6 and a most sudden increase after pH 7 to reach the maximum fluorescence intensity around pH 10 (see Appendix **Figure A.E.2**).

Quercetine (QR) belongs to a group of polyphenolic substances known as flavonoids. QR is a member of the class of flavonoids called flavonols. It is widely distributed in the plant kingdom in rinds and barks [**4**]. Especially rich sources of QR include onions, red wine and green tea. QR is a natural antihistamine and opposes the actions of the histamine in the body.

QR inhibits some inflammatory enzymes, such as lipid peroxidases, and decreases leukotriene formation. QR has anti-inflammatory, antiviral, immunomodulatory, anticancer and gastroprotective activities. QR blocks an enzyme that leads to accumulation of sorbitol, which has been linked to nerve, eye, and kidney damage in those with diabetes. QR also possesses potent antioxidant properties. It protects LDL cholesterol from becoming damaged. QR prevents damage to blood vessels by certain forms of cholesterol and other chemicals produced by the body. QR also works as an antioxidant by scavenging damaging particles in the body known as free radicals. People with diabetes are at higher risk of blood vessel damage from free radicals. For its antioxidant properties it could also be helpful in combination with tumor treatment where radicals are produced.

2.2.2. Methods

2.2.2.1. Preparation of primary NEs

Several oil in water emulsions were prepared varying oil percentage and amount of lecithin used, by adding soybean oil to Lipoid E80 previously weighted with a high precision balance in a beaker. The surfactant was allowed to dissolve in the oil phase by stirring (for 10 minutes at a temperature of 60 °C and at a speed of about 500 r.p.m.) using a high speed blender (RZR 2102 control, Heidolph), and then, after reaching room temperature, it was sonicated for 1.5 min (sonication amplitude of 60%; both pulse-on and pulse-off of 10 s) with an immersion sonicator (Ultrasonic liquid processor Q700, Misonix Sonicators). These two steps were repeated until lecithin was completely dissolved. After measuring the aqueous phase (milliQ water), to obtain the pre-emulsion, the oil phase was added dropwise to the aqueous phase, using for mixing an immersion sonicator for 3 minutes (70% of sonication amplitude, pulse on and a pulse off respectively of 10 and 5 seconds) and then sonication was continued for other 5 min in the same conditions. The pre-emulsion preparation was performed in a large beaker in which a jacket of ice was created, to keep temperature low and avoid pre-emulsion overheating during sonication. Such warming could lead to thermal agitation of pre-emulsion droplets and then increase the probability of coalescence. The pre-emulsion was finally passed at 2000 bar through the high pressure homogenizer (Microfluidics© M-110PS Series Microfluidizer", details of the working

principles of this instruments can be found in the Appendix A.I.2) for 3 single cycles (those that more effectively contribute to reduce the droplet size) and then in continuous steps modality, recycling the product without any reduction of volume and taking out small volumes of emulsion at 50, 100, 150 and 200 steps and in first individual cycles in order to follow the behavior of size, PDI and Z-potential versus number of processing steps.

Tests were conducted to study stability over time and reproducibility of emulsions preparation procedures. The instrument used both for size, PDI and Z-potential measurements is Zetasizer Nanoseries by Malvern© (detailed description are described in the Appendix A.I.3).

2.2.2.2. Chitosan purification

Briefly, a 1% wt acetic acid solution of chitosan (pH=2) was prepared. After complete dissolution of chitosan under magnetic stirring, the solution was filtered and after filtration pH of the solution was changed by adding a solution of NaOH 6M until pH was basic thus allowing the precipitation of chitosan. The polymer was collected by centrifugation (15 min, 4°C, 9000 rpm), redispersed in MilliQ water and recollected by centrifugation (5 min, 4°C, 9000 rpm) several times until all $NaCH_3COO-$ was removed and pH of chitosan suspension was neutral. Then the sample was freeze-dried for 48 h and further dried in oven for 3 h at 80°C to maximize removal of water, since chitosan is strongly hygroscopic as measured by thermogravimetric analysis (TGA) (see Appendix **Figure A.E.1**).

2.2.2.3. Preparation of secondary NEs

It has been seen in preliminary experiments that purified samples of chitosan are necessary for good deposition on primary emulsions. Therefore, starting from purified chitosan, solution at several concentration (0.0025%, 0.005%, 0.00875%, 0.0125%, 0.025%, 0.05%, 0.0875%, 0.125% 0.250%, 0.5%, 0.875%, 1.25% wt), were prepared in 0.1 M acetic acid Milli-Q water. 9 ml of these solutions were diluted 1:4 with Milli-Q water to 36 ml and brought to pH 4 with small addition of NaOH 6 M solution. Then 9 ml of the emulsion diluted to 5% oil phase were added quickly under vigorous stirring and kept under stirring for 15 min to allow uniform chitosan deposition. So the emulsion was diluted 1:5 with chitosan solution (thus final oil concentration was 1% whereas final chitosan concentrations were 1/5 of the initial).

2.2.2.4. Synthesis of FITC labeled chitosan

To carry out some in fluorescence analysis such as in fluorescence microscopy of secondary emulsions, in some preparations it was used a chitosan modified with FITC. Briefly, due to its isothiocyanate moiety FITC could be linked to chitosan's primary amine forming a thiourea bond (**Figure 2.9**).
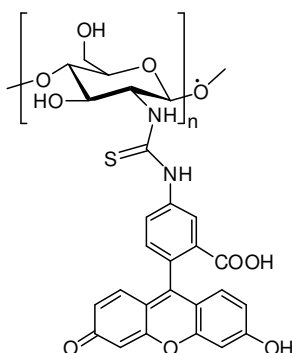
Figure 2.9. Schematic illustration of the synthesized FITC-labeled chitosan.

In particular, 500 mg of purified and dried chitosan where dissolved in 50 ml of aqueous acetic acid solution (0.10 M). After complete dissolution 50 ml of methanol were added. Then 25 mL of a 1 mg/ml solution of FITC in anhydrous methanol was prepared. This solution was slowly added to chitosan solution and the reaction was allowed to proceed in the dark under magnetic stirring for 18h at room temperature. Finally, chitosan was precipitated with a solution of NaOH and the precipitate was collected by centrifugation (9000 rpm; 4°C; 15 min). The obtained FITC-chitosan was dispersed in MilliQ water, washed and centrifuged 6 times until pH had a neutral value and no traces of FITC were visible in the waste washing solutions. As additional evidence that all the FITC was removed, a small amount of the functionalized sample was dispersed in a basic water solution (pH=10) (FITC, is pH sensitive and the fluorescence is very strong in these conditions), allowed to stay and then centrifuged. Negligible fluorescence was revealed at spectrofluorimeter in the solution separated from the dispersed polymer, so the sample could be considered purified. After reaction, the degree of functionalization was determined by means of UV-Vis analysis (see Appendix A.I.8), comparing the absorbance with a FITC calibration line (see Appendix **Figure A.I.3**).

2.2.2.5. DLS characterization

Particle size distribution and Z-potential of emulsions and emulsion-based nanocapsules were determined using a particle electrophoresis instrument (Zetasizer zs nano series ZEN 3600, Malvern Instruments Ltd., Malvern, U.K.). Detailed description of the physical principles of these analyses and of the instrument are reported in the Appendix (A.E.3).

For particles size measurements all the samples were diluted up to a droplet concentration of approximately 0.025% (wt), by using Milli-Q water in the case of primary emulsions and an acetic acid Milli-Q water solution (pH 4, 20 mM) in the case of secondary emulsions. The diluition is important to prevent the overlapping of scattered light intensity, for example, from two droplets if they are extremely close each other (multiple scattering phenomenon) during measurement. A default refractive index ratio (1.52) and 5 runs for each measurement (1 run lasting 100 s) were used in the calculations of the particle size distribution.

For Z-potential measurements the samples were diluted in the same conditions and the analysis was carried out by setting 50 runs for each measurement.

2.2.2.6. Spectrofluorimetry analysis

In order to evaluate polymer coverage on primary emulsions, a FITC emission spectrum analysis was performed (EnSpire Multimode Plate Reader 2300-0000, Perkin Elmer). 100 µl of sample at different FITC-labeled chitosan concentrations (0.01%, 0.00175%, 0.0025%, 0.005%, 0.01%, 0.0175%, 0.025%, 0.05%, 0.1%, 0.175%, 0.25% wt) were loaded in a multi-well (3 replicates for each sample were prepared) and irradiated at 488nm (the light coming from a flash lamp can be filtered in order to have a light with the desired wavelength) Samples were diluted from 1% wt of oil to 0.025 % wt with the same buffer solution used for DLS analysis in order to limit final fluorescence emission. The fluorescence signal was detected at 510 nm. The used flashes number was 100.

2.2.2.7. STED analysis description

A procedure was also developed to allow observation of all the samples with the STED (stimulated emission depletion) high resolution in fluorescence optical microscope. Each sample

was diluted (1:50) in a heppendorf with a 20 mM acetic acid buffer solution at pH 4 and was put in a FD3510 dish for 30 min to allow it to adhere to the surface of the dish. After that, 3 washes with a 5% wt dabco antifade solution were performed and at the end the central part of the dish was left full of dabco during sample observation. Dabco antifade was introduced to avoid the bleaching effect of the FITC-labeled chitosan. Samples were imaged with a Leica TCS STED-CW microscope. The resolution of the microscope was estimated to be < 80nm. For each sample, 10 images were acquired with a field of view of 25.6 x 25.6 μm for a pixel size of 25 x 25 nm. The STED-CW beam power was 430 mW, measured at objective back focal plane. The analysis of the images was carried out by Imagej software.

2.2.2.8. Cryo-TEM characterization

The morphology of the secondary emulsion was observed by transmission electron microscopy (TEM) in cryo conditions. Samples were prepared by putting a droplet of dispersion on the grid; the excess of water was removed by an automatic system (Vitrobot of Leica), described in the Appendix (**A.I.6**) to obtain a thin liquid film on the grid which was immediately immersed into the liquid nitrogen to get a vitreous solid water film. Cryo-TEM images were recorded by a Tecnai 12 electron microscope (Philips, Eindhoven, Netherlands,) described in the Appendix (**A.I.6**) at approximately -170 °C under 120 kV acceleration voltage equipped with a Multiscan 600W CCD camera (Gantan Inc., Warrendale, PA, USA).(Verificare modello cryo-TEM).

2.3. Results and Discussion

2.3.1. Primary emulsions: DLS analysis

In terms of emulsion fabrication, the main effort was to identify the right conditions to obtain NEs with tunable sizes, in a range of interest for bio-nanotechnology applications (below 200nm and down to 100nm), and low PDI (down to 0.1), along with the choice of a biocompatible formulation consisting of soy-bean oil and Lecithin Lipoid E80, both pharmagrade products and used in parenteral nutrition thanks to their well known biodegradability.

As described in detail in the method section, first, the oil phase was prepared by adding a certain amount of Lipoid E 80 to a volume of soy-bean oil. Then the pre-emulsion was obtained by adding the oil phase dropwise to a weighted amount of aqueous phase (Milli-Q water) and emulsified using the immersion sonicator. The pre-emulsions were finally passed at 2000 bar through the high-pressure valve homogenizer (Microfluidics M110PS) for first three individual cycles to strongly reduce the initial size and then continuously by re-filling the reservoir for several steps, thus recycling the product without any loss of volume and taking out small volumes of emulsion at 50, 100, 150 and 200 steps. This method was used for the preparation of all oil-in-water emulsions at different concentrations of oil phase (10, 20, 30 % wt). NEs with different oil and lecithin concentration were classified according to the Lipoid E80/oil phase ratio that remains constant in all oil concentrations, as reported in **Table 2.1**.

Emulsion	Lipoid E80 /Oil phase (g/mg)
L1	0.06
L2	0.12
L3	0.18
L4	0.24
L5	0.3

Table 2.1. List of surfactant formulation.

A first DLS analysis was performed to understand the influence of increasing the number of processing steps on the droplet sizes as well as the lecithin concentration at a fixed concentration of oil of 10 % wt.
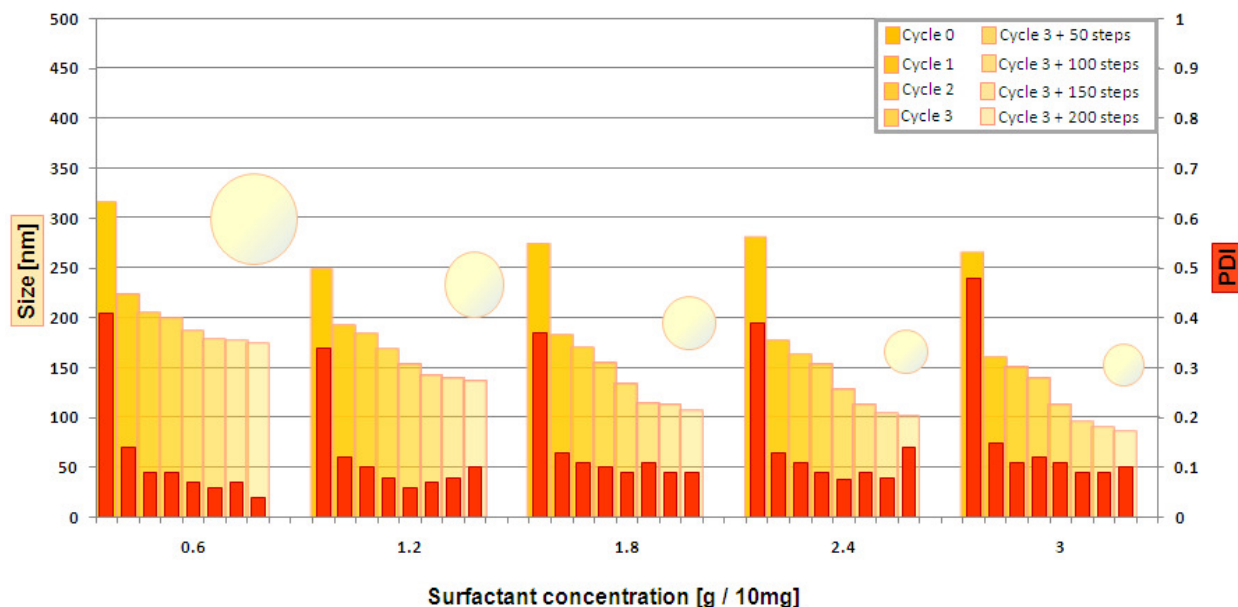
Figure 2.10. DLS results on 10% oil phase emulsions.

As can be seen from **Figure 2.10**, independently from lecithin and oil concentration a longer processing to Microfluidizer led to smaller droplets, but it was decided to stop the process after 200 steps because it was not observed a significant emulsion droplet sizes decreasing with a further increasing of number of microfluidizer steps; on the contrary, in some cases, this over-processing led to emulsion destabilization. Furthermore it was found that using a greater percentage of oil, while maintaining the same surfactant/oil ratio, brought to smaller droplets and smaller PDI (**Figure. 2.11**).

		Diam. (nm)	% Intensity	Width (nm)
Temperature (°C): 25,0				
Count Rate (kcps): 361,2				
Cell Description: Clear disposable zeta cell				

Duration Used (s): 200
Measurement Position (mm): 5,50
Attenuator: 6

		Diam. (nm)	% Intensity	Width (nm)
Z-Average (d.nm): 99,94	Peak 1:	107,2	100,0	29,62
PdI: 0,056	Peak 2:	0,000	0,0	0,000
Intercept: 0,903	Peak 3:	0,000	0,0	0,000
Result quality : Good				
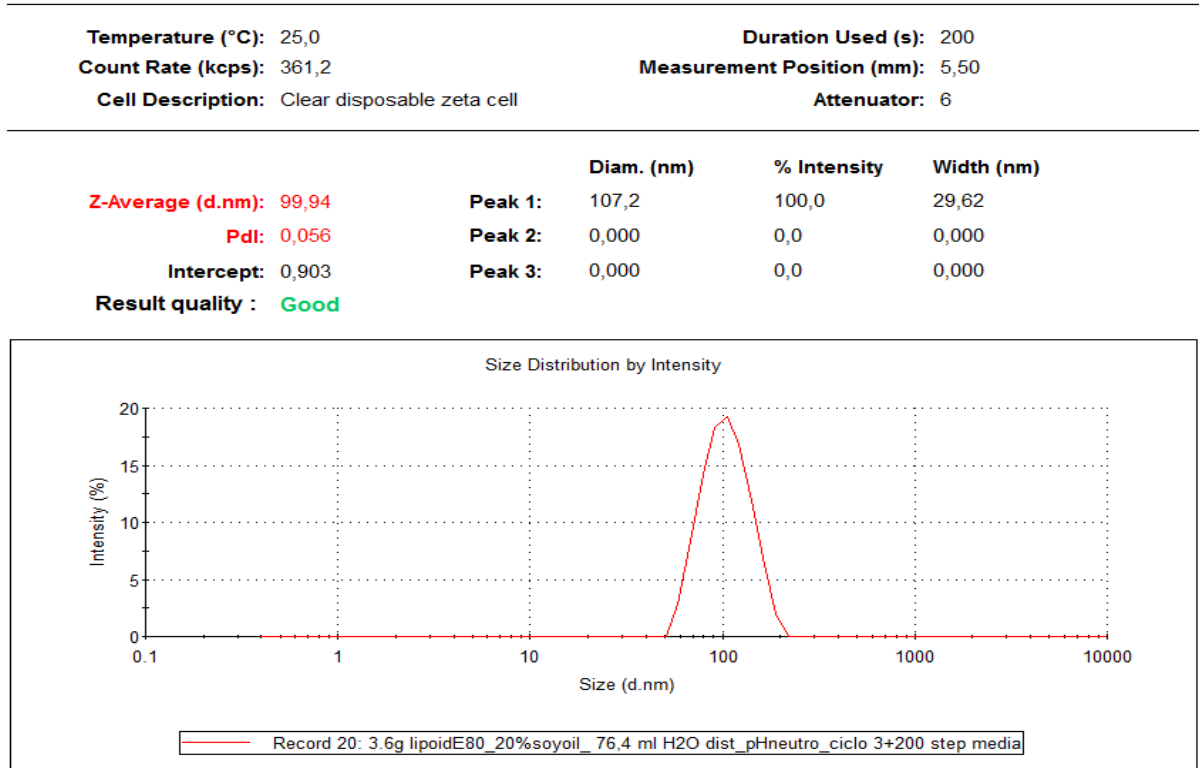
Figure 2.11. Example of droplet size and PDI size distribution measurement.

As reported in the name of the experiment this is a sample corresponding to the sample L3 of the previous experiment. Here we have 3.6g of Lecithing in 20ml of oil whereas in the previous case they were 1.8g in 10ml therefore the same ratio surfactant/oil. This time the average size and PDI (99.94nm, 0.056) were lower than previous case (107nm, 0.09).

Just as an example of Z-potential test, in **Figure 2.12** there is a representation of a typical Z-potential measurement.

		Mean (mV)	Area (%)	Width (mV)
Temperature (°C): 25,1			Zeta Runs: 50	
Count Rate (kcps): 158,5			Measurement Position (mm): 2,00	
Cell Description: Clear disposable zeta cell			Attenuator: 10	

		Mean (mV)	Area (%)	Width (mV)
Zeta Potential (mV): -36,2	Peak 1:	-36,2	100,0	10,1
Zeta Deviation (mV): 10,8	Peak 2:	0,00	0,0	0,00
Conductivity (mS/cm): 0,00398	Peak 3:	0,00	0,0	0,00
Result quality :	Good			

Zeta Potential Distribution

Record 24: 3.6g lipoidE80_20%soyoil_ 76,4 ml H2O dist_pHneutro_ciclo 3+200 step media

Figure 2.12. Example of Z-potential droplet measurement.

Considering the improvement in terms of size and PDI obtained by doubling the oil content, it was decided to repeat the preparation and characterization of all the previous samples at an oil concentration of 20% wt. Also in this case DLS analysis made it possible to observe how the variation in the number of processing passes and steps and of lecithin concentration affected the droplet size and PDI (**Figure 2.13**).
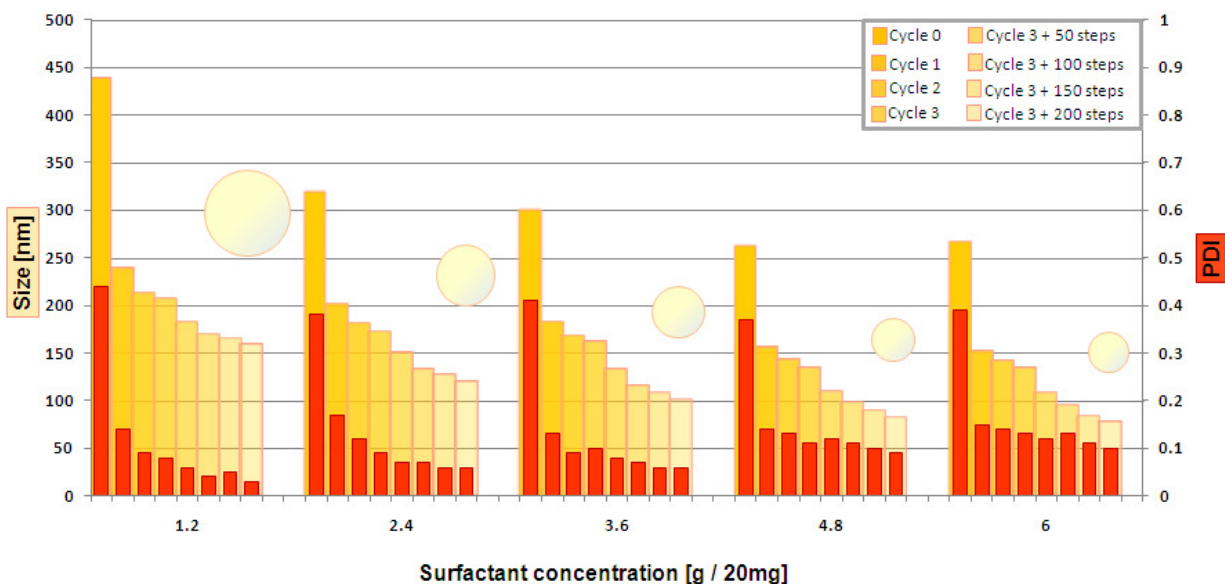
Figure. 2.13. Emulsion size at different processing cycles and surfactant amount.

Like in the case of 10% wt of oil a significant decrease in the emulsion size after the single cycles and a further decrease during continuous processing up to a plateau were observed. In addition, it was confirmed for all the samples the better results compared to the 10 % wt of oil. Remarkably, a reproducible size was attained at each formulation from around 160 nm, with the lowest concentration of lecithin, to around 80 nm with the highest one. L5 was slightly smaller than L4, meaning that a further increase in the amount of lecithin would have been ineffective. In the same way, PDI decreased with the number of cycles, but increased with the amount of surfactant, even though it remained below 0.1. The precise values of size, PDI, and Z-potential for all the samples are summarized in the appendix (**Table A.E.1**) for both 10 and 20% wt of oil.

Each emulsion was characterized in terms of stability by carrying out size and PDI measurements over time as shown in the following **Table 2.2**.

Emulsion Composition	Stability tests								
		0 time	1 day	3 days	1 week	2 weeks	4 weeks	10 weeks	10 weeks 4C
1,2 g lecithin / 20 ml soyoil	Size[nm]	158,3	162	169,5	162,6	160,7	153,5	1010	211
	PDI	0,042	0,028	0,153	0,066	0,052	0,057	0.330	0.259
2,4 g lecithin / 20 ml soyoil	Size[nm]	119	124,5	126,5	126,6	131,1	130,1	149.8	129
	PDI	0,073	0,051	0,05	0,055	0,078	0,055	0.063	0.05
3,6 g lecithin / 20 ml soyoil	Size[nm]	100,8	102,3	105,6	111,9	113,8	131,9	125.6	100.7
	PDI	0,073	0,085	0,097	0,128	0,122	0,137	0.2	0.085
4,8 g lecithin / 20 ml soyoil	Size[nm]	82,33	84	84,92	84,77	83,95	85,34	87.41	86.76
	PDI	0,103	0,107	0,093	0,104	0,089	0,102	0.1	0.106
6 g lecithin / 20 ml soyoil	Size[nm]	77,87	78,58	81,01	80,12	78,51	82,2	82.99	82.1
	PDI	0,1	0,113	0,124	0,116	0,126	0,097	0.099	0.1

Table 2.2. Stability tests on emulsions of different size at room temperature and 4 °C.

As it is possible to see, at room temperature the last two emulsions were quite stable while the first three changed a lot as predictable by the different size. As a matter of fact droplets with bigger sizes are more flexible and can coalesce more easily. By keeping the emulsions at 4°C also the first three gained stability maybe due to the slowing down of the droplets which reduces the efficacy of hits and following coalescence.

To further scale down NEs sizes it was also tried to increase viscosity of the dispersant phase with the addition of glycerol which should reduce emulsion coalescence while processing and stabilize smaller oil nano-droplets as consequence. In the case of formulations including glycerol it was needed to blend the two phases in advance and then process by ultrasound sonicator at the usual conditions. Different concentrations of glycerol were tested in combination with different oil concentrations. After several trials in terms of formulation it was possible to optimize and gain in terms of size reduction without disturbing the PDI. Formulation was varied in terms of both oil concentration, volume ratio between water and glycerol and surfactant concentration (**Figure 2.14**).
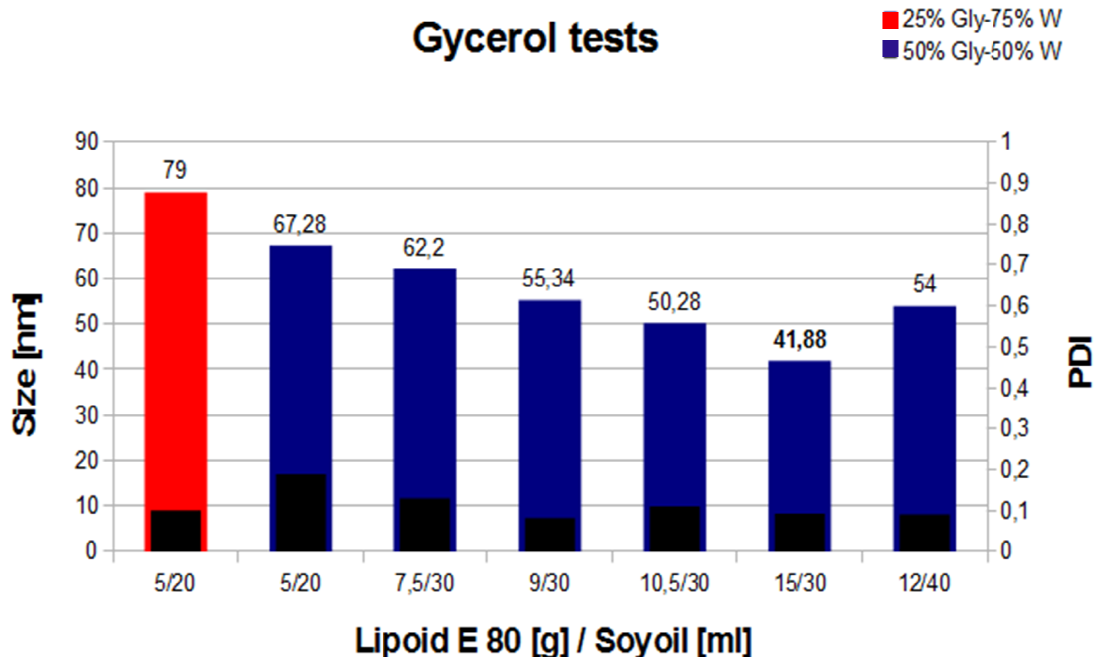
Figure 2.14. Emulsion size at different formulations in presence of glycerol.

The best formulation allowed us to produce NE size down to 42nm. However, these NEs resulted much more unstable over time. Anyway, it was shown how working with the viscosity of the dispersant phase maybe with different substances could allow a further strong reduction of the emulsion size down to few tens of nanometers.

Among the several tests carried out to optimize the preparation method in terms of formulation and equipment, it was also tested the reproducibility of the procedure. In the following **Table 2.3** the average size and PDI for three different preparations with same formulation and procedure are reported.

Procedure	Sample	Mean size (nm)	PDI
1.2% wt Lipoid E80; 10 % wt Soy oil; 88.8 ml H2O distillata Ciclo 3 + 150 step	1	131,4	0,087
	2	127,3	0,073
	3	126,1	0,064

Table 2.3. Reproducibility of an emulsion with a lecithin / soybean oil ratio of 1,2 g / 10 ml.

As it is possible to see there is a perfect reproducibility both in terms of size and PDI. Then, they were weighed 6 g of lecithin and dissolved in 20 mg of soybean oil. It was followed the procedure previously described for the realization of the pre-emulsion. The pre-emulsion, which in this case had a volume of 200 ml, was divided into two equal parts each of 100 ml, therefore with the same lecithin/soybean oil ratio. One of the two pre-emulsions was processed and characterized in the day of preparation while the other one, after 3 days. The results are reported in the following **Figure 2.15**.
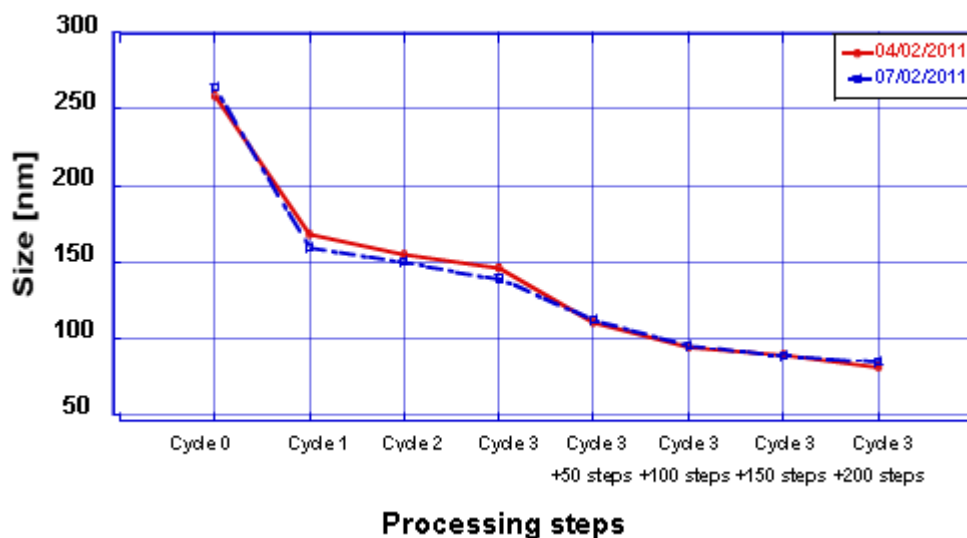
Figure 2.15. Reproducibility of emulsion with a lecithin / soybean oil ratio of 3 g / 10 mg.

As it is possible to see from the graph, emulsions are almost identical for each processing cycle and step. That means once prepared the pre-emulsion, it is not subject to a fast destabilization but it can be processed even after a few days; then the high pressure homogenizer guarantees a perfect reproducibility.

2.3.2. Secondary emulsions

2.3.2.1. DLS analysis

It is well known [**78**] that emulsions with a surface charge can be stabilized using a polyelectrolyte coating; they are then called secondary emulsions, and their stabilization

capability depends on the concentration of the polymer itself. If concentration is not appropriate, stability can be even lower. In this work, not only it was varied the polymer concentration, but it was also attempted to identify an optimal process procedure to improve stability. The main issue in this kind of coating is that polymer concentration inside the mixing cannot be uniform. Therefore, after one day from preparation all the secondary emulsions were homogenized at medium pressure (around 700 bar) following the procedure reported in the experimental part; a beneficial effect on polidispersity and stability was observed. In particular, it was found out that, by re-processing all the secondary emulsions still alive after one month at the same conditions, a further significant enhancement of their long-term stability evaluated in terms of size and PDI over time was obtained. The re-dispersion scheme is reported in the following **Figure 2.16**.
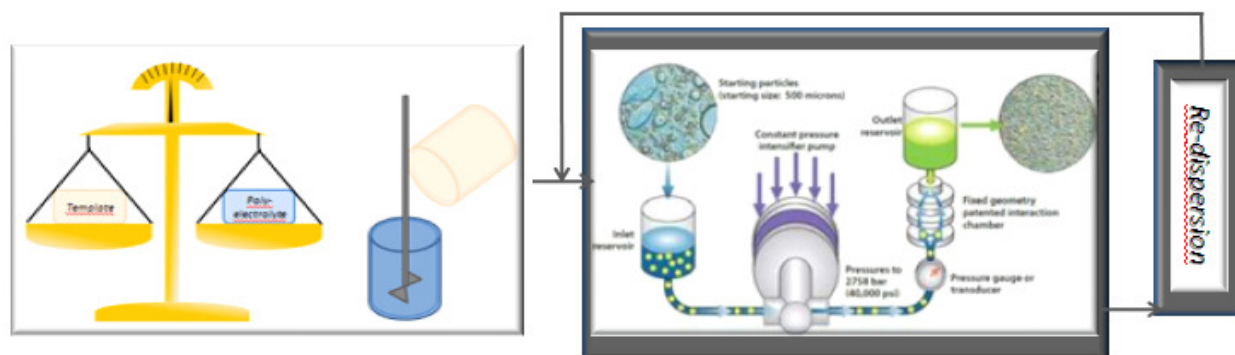
Figure 2.16. Scheme of re-dispersion processing of secondary emulsions.

For instance, the evolution of the size over time for L1 (large), L2 (medium) and L4 (small) double re-processed secondary emulsions (**Figure 1.17.b**) and just for L1, a comparison between double re-processed, single re-processed and no re-processed samples (**Figure 2.17.a**) are reported. (All the other data are in the **Table A.E.2** in the Appendix).
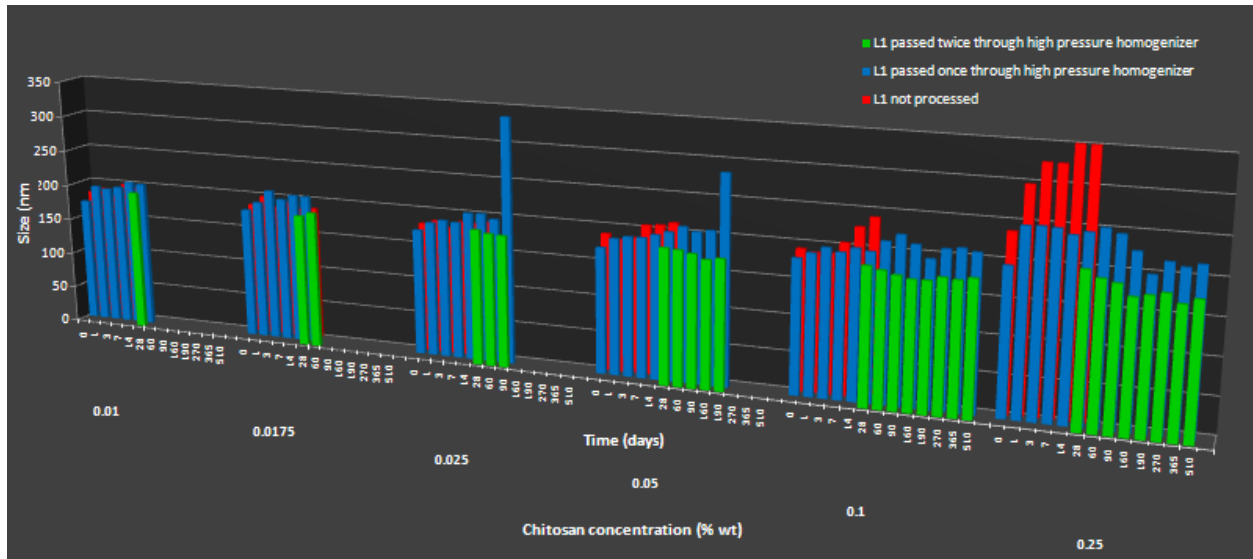
(a)
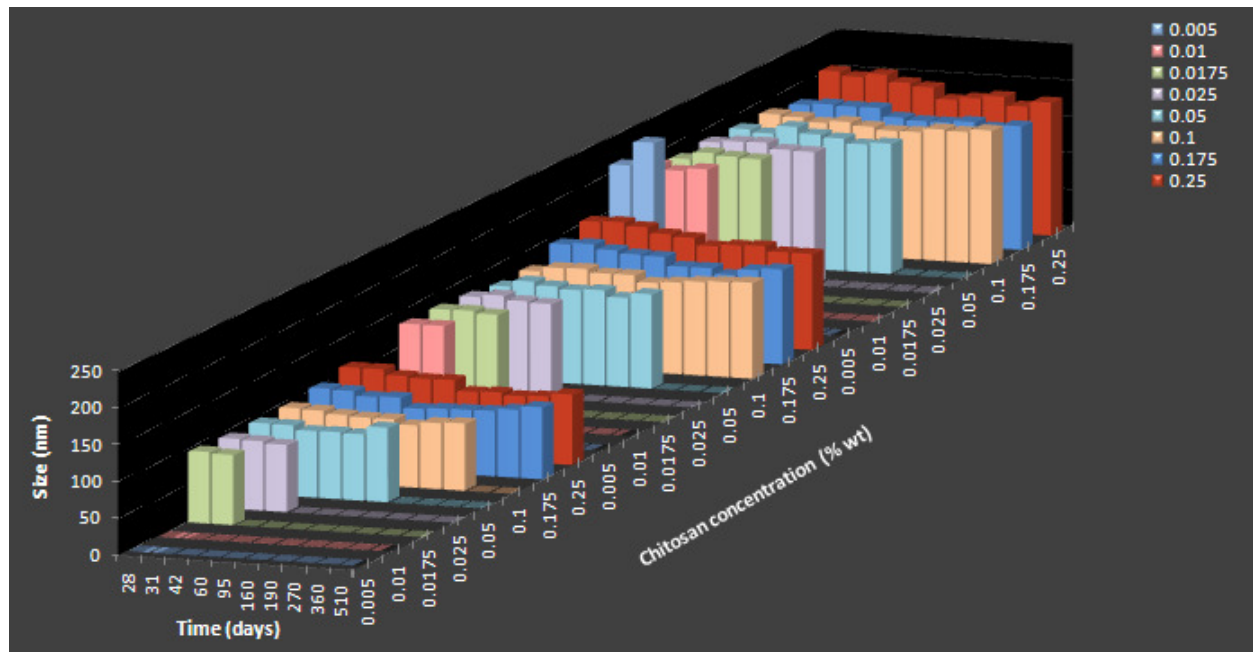
(b)

Figure 2.17. L1 secondary emulsion size at different chitosan polymer concentrations over time processed twice, once and not at all (a); secondary emulsions on L1, L2, L4 processed twice (b).

In particular, from **Figure 2.17.a** it is clear how the double re-processed samples behave better than the single re-processed ones and much better than non-processed ones both in terms of size and possible destabilization time (the same is for PDI, see **Table A.E.2** in the Appendix). For no

re-processed samples, the destabilization trend was already evident in the first month therefore no further data were collected. It is also worth noticing how the size of the double processed samples is slightly higher than the starting primary emulsions meaning no aggregations compared with single re-processed and even more to no reprocessed samples. Data related to double re-processed samples start at 1 month since this time corresponds to their birth. Finally for what concerns polymer concentration it is clear how the stability increased with it. In particular, polymer concentrations needed to give stability were dependent on the emulsion size, as it was predictable looking at the different surface amount; the smaller the droplets, the higher the surface, and therefore the polymer needed. **Figure 2.17.b** confirms this stability trend with polymer concentration independently of starting primary emulsion size. Specifically, a low concentration of chitosan brought to destabilization faster than that of the primary emulsions; specifically, the lower the concentration, the faster the de-mixing as expected. At polymer concentrations below 0.01% wt, secondary emulsions re-processed one time were readily de-mixed, and therefore not suitable for further re-dispersion treatment after 1 month. On the other hand, by increasing polymer concentration, emulsion stability improved maybe due to a more and more complete coverage of the emulsions. However, high polymer concentrations are typically excluded, due to depletion flocculation that we also noticed in different degrees in the case of single and no re-dispersion process, as shown in the **Figure 2.17.a**. On the contrary by double re-dispersing this aggregation was avoided due to an enhanced homogenization of the polymer in solution. In this way it was possible to obtain unprecedented ultrastable secondary emulsions.

2.3.2.2. Granulometric analysis

In terms of stability, the micrometric percentage of secondary emulsions was also evaluated. Indeed, in the field of lipid injectable emulsions for parenteral nutrition, the volume percentage of particles larger than 5 µm has to stay below 0.05%, which is the maximum value specified by United States Pharmacopea (USP) (Chapter729). In **Figure 2.18** it is shown the size distribution of a primary emulsion during the first two weeks after preparation and the same emulsion stabilized by double re-dispersion and by using chitosan at the last three polymer concentrations.
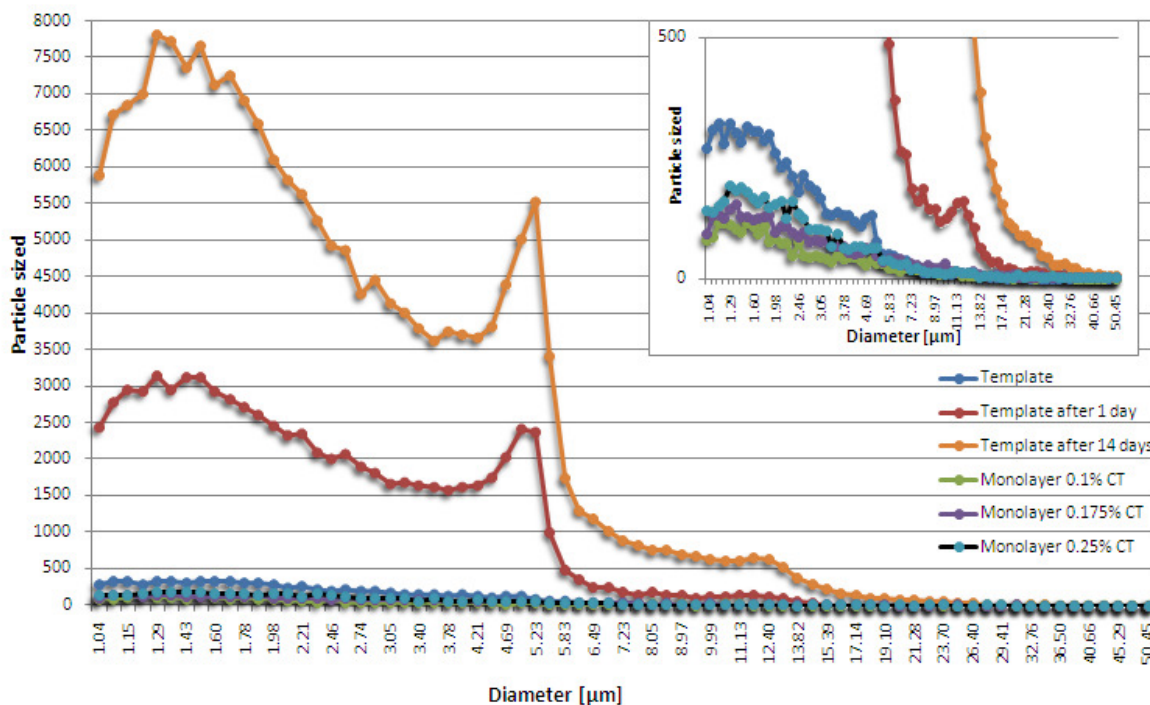
Figure 2.18. Particle size distribution by granulometer analysis. The inset magnify bottom part of the graph.

The difference is evident and by quantifying the percentage of volume fraction above 5 µm in size it was found that emulsions with no polymer coating after 2 weeks had already overcome the specified threshold, while the stabilized secondary emulsions after 7 months still met the specification standard (see **Table 2.4**).

Sample	Days after	% wt of particles > 5
Template	0	0.001
Template afetr 1 day	1	0.015
Template after 14 days	14	0.069
Monolayer 0.1% CT	210	0.029
Monolayer 0.175% CT	210	0.034
Monolayer 0.25% CT	210	0.051

Table 2.4. Amount in % wt of particles above 5 µm in size in the case of L4 for a primary emulsion in first 2 weeks and for secondary double re-dispersed emulsions at the three highest concentrations of polymers (0.1, 0.175, 0.25 % wt) after 7 months.

2.3.2.3. Morphological analysis

To support the DLS analysis L1, L2 and L4 secondary emulsions - coated with chitosan (0.1% wt) and double processed were analyzed by in fluorescence microscopy. This analysis was performed using chitosan labeled with FITC. In **Figure 2.19** the absorption (left) and the emission (right) spectra of the chitosan labeled FITC are reported.
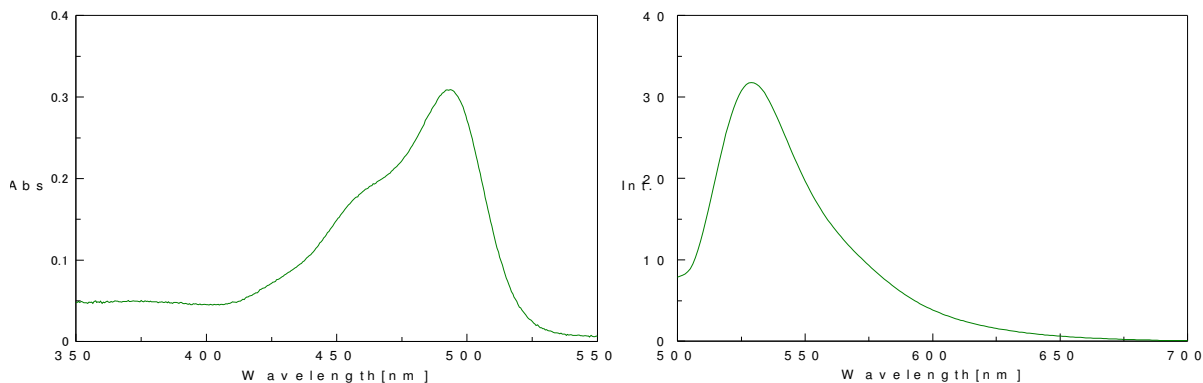
Figure 2.19. Absorption (left) and emission (right) spectra of FITC labeled chitosan.

In particular, it was necessary to carry out a STED analysis due to the expected small size, as demonstrated by the comparison with a confocal analysis (**Figure 2.20**).
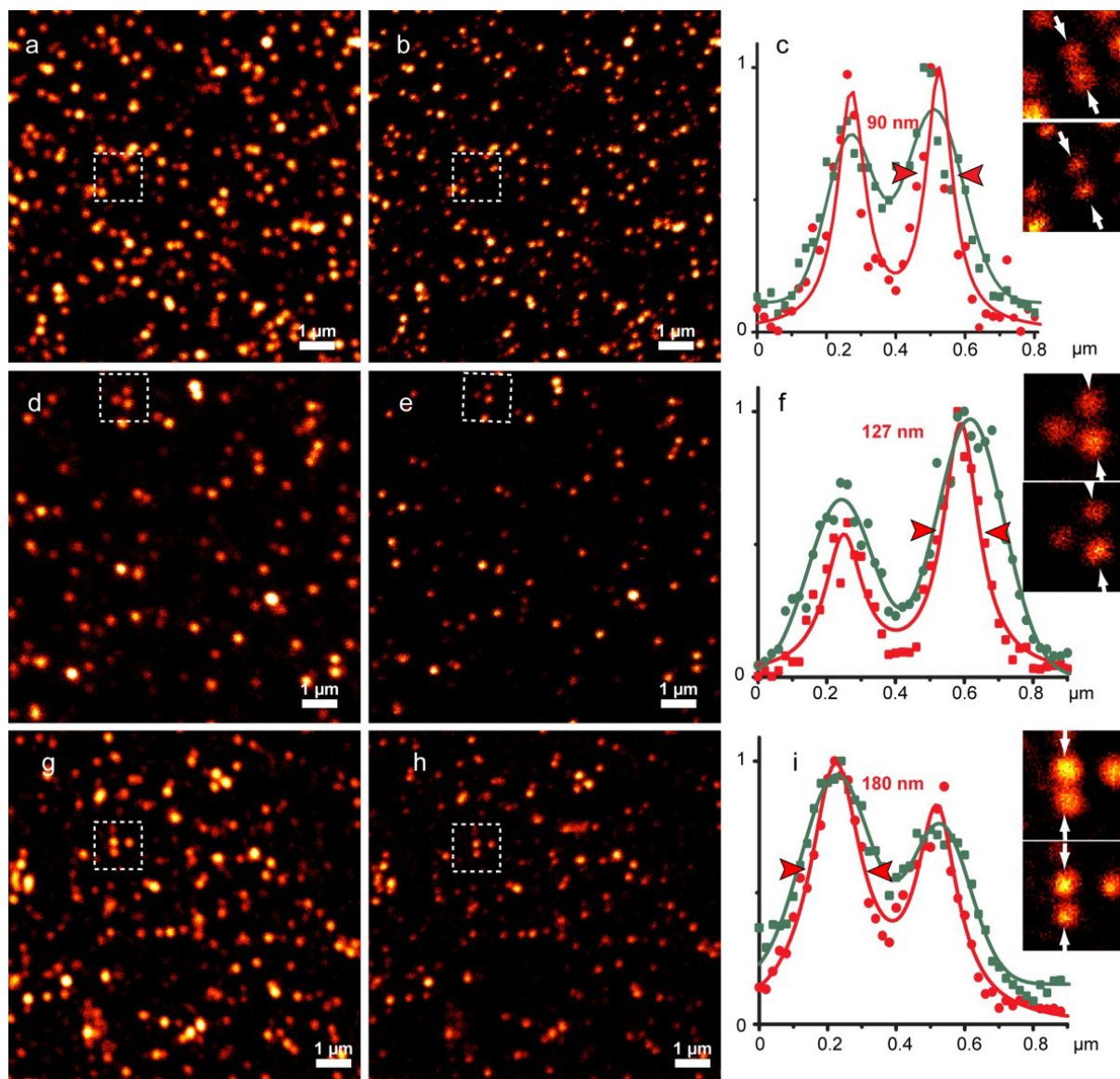
Figure 2.20. In fluorescence microscopy analysis by confocal and STED on L1, l2, l4 based secondary emulsions.

The results are consistent with the analysis carried out in the conventional way by DLS.

In terms of morphological analysis a Cryo-TEM was carried out too. To better distinguish the shell from the oil core a tomography analysis was needed. It is shown this analysis for a stable secondary emulsion built up on the L4 template at 0.1% chitosan concentration after five months (**Figure 2.21**). Indeed, L4 template is the right compromise between smallest sizes and suitable PDI.
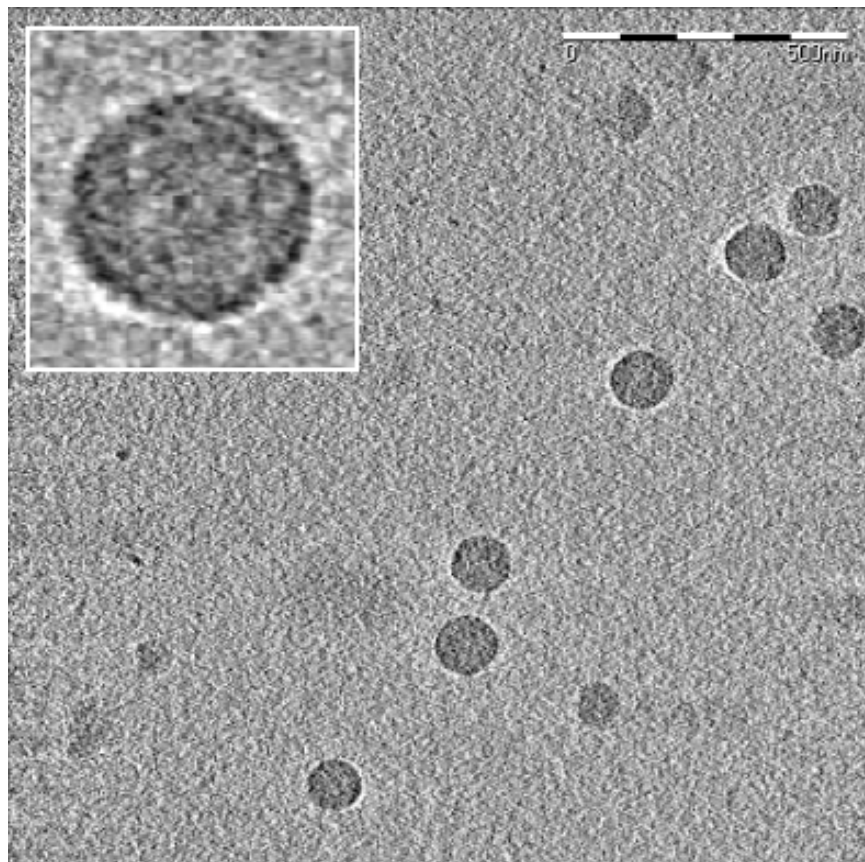
Figure 2.21. Cryo-TEM tomography of a chitosan based secondary emulsion and magnification (Top on the left) showing the nanoshell.

As expected for this system from DLS measurements, size is slightly below 100 nm and the shell is around 5 nm.

2.3.2.4. Sprectrofluorimeter analysis

The use of nanoemulsions as template for further build up of oil core based nanocapsules and in particular layer-by-layer polymer nanoshells on liquid templates can be very advantageous in drug delivery [85, 86]. Typically, for secondary emulsions a significant excess of polymer in solution is avoided in order to prevent further deposition due to aggregations.

There is a model reported in literature which evaluates the amount of polyelectrolyte to reach saturation level on emulsion droplets [87]. This model considers polymer only on droplet surface until complete saturation and uses the following expression:

$$C_{Sat} = \frac{6\varphi\Gamma_{Sat}}{d}$$

where φ is the droplet volume fraction, Γ_{Sat} is the surface load with polyelecrolyte at saturation (in Kgm^{-2}), d is the volume-surface mean droplet diameter (in m), and C_{Sat} is the minimum concentration of polyelectrolyte in the whole system required to saturate the surfaces (in kgm^{-3}). This equation shows that polyelectrolyte concentration required, to completely saturate particle surface, increases with particle concentration, surface load, and the inverse of mean particle size. For a particular system, this concentration can be determined empirically. Indeed, in literature it is proposed to use the Z-potential measurement as method to evaluate the saturation concentration of the polymer around the primary emulsion.

Here, to estimate the saturation concentration, we proposed a novel method based on the use of a fluorophore chemically labeled to the polyelectrolyte, in particular, FITC-labeled chitosan. With this method we evaluated the emission behavior of secondary emulsions, based on L4 template, as an example, at increasing polymer concentrations (**Figure 2.22**). Fluorescence was normalized with respect to the polymer concentration itself.
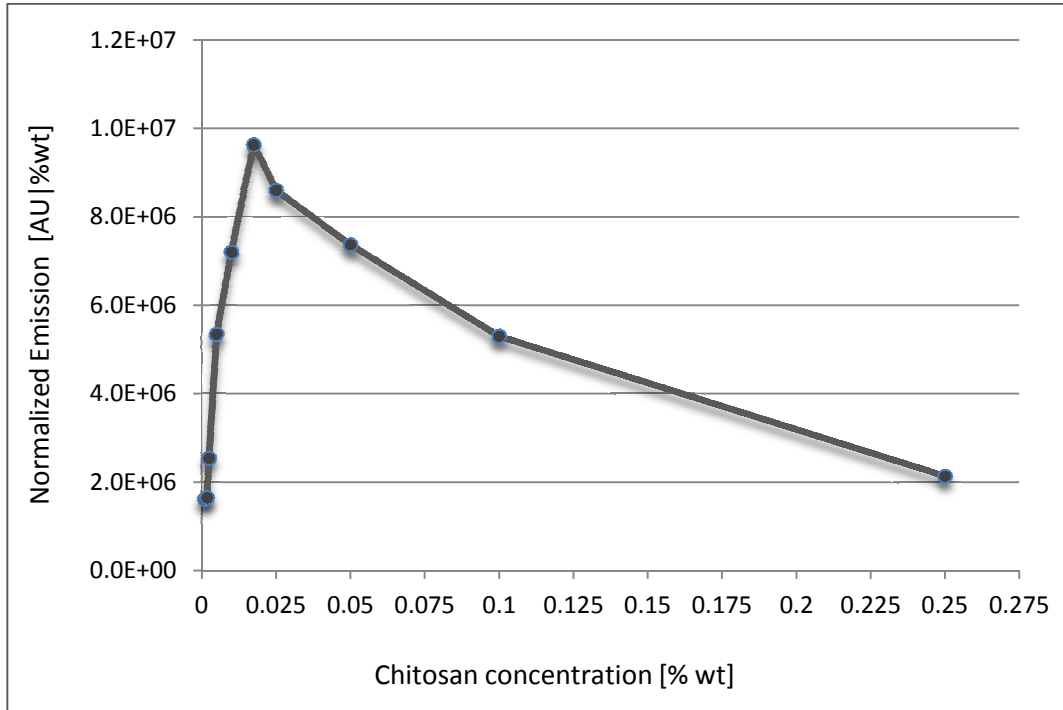
Figure 2.22. Emission analysis by spectrofluorimeter on secondary emulsions at FITC labeled chitosan concentrations ranging from 0.001 to 0.25 % wt, to identify saturation concentration.

69

An initial increase of the emission was observed up to a maximum followed by a decreasing curve. We explained the presence of the peak considering that after oil saturation, there is a significant increase of the polymer content in solution which determines the typical decresing curve of free polymer in solution. This maximum was therefore associated with the saturation of the oil surface, as confirmed by the successful further deposition attempts on secondary emulsions at around this chitosan concentration. Compared to the zeta potential method, which evaluates the saturation concentration by measuring the plateau of the zeta potential, the proposed method is much more sensitive, being able to identify very accurately the emission peak (see **Figure A.E.4** in the Appendix).

The comparison between these samples and free FITC labeled chitosan in solution at the same concentrations (**Figure 2.23**) (from 0.01 % wt to 0.1 % wt of chitosan) it is also evident that after the saturation peak the slope of the two curves is different until concentrations up to 0.1% wt. This was attributed to a complete coverage of the primary emulsions which would also explain the progressive improvement of the stability that was observed over months in the previous described experiments of stability on secondary emulsions.
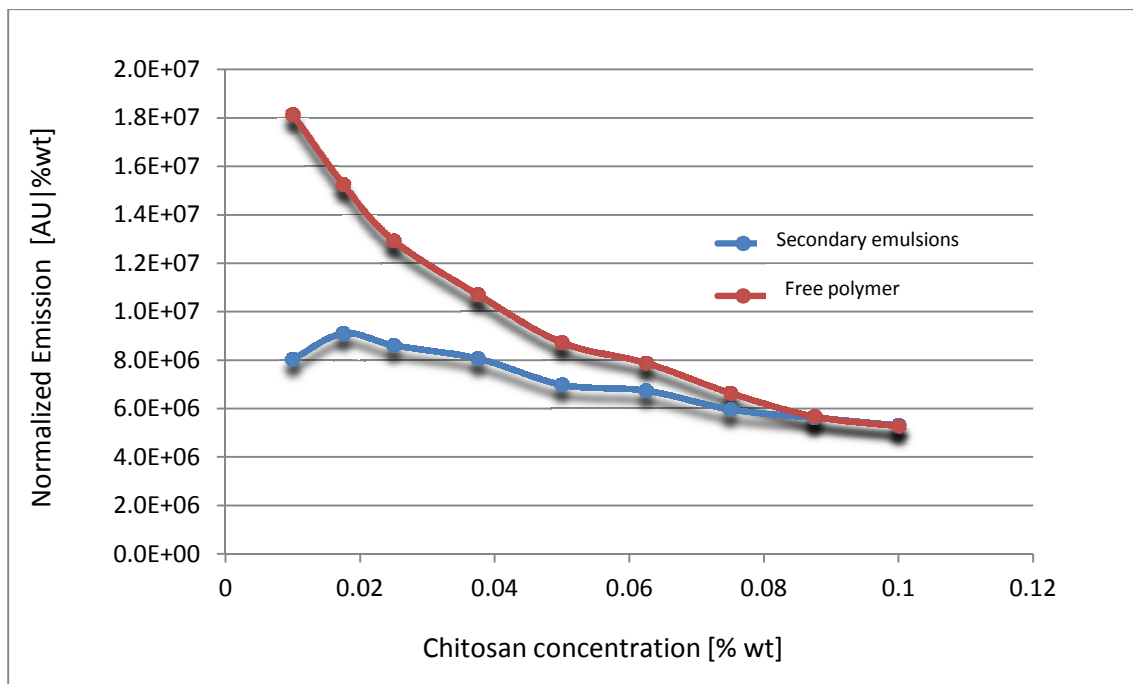
Figure 2.23. Emission comparison by spectrofluorimeter between secondary emulsions and free FITC labeled chitosan in the range between 0.01 and 0.1 % wt.

In the Appendix (**Table A.E.3**) the emission data at different concentration for FITC labeled chitosan alone and in the presence of nanoemulsion are reported.

The proposed method not only provides a very accurate way to identify saturation concentration, but it also shows that saturation is a relative concept. Indeed, after a main saturation, the real complete coverage happens only at much higher polymer concentrations maybe due to equilibrium between polymer on emulsion and polymer in solution. Moreover, even at very low polymer concentration there is such equilibrium as demonstrated by the increase of the normalized emission which can only be attributed to the increase of polymer in solution which is more fluorescent than polymer on emulsion.

2.3.2.5. Loading analysis

As anticipated in method section, to demonstrate loading capability, oil was pre-loaded with a lipophilic molecule like NR fluorophore. In **Figure 2.24** it is reported a confocal analysis of an L1 based secondary emulsion (0.1 % wt of chitosan) where oil was loaded with Nile Red and chitosan labeled with FITC.
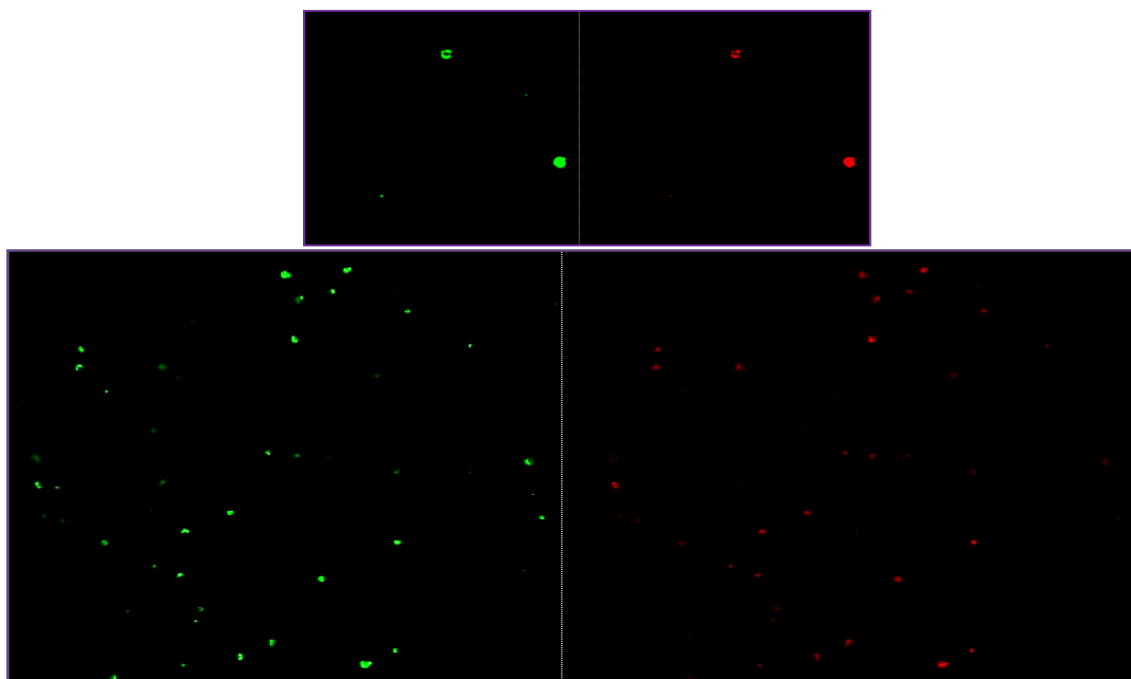
Figure 2.24. Sample with DABCO antifade to stabilize and visualize CT-FITC.

It is evident by the co-localization of the two colours oil loading capability and encapsulation capability of the chitosan. Moreover, the presence of NR clearly did not affect the monodispersion feature of the secondary emulsion.

In terms of lipophilic molecules loading it was also tried to embed a real drug molecule like QR into oil (400 µM). Also in this case emulsion preparation was not affected by the presence of the molecule as well as the coating with chitosan even though it was needed a minimum concentration of chitosan (0.0175 % wt) higher than usual (0.01 % wt). In the following **Table 2.5** DLS results are reported for primary and secondary emulsion.

	Size (nm)	PDI	Z-pot (mV)
Emulsion	207.3	0.073	-35
Monolayer 0.01 % wt	258.2	0.234	+ 21.7
Monolayer 0.0175 wt	212.8	0.092	+ 22.6

Table 2.5. DLS results on primary and secondary emulsion loading quercetin.

Chapter III: Natural polymer nanocapsules via Layer-by-Layer on oil core templates

3.1. Introduction on Nanocapsules

3.1.1. Methods for preparation of nanocapsules

As previously said, among different nanocarriers, nanocapsules present the advantage to really protect drug or biomolecules from degradation and they present the highest possible payloads (till 80 % or more) [**88**]. Of course payload depends on the kind of capsule and method used for production. Moreover, always due to the complete insulation of the inner phase, nanocapsules can mask unpleasant tastes. Finally, as in the case of the other NCs, due to the small size they can improve the biodistribution of active substances which is extremely advantageous especially in the case of lipophilic active substances.

Polymer nanocapsules can be produced starting from monomers or preformed polymers. In the first case (e.g., emulsion polymerization and interfacial polymerization), one limitation is in the consequence to work with synthetic polymers. Moreover, even washing the suspension after preparation, there is always the risk to have some contaminants like monomers residue or chemical initiators typically used. For these reasons the attention was just focused on the second case based on the use of preformed polymers.

Generally, the main methods used for the preparation of nanocapsules starting from preformed polymers are: nanoprecipitation, emulsion-diffusion, emulsion-coacervation, polymer-coating and LBL. It will be provided a brief description of these methods including some details on the procedures and technological advantages, as well as examples of polymers and encapsulants.

3.1.1.1. Nanoprecipitation method

The nanoprecipitation method also called solvent displacement or interfacial deposition is based on spontaneous emulsification formed when the organic phase, containing the dissolved polymer, is added under stirring to the aqueous external phase (**Figure 3.1**) [**89**]. However, spontaneous emulsification is not observed if the coalescence rate of the formed droplets is sufficiently high.
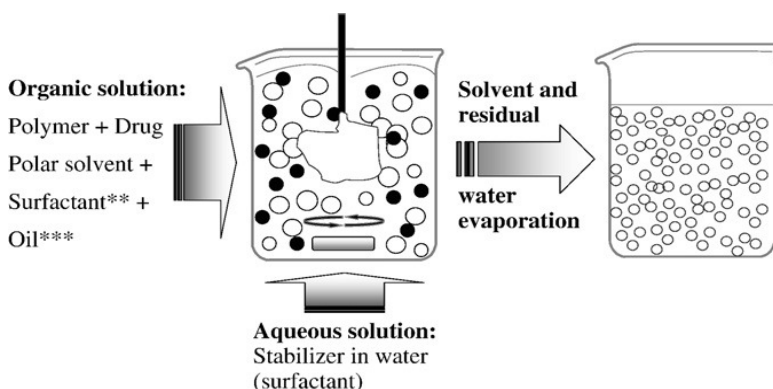
Figure 3.1. Schematic representation of the nanoprecipitation technique.

The inner organic phase contains polymer, active substance and optionally lipophilic tensioactive whereas the external water phase just contains a surfactant. If the organic phase includes an oil, which is immiscible with water, interfacial deposition is always guarantied due to the fact that even after diffusion of the solvent from the inner to the outer phase there is always an organic phase with a surface where polymer can deposit. On the contrary, in absence of oil, solvent diffusion could also bring to the formation of bulky polymer nanoparticles. It depends on the comparison between polymer precipitation and solvent diffusion. However, when capsules are obtained they are hollow whereas in the previous case they are filled with an oil core.

The polymers commonly used are biodegradable polyesters, especially PCL, PLA and PLGA. Considering the oil-based central cavities of the nanocapsules, high loading efficiencies are generally reported for lipophilic drugs when nanocapsules are prepared (up to 70 %) [**88**].

Up to now, this is one of the most used methods thanks to the simplicity of its procedure and low cost. However, some limitations regard the kind of polymers used which are synthetic and then, even though biodegradable they can produce possible side effects [**56**]. Moreover, the

simplicity of the method is translated in the simplicity of the final capsules and therefore low versatility in term of multifunctional behavior which on the contrary is more and more desired especially in drug delivery.

3.1.1.2. Emulsion diffusion method

This method also involves the diffusion of polymer solvent from an emulsion formed by emulsifying oil phase in water phase. In this case, polymer is dissolved in a partially water-soluble solvent whereas the external phase is water saturated with such solvent in order to ensure the initial thermodynamic equilibrium of both liquids. In fact, to produce the precipitation of the polymer and the consequent formation of nanocapsules, it is necessary to promote the diffusion of the solvent of the dispersed phase by dilution with an excess of water. The procedure is illustrated in **Figure 3.2** [**88**].
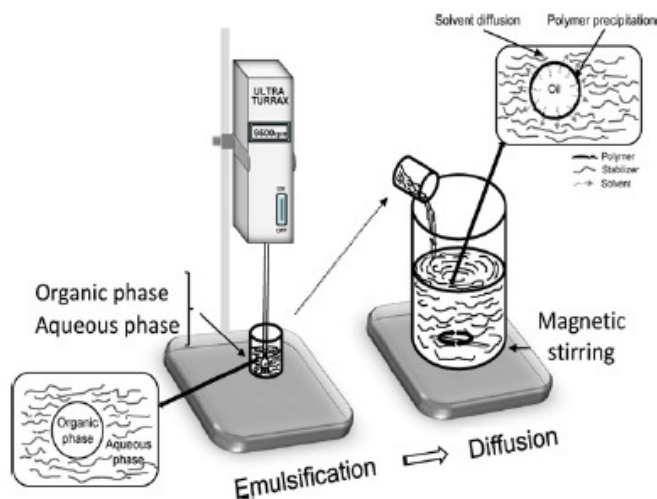
Figure 3.2. Schematic illustration of the Emulsion Diffusion technique.

Organic phase contains polymer, active substance, solvent partially soluble in water and oil. The polymers commonly used are biodegradable polyesters especially PCL, PLA, but also poly(hydroxybuttyrate-co-hydroxyvalerate) (PHBHV). Regarding the solvents, ethyl acetate is the first option even though propylene carbonate, benzyl alcohol and dichloromethane have also been used. Finally, regarding the external phase typically it is used water with poly(vinyl

alcohol) (PVA) or poloxamers or other stabilizing agents as surfactant. Solvent and a great quantity of water are eliminated by evaporation.

This technique presents several advantages, such as high encapsulation efficiencies in the case of lipophilic drugs (generally >70%), the use of pharmaceutically acceptable organic solvents, no need for homogenization, high batch-to-batch reproducibility, ease of scale-up, simplicity, and narrow size distribution [**89**]. Disadvantages are the high volumes of water to be eliminated from the suspension and the leakage of water-soluble drug into the saturated-aqueous external phase during emulsification, reducing encapsulation efficiency. However, preliminary results have been provided on the formation of nanocapsules made of PCL where water dilution effect was replaced by the use of high pressure treatment to induce the diffusion of organic solvents during the emulsion-diffusion procedure [**90**] which could economize the total processing time.

The same considerations regarding capsule materials and simplicity said in the case of nanoprecipitation are also true in this case.

3.1.1.3. Emulsion-Coacervation method

The emulsion-coacervation process is mainly presented as a strategy for the preparation of nanocapsules from naturally occurring polymeric materials. Up to now, sodium alginate and gelatin have been mostly used though synthetic polymeric materials can also be used. The procedure involves the o/w emulsification of an organic phase including oil and active substances with an aqueous phase dissolving polymer and stabilizing agent, by mechanical stirring or ultrasound. Then, coacervation process can be performed by using electrolytes, by adding a water miscible non-solvent or a dehydration agent or by varying temperature [**88**]. Finally, to obtain a rigid nanocapsule shell structure, polymer film can be stabilized by physical intermolecular or covalent cross-linking, which typically can be achieved by varying pH or temperature or by adding a cross-linking agent. The procedure is illustrated in **Figure 3.3**.
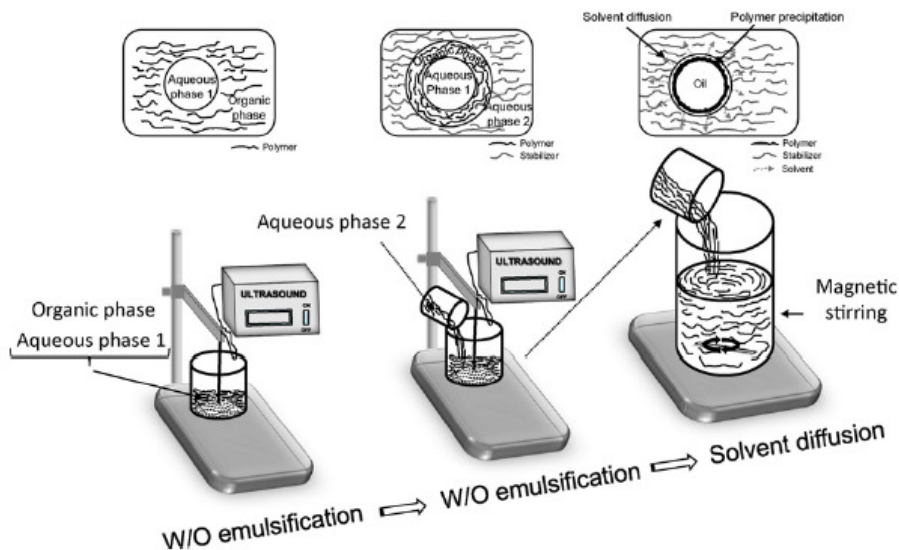
Figure 3.3. Schematic illustration of polymer capsules preparation by emulsion coacervation method.

In terms of loading efficiency it is generally much lower (below 50 %) than in the two previous methods. Moreover, due to the little literature available on this method and to the different methodologies used each time the method is considered premature for general criteria for materials and composition usable. In terms of materials there are also examples of natural polymers like chitosan deposited with this technique; however again the simplicity of the final product makes them low versatile in terms of multi-functionality.

3.1.1.4. Polymer coating

This method is similar to coacervation, though polymer solution is added after emulsification followed by polymer adsorption at the interface of the emulsion. Sometimes, such a process is defined as coacervation. As an example, this method was chosen to produce PLA capsules using thyme oil as the core material [91]. First, a thyme oil emulsion in water stabilized with Tween 20 (as surfactant) and a PLA solution in dimethylformamide (DMF) were prepared. Thereafter, the PLA solution was dropwise to the previously prepared o/w emulsion. Upon contact with water, the homogeneous solution of PLA in DMF promoted the precipitation of PLA around the thyme oil core. Capsules were hardened by adding octamethylcyclotetrasiloxane (OCMTS) that acts as a nonsolvent for the PLA, thus promoting capsules solidification. The complete flow process is represented in **Figure 3.4**.
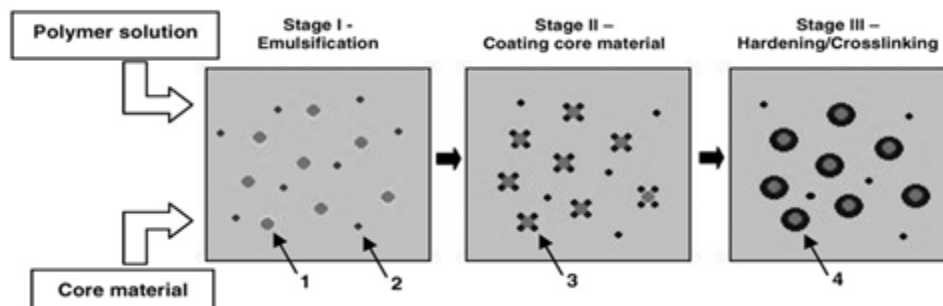
Figure 3.4. Schematic illustration of microcapsule preparation by polymer coating.

In terms of limitations the same consideration seen in the case of coacervation can be replaced here even though slightly higher loading capabilities have been registered (up to 60 %).

3.1.1.5. Layer-by-Layer method

Among various methods LBL technique - consisting in an alternate deposition of polyelectrolytes with opposite charge – is the only one capable to allow a fine control of the thickness at nanometric level (since any layer can be nanometric) and give a multifunctional behavior to the capsule. Indeed, with a multilayer system it is possible to embed magnetic (e.g., Fe_3O_4) or plasmonic nanoparticles (e.g., Au) which can be used both for imaging or to determine capsule rupture under external stimuli [2]. It is possible to embed biomolecules between layers which can be isulated each other. Polyelectrolytes can also bring biomolecules such as DNA, small-interfering RNA (si-RNA) and enzymes by conjugation with polymer chain. The outer layer can have some modifications for active targeting and or for long circulation capability. Due to their charge they can be pH responsive and release their cargo by physiological or external induced pH variation [92, 93]. Therefore, there is a huge interest in using LBL nanocapsules in the field of drug delivery [94].

3.1.1.5.1. Layer by Layer on solid templates

This method was first introduced to deposit polyelectrolyte multi-layers on flat substrates (**Figure 3.5**) [95].
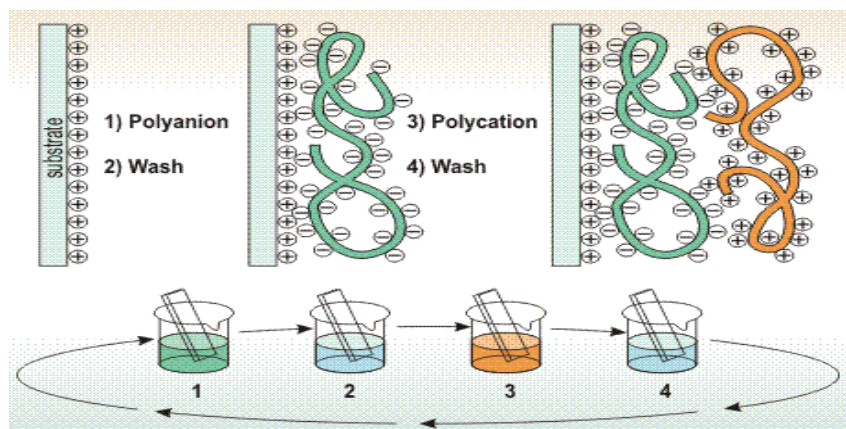
Figure 3.5. Scheme of the layer by layer on flat surfaces.

As represented in the scheme, LBL technique is based on the absorbtion of a certain number of alternate layers of polyelectrolytes of opposite sign (polymers presenting ionic moieties along the backbone chain) onto a charged surface. The assembly of the shell is simply led by Van der Waals and ionic interactions between functional oppositely charged groups. All the parameters affecting polyelectrolyte charge have an impact on the deposition conditions. However, an important parameter is the molecular weight of the polyelectrolytes which can determine a linear or an exponential growth [96].

For the realization of nanocapsules this method requires a colloidal template onto which polyelectrolytes of opposite charge are alternatively deposited [88].

They are typically fabricated using a solid template such as $CaCO_3$ [97, 98], silica [99] and mesoporous silica (MSN) nanoparticles, melamine formaldehyde (MF) [93] or polystyrene (PS) latex nanoparticles [100] upon which the LbL shell is constructed. The cores can be subsequentely dissolved by using the proper solvent like ethylenediaminetetraacetate (EDTA) in the case of $CaCO_3$, HCl solution for MF beads or HF/NH_4F for silica cores. In the **Figure 3.6** it is reported a schematic illustration of the LBL method applied on silica template.
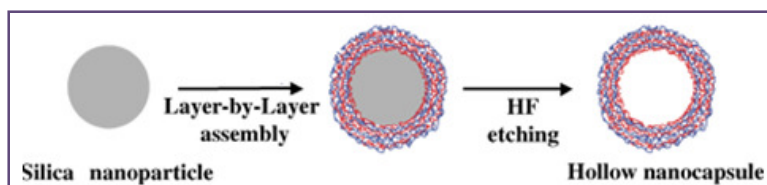
Figure 3.6. Production of hollow nanocapsules.

Generally, the drug is loaded by swelling holow capsule once varied the permeability of the multilayer shell through variations in pH, solvent polarity, ionic strength or temperature. In the case of the post-loading method, the necessity of removing the core can determine the damage of the constructed capsule or some residual core can remain in the shell toghether with the active molecule. For istance, in the case of MF capsule, it is demostrated that there is incomplete elimination of melamine formaldehyde oligomers (formed during dissolution) and that they have biological incompatibility [**101**].

Alternatively, in the case of biocompatible [**102, 97**] porous inorganic cores such as MSN or porous $CaCO_3$, the drug can be pre-loaded inside the porous templates by diffusion, followed by the LbL coating. However, adsorption is influenced by diffusion into pores and depends on molecular weight of drug. Therefore, loading can be difficult and the amount of drug loaded can be insufficient and variable depending on the system conditions.

The choice of the initial core significantly influences the properties of the capsules such as their size distribution and the strategy used for loading the active molecules inside the cavities. In that sense, the main advantage of using capsules built up on organic solid cores is that they are typically characterized by a good monodispersity, but the capsules synthesized are generally bigger than 200 nm [**88**] therefore bigger than the ones useful in drug delivery especially if extravasation is the mechanism exploited for delivery. LBL capsule sizes below 200nm can easily be prepared starting from a dispersion of drug crystals [**103**] or nanoparticles meant to be used for therapy by their own as in the case of gold nanoparticles [**104**].

3.1.1.5.2. Layer by Layer on liquid templates

However, a general strategy to obtain LBL nanocapsules with sizes lower than 200 nm and down to 100 nm and embedding single drug molecules, instead of crystals, is based on the use of a liquid template. In this method the core part of the capsule is made of emulsion droplets (O/W emulsion, generally stabilized with surfactants) and the shell is made with the same technique [**85, 86**] The difference is that the core is not removed and the drug can be previously loaded by simple mixing with the oil phase or any organic phase immiscible with water solutions and, thus the preparation is simpler and there is a major efficiency in drug loading. Moreover, the use of emulsion droplets as a liquid core gives the possibility to encapsulate high payloads of oil

soluble active molecules. Furthermore, template is not sacrificial therefore there is no need for the use of robust synthetic polymers to afford template removal conditions. Natural polymers like chitosan, sodium alginate, heparine, ialuronic acids, and so on can be easily used in this case.

Actually, there is no much literature on the use of oil template for layer by layer due to the polydispersity and following instability of such templates [105]. However, their development could really opens new possibilities for applications in many fields such as the cosmetic, medicine, pharmacy and food industries [106-109]. For example, capsules with liquid cores can be used in drug delivery systems or as microreactors [110-115]. Liquid core can be chosen depending on the type of drug dissolved. Also the choice of surfactant is fundamental, especially for stability and further deposition of LbL shell; finally the choice of polymer composing the shell is important depending on the administration route and the target environment.

Considering the above considerations, the main topic of this PhD work was the study of LbL nanocapsules on a liquid core.

3.1.2. Multi-layer cross-linkage

Biodegradable nanocapsules should be resistant to physiological environment like blood in order to survive until reaching target site. In the case of multilayer polymer shell single polymer layers are kept together by electrostatic or hydrogen bonds. In literature we can find several examples of cross-linking [116, 117] where cross-linking is achieved exploiting the reactivity of suitable functional groups inserted on the nanocapsules during their build-up or a as a post-functionalization process. For example, amide formation with carbodiimide coupling between chitosan amine and alginate carboxylates could be realized. In this procedure one of the problems is the possible destabilization due to the addition of reactant to the nanocapsule suspension. Furthermore additives such as catalysts, coupling agents or functionalizing molecules can permeate the layers and contaminate the nanocarriers, bringing problems for eventual subsequent applications. So it would be ideal to previously functionalize the polycation and polyanion that are forming LbL nanocapsule shell, carefully purifying them from side products or unreacted molecules and then use them. Furthermore it would be advisable to create a method of cross-linking not too invasive, such as for example photo-cross-linking reaction

even better if with no photo-initiator needed. For instance thiol-ene based chemistry was proposed as advantageous method for the stabilization and functionalization of polymer capsules [118]. This process is photo-initiated, the reaction can be performed at room temperature in the presence of oxygen, and the process is environmentally benign. Importantly, this process does not require any potentially toxic metal catalyst. Furthermore, the vast array of commercially available molecules and biomolecules with either thiol- or ene-functionality makes this a powerful technique to introduce functionality.

Herein, we also decided to exploit a photo-click chemistry reaction based on thio-ene reaction between polymer layers. However, compared to literature this reaction has been applied to completely biodegradable polymers such as chitosan as polycation and sodium alginate or heparin as polyanion. A scheme of this reaction is reported in the following **Figure 3.7**.

$$R_1 \diagup SH \; + \; \diagdown R_2 \quad \xrightarrow[\text{(254 or 365 nm)}]{h\nu} \quad R_1 \diagup S \diagdown \diagup R_2$$
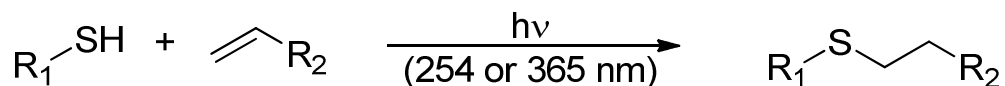
Figure 3.7. Scheme odium alginate chemical structure.

Actually due to the advantage to work on deformable template, we also claim cross-linkage could pave the way for the consolidation of certain shape different from sphere. In other words while deforming in flow such oil core based nanocapsules polymer multi-layer could be cross-linked to consolidate such elongated or in general deformed shape. Reaction should be activated from the outside and this could be done by photo-activation. Indeed it was shown that spherical NPs tend to stay in the center of the capillary blood flow, thus adversely impacting their extavasation trough the fenestrations that are associated with the tumor neovasculature as well as limiting their ability to recognize specific molecular markers on the tumor-associated endothelium. On the contrary, non-spherical shapes facilitate the carrier in its way towards the vessel walls with the advantage to promote extravasation and avoid phagocytic cells [119; 33]. Moreover, there are some studies showing capability of elongated shapes to better elude RES system and enhance the circulation time without any specific surface treatment like PEG-ylation [35].

The general idea was to functionalize chitosan with a thiol group (N-acetylcysteine), firstly varying the type of chitosan (low molecular weight chitosan, depolymerised chitosan or glycol chitosan) in order to improve the degree of functionalization, and then using sulphur rich

chitosan to link covalently with biopolymers like sodium alginate or heparin modified with allylamine (**Figure 3.8**).
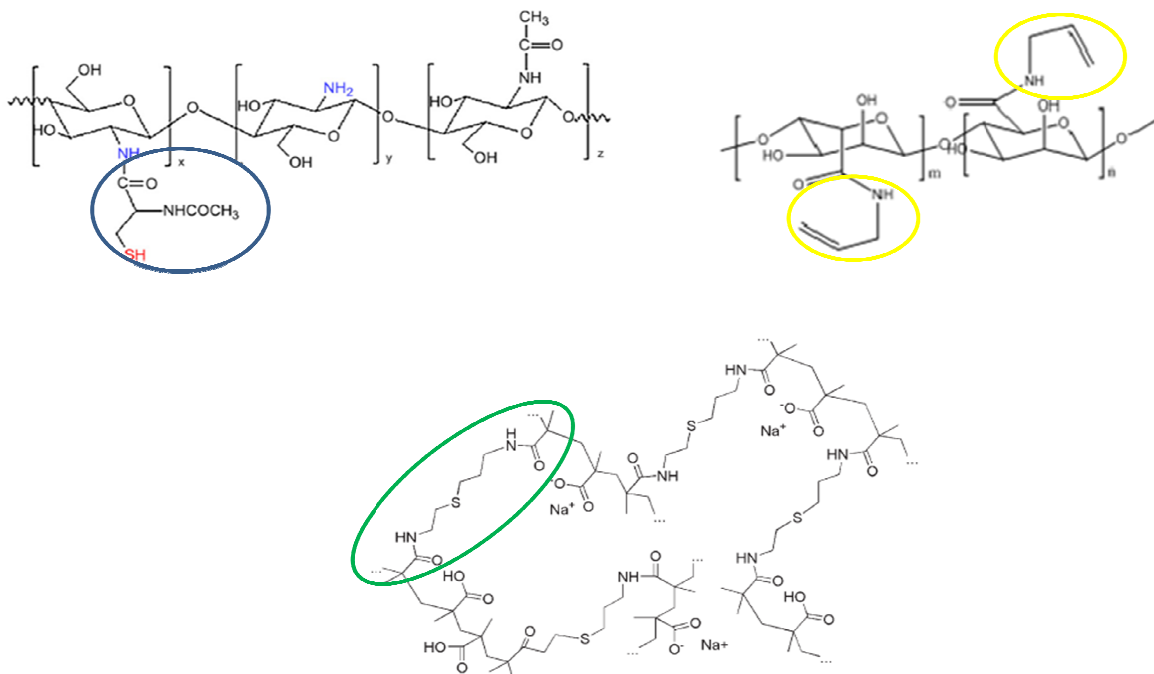
Figure 3.8. Scheme of reaction between thiolated chitosan and allylamine-sodium alginate.

Sulfur-rich chitosan are already known to be useful for several bio-applications by their own. For instance, thiolated chitosans were successfully used as mucoadhesive drug delivery system, as they are able to form covalent bond with mucus glycoproteine [120]. Moreover, thiolated chitosan were used for the formation of disulfide bridges linking chitosan polymer layers of a biodegradable nanocapsule to be used in the field of drug delivery [121].

3.2. Materials and Methods

3.2.1. Materials

For the built up of layer by layer nanocapsules on oil core, chitosan as polycation and sodium alginate and heparine as polyanions were employed. Chitosan LMW is the one used in the previous chapter. Sodium alginate from brown algae (low viscosity, 100-300 cP in 2% solution

at 25°C) and heparin (Heparin sodium salt from porcine intestinal mucosa, 17-19 KDa) were purchased from Sigma Aldrich. Polyelectrolytes were functionalized in order to obtain crosslinkable materials for achieving more rigid and resistant nanocapsules. All the reactions were amide formation reaction catalyzed by a water soluble carbodiimide. Reagents like N-Acetyl-L-cysteine, (NAC, m.w.=163.19 g/mol), 5,5′-Dithiobis(2-nitrobenzoic acid) (DTNB) (Ellman reagent) (m.w.=396.35 g/mol), allylamine (m.w.= 57.09 g/mol; d= 0.761 g/mL at 25 C), 1-hydroxybenzotriazole hydrate (HOBt, m.w.= 135.12 g/mol) were purchased from Sigma Aldrich, wherease N-(3-Dimethylaminopropyl)-N′-ethylcarbodiimide hydrochloride (EDAC·or the same EDC, m.w. =191,70 g/mol) was purchased from Thermo scientific. All reagents were used without further purification except chitosan used for LbL that needed to be purified as described above. Glycol chitosan, purchased from Wako Chemicals, was also tested to improve the degree of modification of chitosan. To evaluate multilayer cross-linkage, modified polymers were deposited on carboxyl latex (4% w/v 0.1 µm) purchased from Invitrogen. Photo-reaction was tried with no photoinitiator but also for comparison in presence of a photoinitiator like Irgacure 2959 purchased by Ciba Specialty Chemicals. Dialysis Membranes were purchased from Spectrum Laboratories Inc. Finally, to purify secondary emulsions from the excess of polymer and make possible further deposition of polymer layers, magnetic carboxilate nanobeads, purchased from TurboBeads, were used.

Sodium alginate is a natural polymer, extracted from marine brown algae and consists of linear chains of α-L-guluronic acid and β-D-mannuronic acid residues joined by 1,4-glycosidic linkages (**Figure 3.9**).
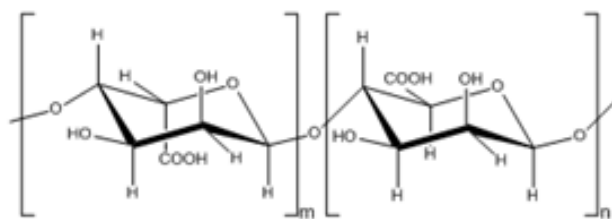
Figure 3.9. Sodium alginate chemical structure.

It can be cross-linked using calcium chloride, with formation of insoluble calcium alginate particles on a nanometer scale depending on the concentrations of sodium alginate and calcium chloride. Low stability and loss of encapsulated materials have been observed with capsules formed by an alginate polymer, but these problems can be overcome by using cationic polymers such as chitosan covering the alginate layer [**122**].

Heparine is a natural polysaccharide being major component of extracellular matrix (ECM), is a negatively charged linear glycosaminoglycan (GAG) consisting of repeated sulfated disaccharide [**123**]. It is also known to have diverse biological functions such as anti-coagulation, anti-inflammation, anti-angiogenesis, and anti-tumor cell proliferation. For metastatic cancer cells, heparanase and heparinase, which degrade heparine, are overexpressed in the ECM. Its chemical structure is reported in **Figure 3.10**.
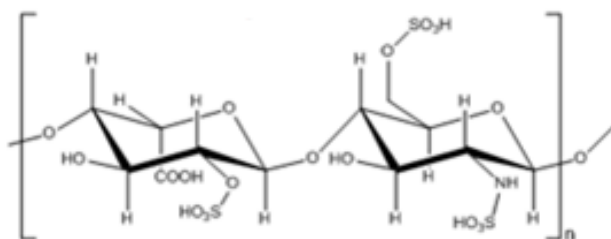
Figure 3.10. Heparine chemical structure.

Being negative charged it can be used as polyanion in the build up of layer by layer polymer films as demonstrated in the case of a flat substrate [**124**].

Magnetic carboxylated nanobeads are highly magnetic nanoparticles with diameters of below 50 nm. The surface of the particles is covalently functionalized with carboxyl groups (> 0.1 mmol/g) and can be used for further functionalization and for the recovery of chemical and biological compounds from complex mixtures. The stock magnetic nanobeads concentration used to perform tests was 3%.

Glycol chitosan is a derivative of chitosan. While chitosan has demonstrated biocompatibility, its usage is limited by its poor water solubility. glycol chitosan, chitosan

conjugated with ethylene glycol, is water soluble at the entire pH ranges and, at the same time, it retains its positive charge at physiological pH values [125, 126] (Figure 3.11).
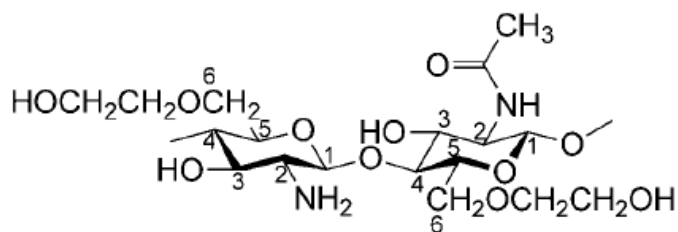
Figure 3.11. Chemical structure of glycol chitosan.

Due to its positive charge it was already used in the layer by layer alternated with bovine serum albumin (BSA) to be applied for protein delivery [127].

3.2.2. Methods

3.2.2.1. Chitosan depolymerization and molecular weight determination

During this work there was a need to reduce the molecular weight of chitosan both to improve deposition capability in the LBL (from the third layer on) and try to improve solubility thus degree of modification with NAC. The method chosen for chitosan de-polymerization was based on NO_2 de-polymerization reaction, which is fast and can be conducted in mild conditions. Furthermore, with this method it is possible to easily control the degree of de-polymerization of the polymer by choosing the appropriate D-glucosamine/$NaNO_2$ molar ratio and temperature at which reaction is conducted. By controlling the degree of de-polymerization it is possible to obtain a wide range of chitosans with different molecular weights (Figure 3.12) [128, 129].
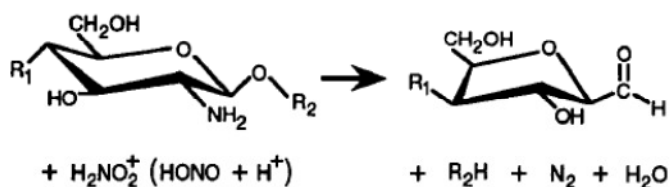
Figure 3.12. Scheme or chitosan de-polymerization reaction by means of HNO2 FITC calibration line for determination of chitosan-FITC degree of functionalizaton.

500 mg of chitosan LMW were dissolved gradually in 25 mL of HCl 1 M at room temperature. Dissolution was brought to completion by adding slowly the samples to solution under stirring. All chitosan solutions were heated at 50°C and this temperature was kept stable during all the reaction time. Different amounts of $NaNO_2$ were added in order to obtain chitosan with different molecular weights. After 45 minutes the solution was cooled at room temperature and a mixture of $MeOH/NH_3$ (7:3) was added gradually until basic pH (pH=10) was reached to allow the precipitation of de-polymerized polymers. The solution was then filtrated with a Buchner funnel and washed with MilliQ water until reaching neutrality. Chitosan was recovered and freeze-dried for 48 h. In particular, 4 different D-glucosamine/$NaNO_2$ molar ratios were tried:

- 1,725 mg of $NaNO_2$ molar ratio CT/$NaNO_2$ 0.0031118/2,500x10^{-5}
- 4,3 mg di $NaNO_2$ molar ratio CT/$NaNO_2$ 0.0031118/6,2319x10^{-5}
- 9,7 mg di $NaNO_2$ molar ratio CT/$NaNO_2$ 0.0031118/1,4058x10^{-4}
- 17,25 mg di $NaNO_2$ molar ratio CT/$NaNO_2$ 0.0031118/2,5x10^{-4}

The molecular weight of each sample was measured by viscosimetry, according to literature [130]. Specific viscosities of chitosan LMW and de-polymerized chitosan in 2% HAc/0.2M NaAc were measured using an Ubbelohde capillary viscometer at a controlled temperature (25 ± 0.01 °C) in a water bath. From these measurements it was calculated the molecular weight of five different samples by using the Mark-Houwink equation. The details are reported in the Appendix (**A.E.7**) (see also **Figure A.E.5**) as well as the results of the different molecular weights corresponding to the different concentrations of $NaNO_2$ (**Table A.E.4**).

3.2.2.2. Layer by Layer on saturated secondary NEs

For the layer by layer, both sodium alginate and heparin were used as polyanions with heparin behaving better in terms of deposition. For the first layer, we started from secondary emulsions with an oil concentration of 1% wt and a chitosan concentration of 0.01% wt (L1 and L4 were chosen as template). These secondary emulsions were re-dispersed at least once through the high-pressure homogenizer for 100 continuous steps at a pressure of 700 bar before further deposition according to the process described in Chapter II.

Case of sodium alginate as polyanion: For second layer deposition, secondary emulsion was diluted 1:2 with a solution of alginate dissolved in MilliQ water. In particular, secondary emulsion was added to the polyelectrolyte solution under stirring for 15 minutes. The same procedure was adopted for third layer deposition where the previous bi-layer suspension was diluted 1:2 with a solution of chitosan dissolved in a solution of chitosan dissolved in MilliQ water at pH 4. Both bi-layers and three-layers oil core based nanocapsules were passed, after one day from deposition, in the Microfluidizer for 100 steps at 850 bars. All the LbL nanocapsules were stored at room temperature.

Case of heparin as polyanion: The second layer was deposited after one day, by preparing a solution of heparin in Milli-Q water and using this solution to dilute the secondary emulsion 1:2. The tri-layer was prepared by depositing, after one day, chitosan dissolved in an acetic acid Milli-Q water solution (pH 4, 20 mM) and using this solution to dilute the dispersion again 1:2. This time bi-layer did not need any passage through the high pressure homogenizer. For the tri-layer in order to keep monodispersion with no re-dispersion processes, it was used a chitosan with a lower molecular weight, chitosan-B (17 kDa), obtained by using the previous described de-polymerization process. Then, it was also demonstrated the capability to produce multi-layer up to five layers by alternating chitosan-B and heparine with the same dilution and using again Milli-Q water for heparine and acetic acid Milli-Q water solution for chitosan (pH 4, 20 mM).

3.2.2.3. Layer by Layer on ultra-stable secondary NEs

As seen in the previous chapter, it was possible to produce ultra-stable secondary emulsions by implementing an optimized re-dispersion process in combination with high concentrations of polymer. In these conditions, due to the excess of polymer in solution further deposition of polymers by means of the layer by layer method is prevented. However we developed a method to purify and deposit on ultra-stable emulsions.

Secondary emulsions purification: To purify emulsions from the excess of chitosan LMW a new fishing-based method was established. It consists in the use of 30 nm magnetic and carboxylated beads. Particularly, starting from a stock dispersion at 3 % w/v of beads in water

solution it was diluted at different concentrations and mixed in the same amount of volume with the secondary emulsion (chitosan ratio with oil 0.1:1) with a stirrer for 30 min at 1500 r.p.m. to allow the chitosan polymer in solution to cover the magnetic nano-beads. The mixture was then moved in an eppendorf and kept in a magnetic rack overnight in order to separate magnetic nano-beads covered with chitosan from the secondary emulsion. At the end, to check the absence of magnetic nano-beads in the secondary emulsion a centrifugation step was performed. The secondary emulsion was centrifuged for 30 min at 13000 r.p.m., at a temperature of 25°C and no magnetic nano-beads were noticed. Moreover, the right amount of nano-beads was also evaluated by carrying out a DLS analysis on the purified chitosan, by monitoring capability of bi-layer deposition, as well as by energy dispersive x-ray (EDX) spectroscopy analysis of lyophilized samples to check the chemical composition of the system.

Multilayer deposition: A second layer of Heparine was deposited on the secondary emulsion, and again chitosan was finally deposited as third layer. For the first layer we started from an oil concentration of 1% wt (L1 and L4 were chosen as template) and an excess of chitosan concentration of 0.1% wt. After double processing and purification, heparin was deposited at different concentrations to first verify capability to deposit, which was instead prevented with no purification and then to identify right concentration. After few hours a tri-layer was prepared by depositing reduced molecular weight chitosan (chitosan-B) at different concentrations to verify again deposition capability. Then, preliminary penta-layers were also obtained by alternating chitosan-B and heparine with the same dilution (1:1) and using again Milli-Q water for heparine and acetic acid Milli-Q water solution for chitosan (pH 4, 20 mM).

3.2.2.4. Chitosan modification with N-Acetylcysteine

Low molecular weight, depolymerized and glycol chitosan were used for modification with N-Acetylcysteine. Their de-acetylation degrees determined with nuclear magnetic resonance (NMR) experiments were 84%, 84.5, 87.5 % respectively. For modification reaction 0.5 mM of chitosan was dissolved in 10 mL of MilliQ water. Variable amounts of HOBt (**Table 3.6**) were added and pH was adjusted to a value of 4 with HCl 1 M to allow complete dissolution in the case of low molecular weight and chitosan-B. Then, different amounts of NAC and EDC (**Table**

3.6) were added to the solution. The pH was adjusted and maintained to a value of 5 for all the reaction (3h, RT). Samples were dialyzed (dialysis tubing of 12-14 kDa c.o.; 4 cycles of 1% NaCl at pH 3 solution and 4 cycles without NaCl with a HCl pH 3 solution; 3 h each dialysis cycle) and freeze-dried for 48 h.

EDC is a common coupling agent used to form an active ester with cysteine. Indeed, the byproduct of the reaction between this ester and the amine group of the chitosan is the urea which is a good leaving group. However, the ester group could react with water forming acilurea subtracting NAC to the reaction therefore HOBt is used to form a less reactive ester which react with the amine group of chitosan with higher probability.

Ellman test for free thiols groups. 2 mg of each chitosan-NAC sample were weighted and dissolved in 0.5 ml of acetic acid solution at pH 3. After partial or complete dissolution with sonication, 3.5 ml of a solution of DTNB in a buffer phosphate solution at pH 8.03 (0,2 mg/ml) were added and the reaction was allowed to proceed in the dark at room temperature for 2 h under magnetic stirring. The final pH was 7.4. Absorbance values of TNB^{2-} were registered at 412 nm. The TNB^{2-} and so the sulfhydryls groups concentration were determined by means of a calibration line constructed in the same conditions by allowing the reaction between standard amounts of free N-acetyl-L-cysteine with DTNB. ε of TNB^{-} was $12{,}7 \cdot 10^{4}$.

3.2.2.5. Sodium alginate and heparine modification with Allilammine

Heparin (100 mg, 0.150 mmol of –COOH groups) or sodium alginate (100 mg, 0.505 mmol) was dissolved in 10 ml of MilliQ water. After complete dissolution Allylamine (112.5 µl, 1.5 mmol) was added to the solution and pH adjusted to a value of 6.8. Then, HOBt (81.22 mg, 0.6 mmol) and EDC (115.2 mg, 0.6 mmol) were added. The pH was adjusted again to 6.8 and maintained to this value for all reaction time (6h, RT). Samples were finally dialyzed (with dialysis tubing of 6-8 kDa c.o.; 4 cycles of 1% NaCl and 4 other cycles with MilliQ water) and freeze-dried for 48 h. Preliminary tests of sodium alginate functionalization with allylamine were conducted to optimize the procedure and they are reported in the Appendix (**Table A.E.5**).

3.2.2.6. NMR spectroscopy

Modified chitosans and alginates structures were investigated by NMR technique using a Bruker 600 MHz NMR spectrometer. The experiments were run at 25°C; D_2O with 1% TFA was used as solvent for thiolated and unmodified chistosans while modified and unmodified alginate samples were dissolved in D_2O.

3.2.2.7. Cross-linkage tests on modified multi-layer

Click chemistry reaction was first demonstrated on modified chitosan in contact with allylamine and finally between modified polymers.

In the first case 8 mg of thiolated glycol chitosan were dissolved in 2 ml of acetic acid 0.1 M, pH 4, in a flask or in a beaker. Then 2.5 µl of allylamine and in some cases 3.6 mg of photoinitiator were added. Finally half sample was irradiated under stirring with UV light at 365 nm or 254 nm using a UV Hand Lamp (Spectroline® E-Series UV lamp, output 6 W) fixed at a distance of 3 cm or a High Intensity Lamp (Blak-Ray® UV, Ultraviolet Lamp with Spot Bulb, output 100 W) fixed at a distance of 10 cm equipped with a water bath to avoid overheating. Some tests were conducted under nitrogen. After 2 hours of irradiation the reduction of thiol group amount, respect to the not irradiated sample, was determined using the Ellman's test on both samples and making the subtraction.

In the second case, to easily see and quantify the reaction effectiveness, modified polymers were deposited on PS NPs with sizes similar to that of the emulsions (100 nm) but more easily manageable. First, 10 ml of a water dispersion of PS NPs (0.5 % w/v) were added, under vigorous stirring, to 40 ml of a solution of glycol chitosan (0.032 % w/v) in acetic acid (20 mM). After 15 minutes the stirring was stopped and the solution processed through a high pressure homogenizer (Microfluidics M110PS) at mild conditions (600 bar, 100 steps, 4°C) to improve PDI value. Then, 25 ml of a water solution of heparin (0.05% w/v) under vigorous stirring were added to 25 ml of monolayer solution (0.1% PS microspheres; 0.0256% glycol chitosan). After 15 minutes the stirring was stopped and the product measured by DLS in the usual conditions. To evaluate photo-reaction between layers, the solutions were concentrated to 2 mL by centrifuge (13000 rpm, 10 minutes, 4 °C), re-dispersed in water and sonicated (10 minutes, 40 MHz, 50 % of power, 4 °C). 1 mL of solution was irradiated with UV light for 2 h, while 1 mL

was stored at room temperature for 2 h, in presence of natural light and atmospheric oxygen. Then 0.5 mL of each sample was added to a solution containing Ellman's reagent, according to Ellman's test shown above. After 2 h, each sample was centrifuged (13000 rpm, 15 min) and supernatant was collected for UV measurement.

3.3. Results and Discussion

3.3.1. Layer by Layer on saturated secondary NEs

On secondary emulsions with no significant excess of polymer it was demonstrated the capability to grow a polymer multilayer by keeping monodispersion feature. In particular, it was used the LBL method by exploiting the positive feature of the secondary emulsions. As polyanion alternating to the chitosan they were used both sodium alginate and heparin as said. In particular we observed a much more control in the deposition of the heparin. Indeed, with sodium alginate it was needed a re-dispersion process to re-gain monodispersion while with heparin, once found the right concentration such a process was not needed. For the first layer, we started from secondary emulsions with an oil concentration of 1% wt and a chitosan concentration of 0.01% wt. This chitosan concentration was chosen for several reasons. First at 0.01 % wt Z-potential was switched and almost completely saturated meaning a high coverage level to further deposit the polyanion. Moreover, in terms of spectrofluorimeter analysis this concentration was approaching the emission peak (at 0.175 % wt) which we associated to the saturation concentration. Finally, testing concentrations above 0.01% as starting point for further depositions usually there was a worse PDI or even a second peak for higher and higher concentration meaning aggregation due to a significant excess of chitosan in solution.

3.3.1.1. Case of sodium alginate as polyanion

As described in materials and methods section for second layer deposition, after the dilution 1:2 of the secondary emulsion with the solution of alginate dissolved in MilliQ water, it was needed to pass the bilayer in the Microfluidizer for 100 steps at 850 bars. The same happened after the deposition of the chitosan as third layer. In terms of polymer concentrations we started from a

secondary emulsion at a concentration of chitosan of 0.01 % wt. This monolayer was mixed with a solution of sodium alginate with the same concentration 0.01 % wt identified as good concentration. Indeed, previous attempts of using different chitosan/sodium alginate ratios (1/3; 1/2; 1/5; 5/1 3/1) brought to quick destabilization. Finally, the bilayer system with a final concentration of sodium alginate of 0.005 % wt was mixed with a chitosan solution at a concentration of 0.005 % wt and this allowed complete switching of Z-potential. In **Figure 3.13** it is reported the DLS of a final tri-layer obtained as described.
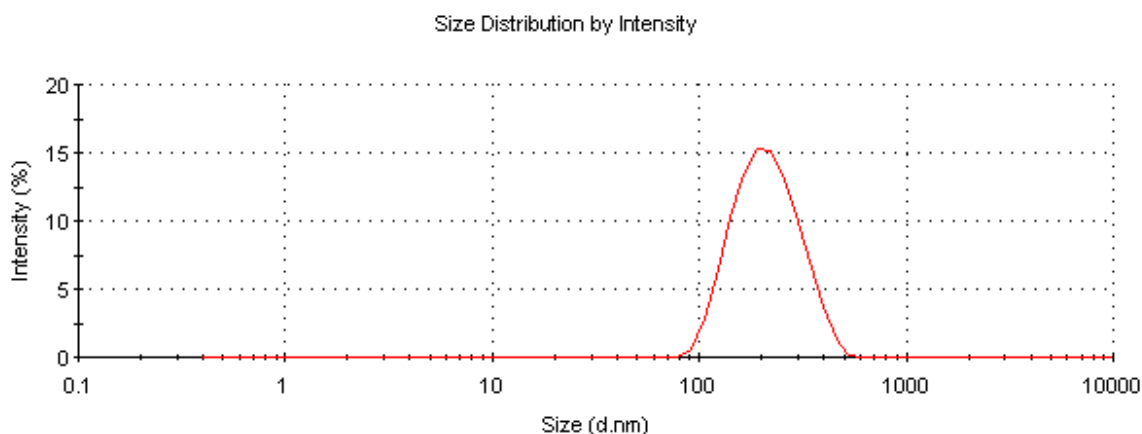
Figure 3.13. DLS of the final tri-layer with chitosan (monolayer) sodium alginate (bilayer) and chitosan (trilayer).

The final trilayer was monodisperse (size 196.5 nm and PDI 0.106) and with a positive Z-potential positive, as expected, and equal to 50 mV. Due to the labeling of the third layer with FITC it was also possible to perform a STED analysis as reported in the **Figure 3.14**.
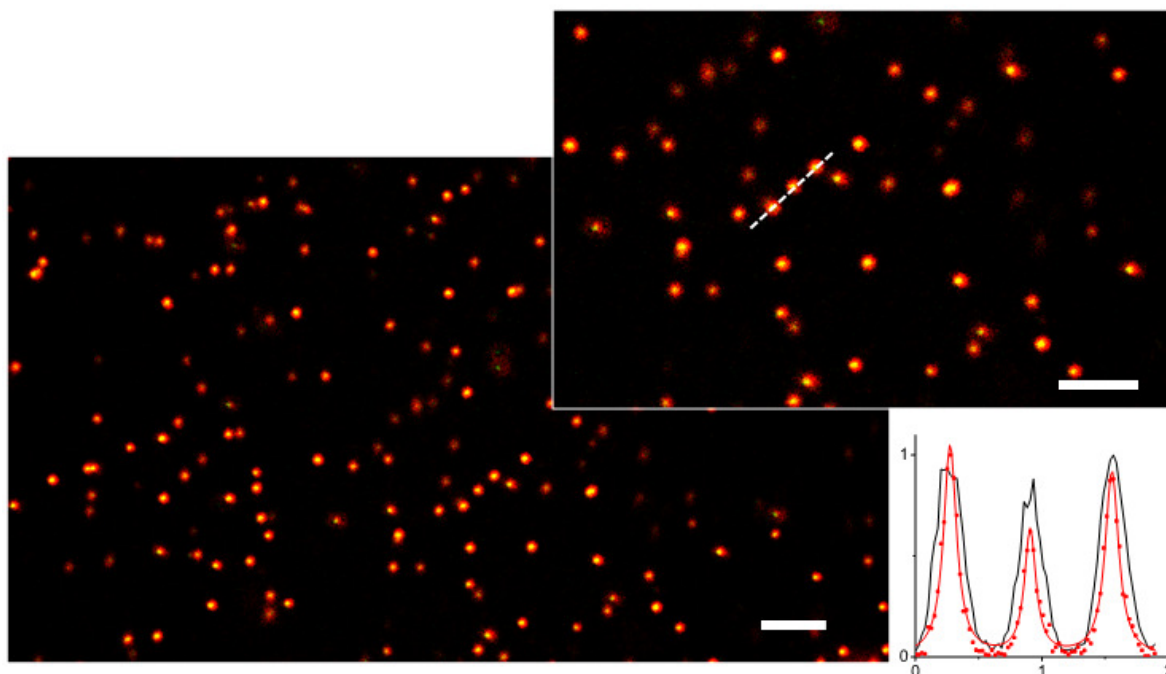
Figure 3.14. STED image of final tri-layer with chitosan (monolayer) sodium alginate (bilayer) and chitosan-FITC(trilayer). Scale bar is 2 µm.

Even after few days the trilayer kept is monodispersion feature and the size was around 180nm therefore in agreement with DLS.

3.3.1.2. Case of heparin as polyanion

To optimize the deposition of the second layer different heparin concentrations were tried. Starting from L1 based secondary emulsion template and from a heparin stock solution 0.27 % wt in Milli-Q water, different dilutions were tried as schematized in the **Table 3.1**. In particular, after mixing heparin and secondary emulsion (as said 1:1), the bi-layer with lower heparin concentration (Bi 5) demixed very soon. Instead the other samples were all stable over time, with PDI below 0.1 and with stabilities increasing with the concentration of heparin. Therefore it was chosen Bi 4 in order to have the minimum amount of free heparin in solution and considering that it was anyway stable over few days thanks to the almost complete switching of the Z-potential.

Heparin code	Heparin % wt	Heparin % wt	Chitosan % wt	Z-pot bilayer (mV)	Size bilayer (nm)	PDI bilayer
	before mixing	*After mixing*				
Bi 0	0.27 (No dil)	0.0135		- 39.2± 6.54	196.9	0.041
Bi 1	0.135 (dil. 1:2)	0.0675		-31.7± 6.99	200	0.04
Bi 2	0.09 (dil. 1:3)	0.045	0.005	-33±7.01	193.7	0.06
Bi 3	0.054 (dil. 1:5)	0.027		-27.4± 6.01	211.4	0.092
Bi 4	0.027 (dil. 1:10)	0.00135		-28.9±5.96	200	0.077
Bi 5	0.02(dil. 1:27)	0.01		Aggregates		

Table 3.1. Summary of the heparine concentrations tried on L1 based secondary emulsions at 0.01 % wt of chitosan. Results are referred to samples just after mixing. Starting template was 180nm (around 20nm more than usual being few months old).

To optimize tri-layer preparation on Bi 4 as bilayer, the same procedure was used to find the best chitosan concentration as tri-layer. In particular, it was used a stock solution of chitosan 0.27 % wt in acetic acid Milli-Q water (pH 4, 20 mM) and it was diluted at different concentrations by using the same solution (pH 4, 20 mM) as shown in the **Table 3.2**. In this table DLS results related to the different tri-layers built up with chitosan LMW and chitosan-B are also reported.

Heparin code	Chitosan % wt	Chitosan % wt	Heparin % wt	Chitosan LMW	Chitosan-B
	before mixing	*After mixing*			
Tri 0	0.27 (No dil)	0.0135		Size=298.6 nm	Size=218.4
				PDI=0.204	PDI=0.080
				Z-pot=68.2±5.2 mV	Z-Pot=52.3±6.03 mV
Tri 1	0.135 (dil. 1:2)	0.0675		Size=216.5 nm	Size=214.5 nm
				PDI=0.115	PDI=0.059
				Z-Pot=49.8±7.11 mV	Z-Pot=45.1 mV±6.23
Tri 2	0.09 (dil. 1:3)	0.045	0.00675 (= B4)	Size=244.5 nm	Size=216.3 nm
				PDI=0.151	PDI=0.063
				Z-Pot=57.1±6.30 mV	Z-Pot=46.03±6.07 mV
Tri 3	0.054 (dil. 1:5)	0.027		Size=212.4 nm	Size=206.3 nm
				PDI=0.064	PDI=0.058
				Z-Pot=46.9±7.33 mV	Z-Pot=44.5±5.92 mV
Tri 4	0.027 (dil. 1:10)	0.00135		Aggregates	Size=218.1 nm
					PDI=0.070
					Z-Pot=42.5 ±5.73 mV
Tri 5	0.02(dil. 1:27)	0.01		Aggregates	

Table 3.2. DLS results for tri-layer deposition both in the case of chitosan and chitosan-B.

From the comparison between chitosan LMW and chitosan-B it is evident how the lower molecular weight behaves better for each concentration. In the case of chitosan LMW only the sample Tri 3 is acceptable. On the contrary for chitosan-B it is possible to use concentrations of polymers ranging from Tri 4 to Tri 1. In particular, in the case of further deposition we used for chitosan-B the minimum acceptable concentration (Tri 4) whereas in the case of samples to be tested as their own we used the concentration Tri 3 which guaranties more stability over time.

By making similar tests on smaller secondary emulsions, in particular on L4 there was no acceptable concentration of chitosan LMW therefore in this case it was just used chitosan B. As an example, **Table 3.3** reprot the DLS results of a trilayer where as heparin it was used the concentration of 0.0276% wt (Bi 4) and as trilayer chitosan-B at the concentration of 0.0552% wt (Tri 3).

	Emulsion			Monolayer			Bilayer			Trilayer		
	Size (nm)	PDI	Z-pot (mV)	Size (nm)	PDI	Z-pot (mV)	Size (nm)	PDI	Z-pot (mV)	Size (nm)	PDI	Z-pot (mV)
L4	98	0.069	-49	105	0.107	+25	110	0.116	-27	126	0.125	+38.6

Table 3.3. Summary of the size, PDI and z-potential of a complete tri-layer on L4.

DLS results reported in the above table confirm a satisfying control on size and PDI.

In this trylayer, last layer of chitosan was labeled with FITC and the oil was pre-loaded with NR as a lipophilic model drug, in order to perform a fluorescence confocal and STED analysis as shown in **Figure 3.15**.
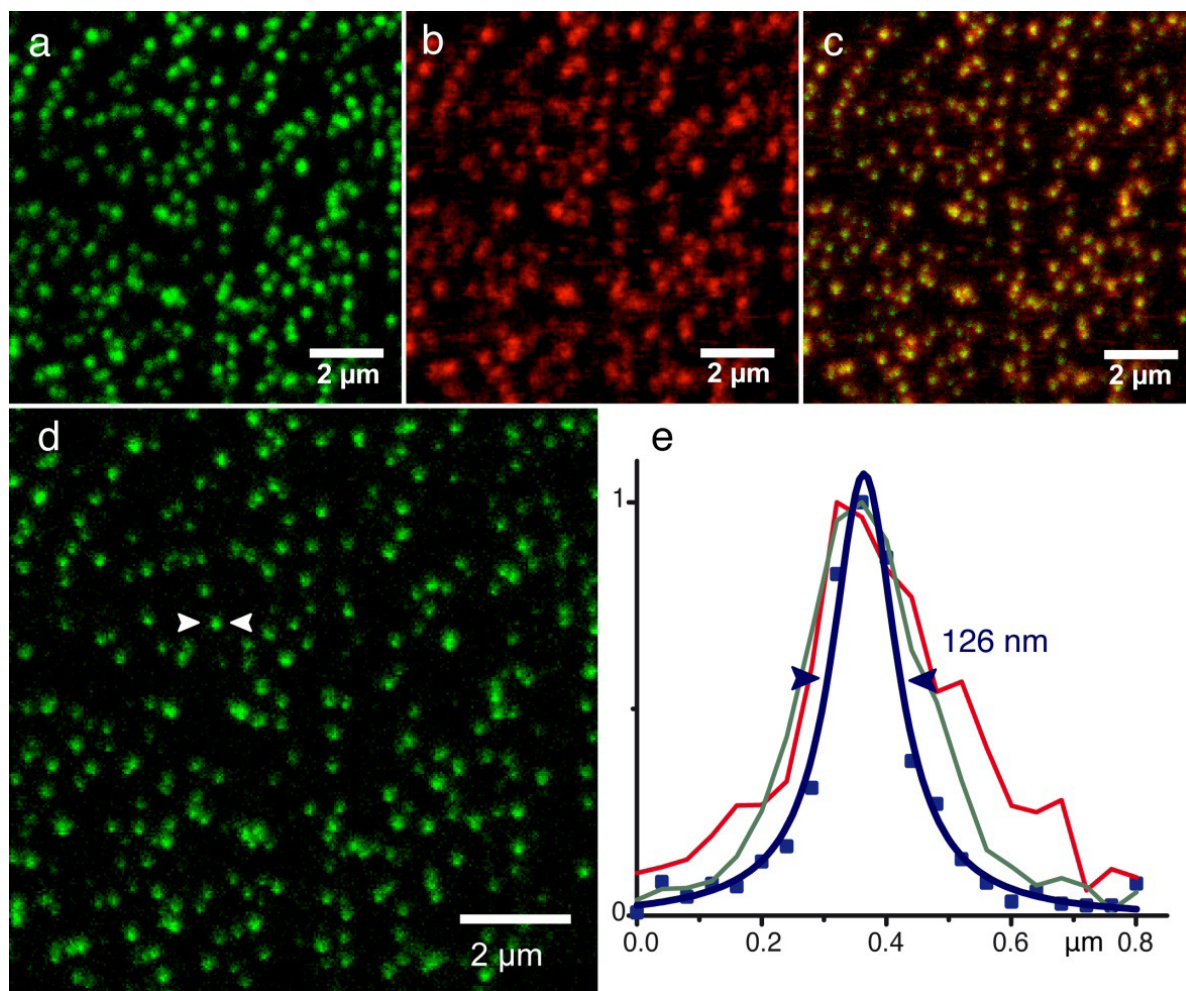
Figure 3.15. In fluorescence analysis of a trilayer made of CT-Heparine-CTB-FITC on L4 oil droplets.

The image confirms the formation of the tri-layer, as demonstrated by the matching of the two colors, green from FITC and red from NR, as well as its loading capability without affecting the monodispersion feature of the nanocarrier itself.

Preliminary tests were also carried out to obtain capsules made of pentalayers. In the following **Table 3.4** the concentrations of the polyelectrolytes used to build up pentalayers are reported. In **Figure 3.16** it is instead reported the DLS analysis from a monolayer to a pentalayer in the case of L1 based template prepared following the concentrations listed in the table.

Layers	Oil	CT-LMW	Hep	CT-B	Hep	CT-B
Mono	1	0,01				
Bi	0.5	0.005	0,0138			
Tri	0.25	0.0025	0.0069	0,0138		
Tetra	0.125	0.00125	0.00345	0.0069	0.019	
Penta	0.0625	0.000625	0.00172	0.00345	0.0095	0.019

Table. 3.4. Summary of the final optimized concentrations in % wt for each layer.
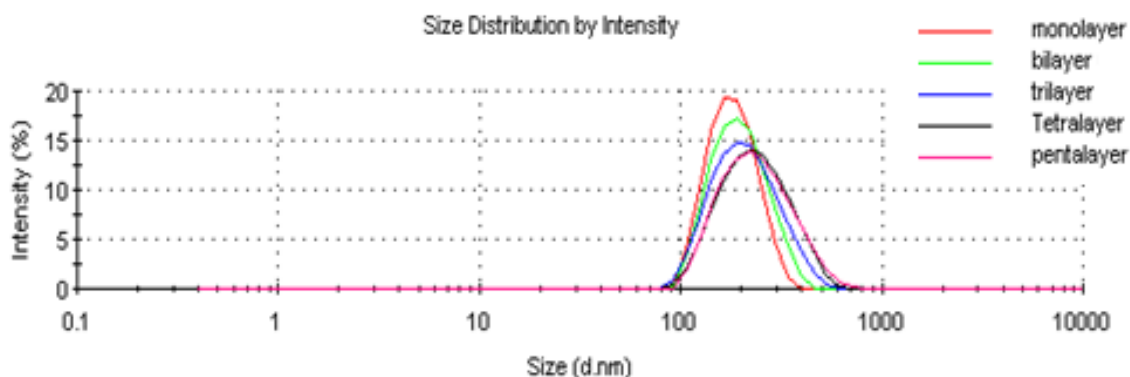
Figure 3.16. DLS analysis from mono to pentalayer built up on an L1 based primary emulsion.

It is possible to see the monomodal feature of all oil core based nanocapsules from single to pentalayer. In terms of monodispersion there is an increase of the PDI with the addition of more and more layers (up to 0.14 for pentalayer). However, by playing with polymer molecular weight it is expected to further optimize monodispersion also in the case of high layers number.

3.3.2. Layer by Layer on ultrastable secondary NEs

Layer by layer polymer nanocapsules are typically prepared by starting from solid templates for two reasons that are the lack of monodispersion and stability of oil templates which instead we were able to obtain by choosing optimal formulation and process. In the previous paragraph multi-layer depositions were made on secondary emulsions characterized by a saturation concentration of the polymer which indeed does not guaranty stability over time. In this section we demonstrate that it is possible to use also the ultrastable secondary emulsions to build up

layer by layer nanocapsules. To do that the excess of polyelectrolyte used for the stabilization of the droplets was properly removed by implementing a nano-beads mediated fishing procedure. This procedure was also originally developed in this work and it was made possible thanks to the monodispersion of the starting secondary emulsions. A scheme of this method is reported in **Figure 3.17**.
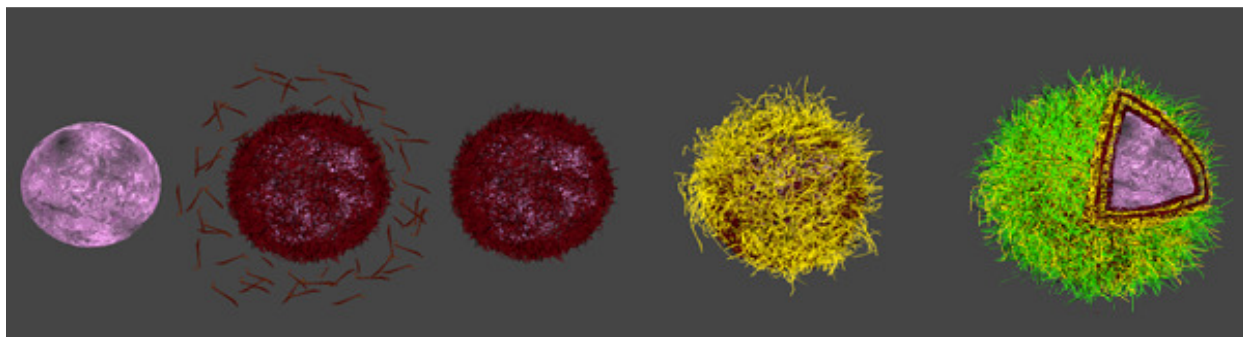
Figure 3.17. Scheme of the Layer by Layer on pre-loaded liquid template by means of a nano-beads mediated fishing procedure to purify secondary emulsions.

As said secondary emulsions stability was only possible with an excess of polymer in solution preventing the deposition of the successive layer. Differently from solid templates secondary emulsions cannot be purified by filtration and centrifugation due to their delicacy. Not even dialysis is feasible mainly due to the charge of polymer and emulsion involved. Anyway, monodispersion feature of our product allowed us to carry out an effective purification by developing a nanobeads-mediated fishing procedure. It is worth noticing that without purification there was no way to deposit any concentration of negative polyelectrolyte even diluting secondary emulsions due to the excess of chitosan in solution while after purification LBL was again possible.

In particular, for purification we used 30 nm magnetic beads which are carboxilated on the surface therefore exhibiting an opposite charge compared to the one of the chitosan thus making possible fishing. This method was successfully proved on the biggest and the smallest secondary emulsions with an excess of chitosan (0.1 % wt). We started from a stock dispersion of magnetic beads at a concentration of 3 % w/v. Generally to not waste too many beads we worked in dilution conditions. Specifically, the secondary emulsion was diluted 10 times with acetic acid solution 20 mM (from 1 % wt of oil and 0.01 % wt of chitosan to 0.1 % wt of oil and 0.01 % wt

of chitosan) whereas the dispersion of magnetic nanobeads was first diluted to 1 % w/v and then a volume between 180 to 60 µl (at 1 % w/v) of such nanobeads was mixed to the previous secondary emulsion. The objective was to identify the right amount of purifying nanobeads in order to obtain a good DLS on the purified secondary emulsion, capability to deposit second layer and no significant beads residue. The first two conditions were obtained for the entire interval in the case of L1 whereas for L4 the right interval resulted between 180 a 75 µl of beads (at 1 % w/v). In **Table 3.5** DLS results of monolayers after purification are reported for the extreme of such range for both L1 and L4 based secondary emulsions.

Then, for the deposition of the heparin different concentrations were tried and the best found was a concentration of around 13 times the one of the first layer of chitosan. Infact, lower concentrations presented a high PDI whereas higher concentrations did not allow chitosan deposition. In previous experiments of layer by layer on secondary emulsion at 0.01 % wt of chitosan the ratio between heparin and first layer of chitosan was 2.76 times therefore 5 times less than here. In other words, in previous case we started from a concentration of heparin of 0.027 % wt (with the first layer of chitosan at a concentration of 0.01 % wt) whereas here we needed five times this concentration divided by 10 times due to the dilution we said previously to avoid wasting of beads (0.027x5/10=0.0135 % wt). We attributed this difference to a higher coverage of oil droplets with chitosan in the case of purified secondary emulsions which indeed required higher heparin to completely switch surface charge. Final heparin concentration after mixing with secondary emulsion was therefore 0.0069 % wt.

After heparine coating it was deposited a third layer of chitosan-B. In particular, the optimal concentration of chitosan was 5 times the one of the heparin (5 x 0.0069 = 0.0345). The DLS results of these depositions are also summarized in **Table 3.5**.

	Beads	Monolayer			Bilayer			Trilayer		
	µl (1 % w/v)	Size (nm)	PDI	z-Pot (mV)	Size (nm)	PDI	z-Pot (mV)	Size (nm)	PDI	z-Pot (mV)
L1	180	183.1	0.081	31.4	179.4	0.062	-29	207	0.085	42
	60	189.6	0.112	28.1	190.4	0.097	-27.6	214	0.093	25
L4	180	92.7	0.077	42.4	92.7	0.099	-35	115.9	0.123	36
	75	96	0.095	26	99	0.095	-29	121	0.124	32.1

Table 3.5. DLS results for trilayer deposition on both L1 and L4 purified secondary emulsions.

In the above experiments, last chitosan layer was labeled with FITC in order to perform a STED analysis while the oil was pre-loaded with NR in order to check loading capability. In **Figure 3.18** the STED analysis on the L4 based (**Figure 3.18.A**) and L1 based (**Figure 3.18.B**) trilayers are reported.

(A)

(B)
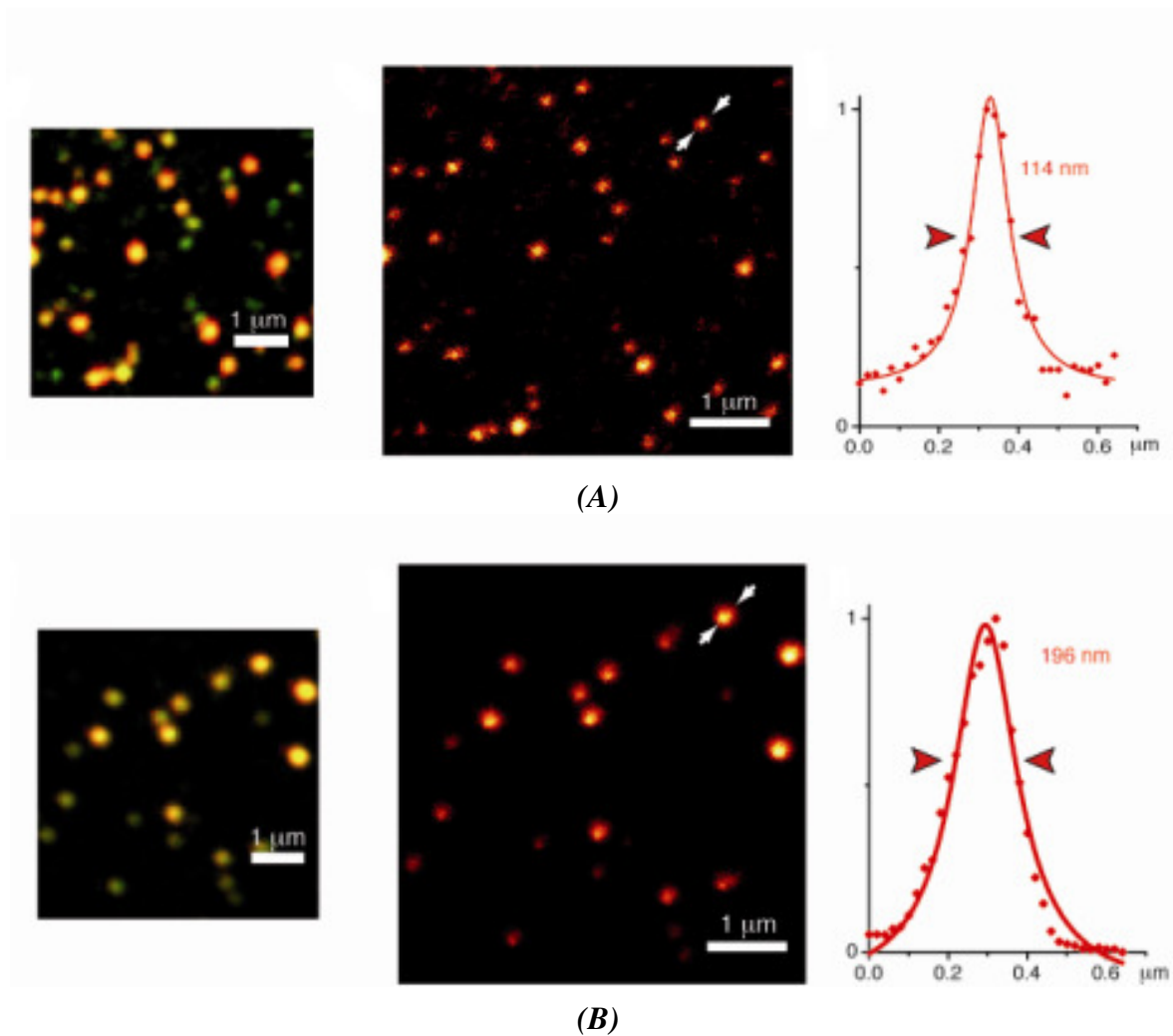
Figure 3.18. Trilayers on L4 (A), L1 (B) secondary emulsions for purified samples (75, 60 μl beads respectively).

STED analysis, in agreement with the DLS measurements, proves the monodispersion feature of the developed nanocapsules on both the sizes as well a perfect match between the bright red fluorescence of the NR with the bright green fluorescence of the chitosan-FITC. This analysis confirms from one side the formation of the tri-layer being only the last layer labeled with FITC and that all the nano-droplets containing the lipophilic drug model are covered by the tri-layer.

Also in this case, regarding the loading aspect it is worth noticing how the presence of the NR did not affect the behavior of the emulsion in terms of size, PDI and templating capability.

For what concerns the dilution it is worth noticing that it did not affect the procedure since with no dilution of the secondary emulsion, purification results were confirmed (see **Table A.E.5** in the Appendix).

Instead, in terms of possible magnetic beads residue it was verified by EDX spectroscopy analysis that by lowering enough the amount of beads useful for separation it is possible to keep it negligible (see Appendix, **Table A.E.6**).

However, apart from the magnetic nano-beads mediated fishing and purification the important thing to remark was the demonstration for the first time of the capability to use an ultrastable emulsion as template to deposit on it once properly purified. That means it is possible to store liquid templates for months and use them whenever needed, like in the case of solid templates, to build up nanocapsules. This was made possible due to monodispersion feature of our emulsion which can guaranty purification by keeping monodispersion and therefore further deposition with low PDI. Nowadays, more and more sophisticated separation systems are being developed also on large scale thus making purification and use of such emulsions scalable at an industrial level.

3.3.3 Multi-layer cross-linkage

3.3.3.1. Chitosan modification with N-Acetylcysteine

In this work it was tried to find the best conditions to improve the degree of functionalization of chitosan without preventing the solubility of the final product, also varying the type of chitosan used (de-polymerized and glycol chitosan). In particular, as anticipated in the methods section chitosan was modified with NAC as reported in **Figure 3.19**.
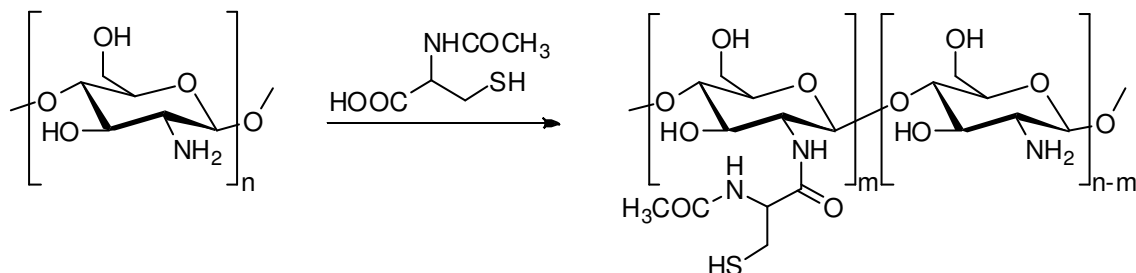
Figure 3.19. Scheme of chitosan reaction with NAC and final chemical structure.

Analysis of modification degree of chitosan with NAC by Ellman test

To evaluate the degree of chitosan modification with NAC it was preliminarly carried out an NMR analysis. Even though it was possible to observe the appearance of a peak at 2.73 ppm associable to CH_2-SH group, another peak partially overlaid with peaks of chitosan in the range between 3.00 and 3.40 ppm and a peak at 4.50 that could be assigned to the anomeric proton H1 of NAC-functionalized units, it was not simple to determine degree of functionalization by NMR analysis. Indeed, the absence of well resolved new peaks did not allow such determination. It was therefore decided to use a well established colorimetric test, the Ellman's test, in order to calculate the amount of thiol groups present.

In this method Ellman reagent (DTNB) reacts with free thiols in slightly basic solution in a thiol-disulfide interchange reaction (**Figure 3.20**).
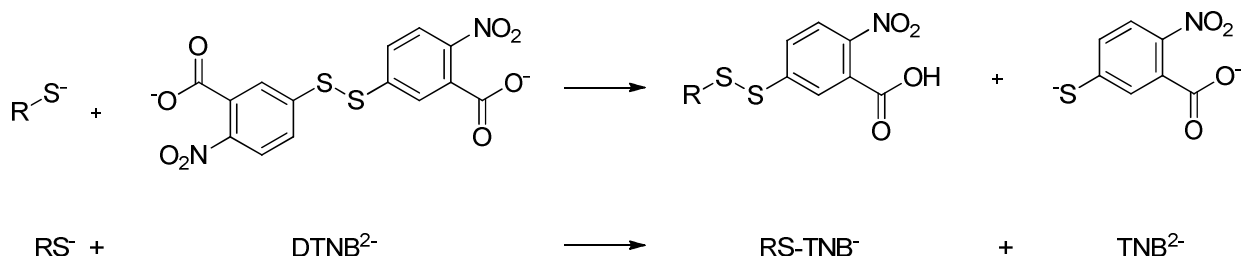
Figure 3.20. Scheme of the reaction between Ellman reagent and free thiols.

TNB^{2-} absorbs light in the UV-Vis range, with a maximum of absorbance at 412 nm. TNB^{2-} formation can be used to assess the number of thiols present due to the stoichiometry of thiolated chitosan to TNB^{2-} formed which is 1:1. So it was calculated a calibration line fot TNB^{2-} using

103

precise amounts of NAC in order to generate known amounts of TNB^{2-}. An ε value of 10320 M^{-1} cm^{-1} was calculated (see Appendix **Figure A.E.6**) by following the method reported in literature [**131**]. It is noteworthy that this test underestimates the degree of functionalization, determining only free and accessible thiols. However, free thiols are the ones involved in the final cross-linking reaction and thus useful to be evaluated. As an example in the Appendix (**Figure A.E.7**) it is reported a spectrum of absorbance of modified glycol chitosan from which it can be possible to quantify TNB^{2-} content, therefore modification degree.

It is important to underline that primary amine groups are crucial for solubilisation of chitosan in water and, consequently, for the degree of thiolation. Indeed, an increase of thiol groups determines the insolubility of the polymer in water as it is reported and as we noticed [**132**].

The degree of functionalization, determined by Ellman test, for some selected chitosan samples with corresponding reaction formulations are reported in **Table 3.6**.

Polysaccharide	HOBt:Chitosan:NAH:EDC	Free thiols %
Chitosan LMW	1:1:4:8	2.2
Chitosan LMW	1:1:4:16	4.3
Chitosan-B	1:1:4:16	4.8
Glycol Chitosan	1:1:4:16	13.2

Table 3.6. Determination of degree of functionalization using Ellman's test.

In the case of chitosan LMW by increasing the EDC amount it was possible to increase modification degree up to 4 %. With chitosan B at the same reaction conditions the % of free thiol was only slightly increased. However, in the case of glycol chitosan, there was a significant enhancement of modification and this kind of modified chitosan, also called glycol chitosan NAC, was therefore used for all the click reactions tests described in paragraph 3.3.3.3.

3.3.3.2. Degree of functionalization by NMR analysis for allylated polyanions

Allylated Sodium alginate

As said in the materials and methods section of this chapter, sodium alginate was functionalized with allylamine. The scheme of reaction and the final structure of the modified polymer is reported in the following **Figure 3.21**.
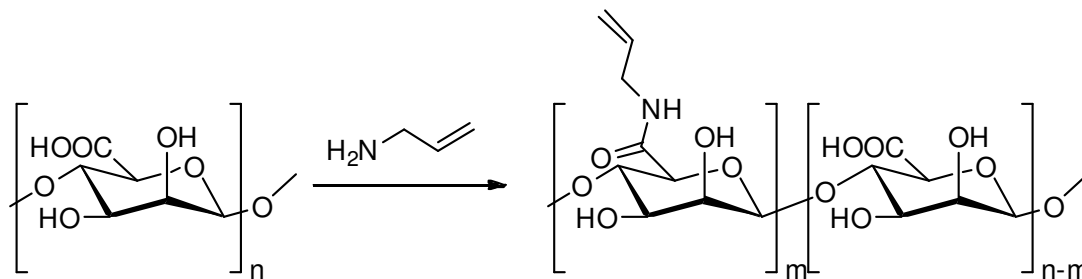
Figure 3.21. Scheme of alginate allylamine functionalization.

Degree of functionalization of alginate was determined by NMR spectra. In particular, tests at different molar ratios between polymer, EDC, HOBt and allylamine were conducted to identify an optimal degree of functionalization (see Appendix **Table A.E.7**) choosing at the end the procedure reported in the materials and method section.

Comparing NMR spectrum of allylated alginate and non allylated alginate (**Figure 3.22**) it can be seen that two signals appear, corresponding to allylic group: the signals at 5.85 and 5.15 ppm, corresponding respectively to CH and CH_2 protons of terminal olefin. Between these two peaks only the one at 5.85 results not overlapped. Therefore, by integration of the peak at 5.85 and and the region between 3.3 and 4.3, related to 5 protons of glucuronic or mannuronic units, it was possible to estimate the degree of functionalization that was ~71 %.
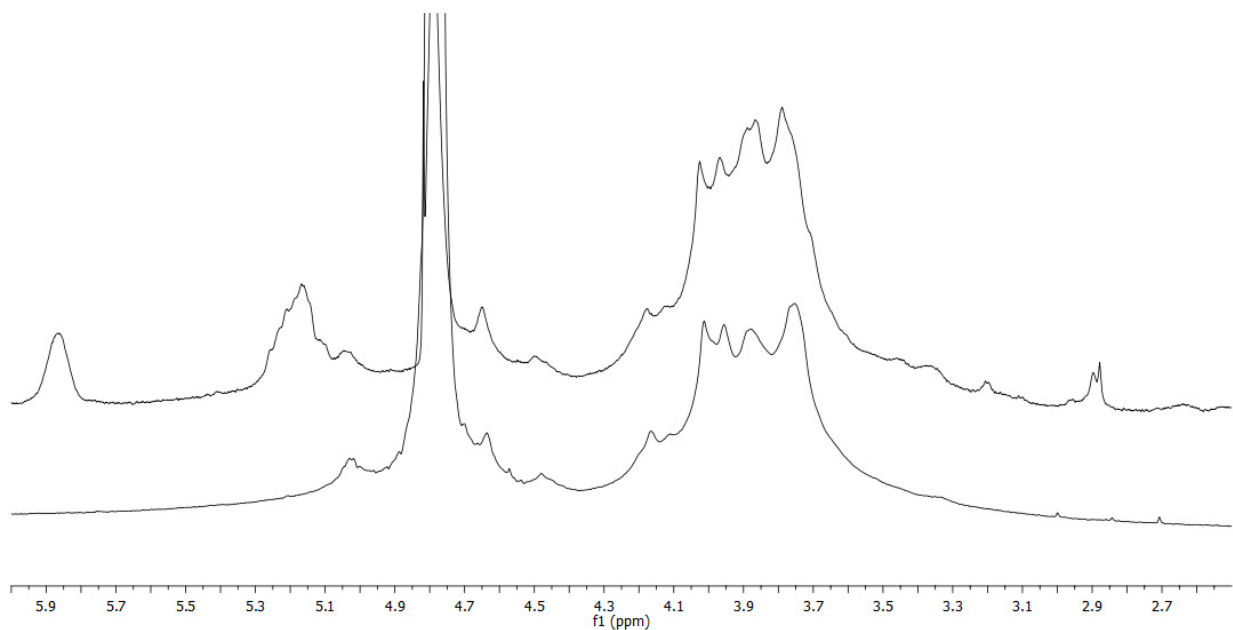
Figure 3.22. Offset 1H NMR spectra of sodium alginate and allylated alginate (on top) in D2O.

Allylated Heparin

The same considerations done for alginate functionalization are also valid for heparin functionalization. As shown in **Figure 3.23** there is a signal at 5.84 ppm related to CH proton of terminal olefin that results not overlapped with heparin signals. So by integration of this peak and the region between 3.00 ppm and 4.40 ppm, related to 10 protons of iduronic and glucosamine units, it was possible to determine the degree of functionalization that is 80.0 %.
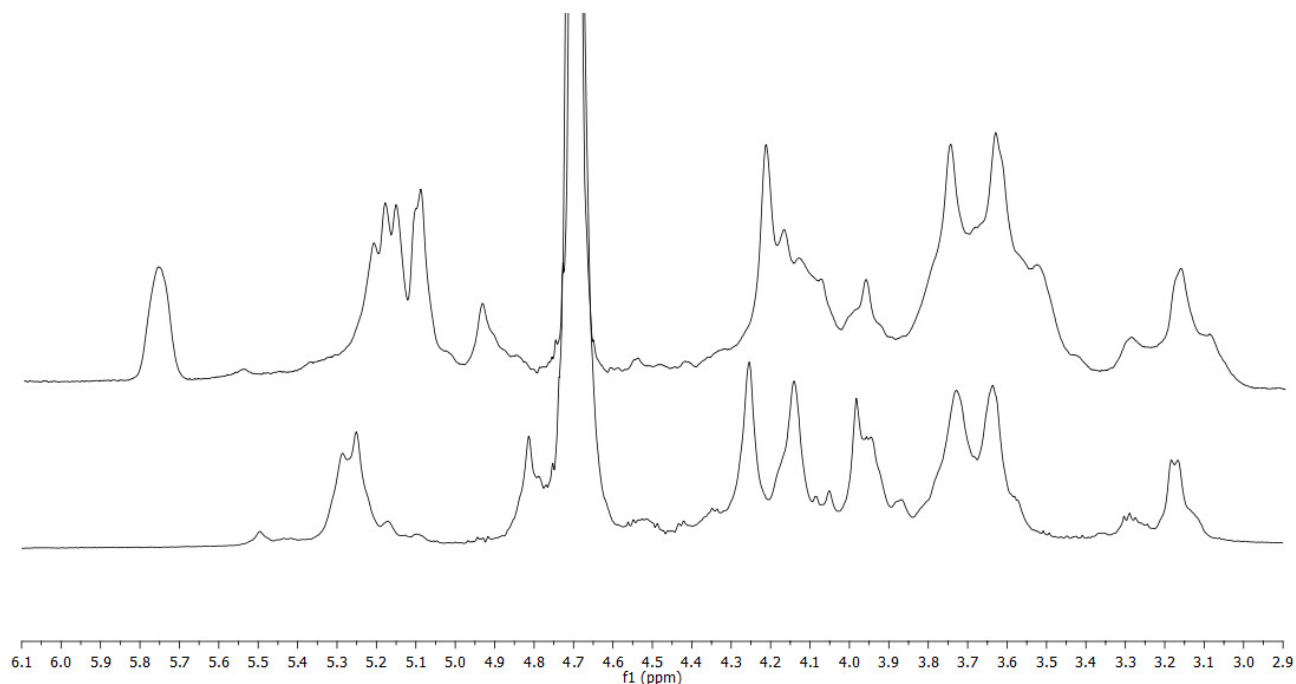
Figure 3.23. Offset 1H NMR spectra of heparin sodium salt and allylated heparin (on top) in D2O.

3.3.3.3. Cross-linkage results

In order to demonstrate the applicability of thiol-ene photoreaction for this thiolated polymer, it was first chosen to optimize the reaction conditions (pH, wavelength, exposition time to light, etc.) carrying out the thiol-ene photo click reaction between thiolated glycol chitosan (the polyelectrolyte with higher degree of functionalization) and just allylamine (**Figure 3.24**).
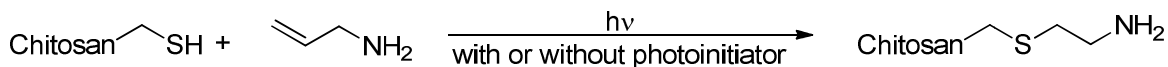
Figure 3.24. Scheme of reaction between modified chitosan and allylamine

To assess the successful of click reaction the reduction of free thiol was determined using the Ellman's test. In **Table 3.7** the conditions used and related reductions of free thiols are shown.

	Irradiation source (nm)	Time exposure	Sperimental condition	Photoinitiatior	% reduction of free thiols
1	Sunlight	2h	In N_2	No	1.4 %
2	365 (Hg lamp)	2h	In N_2	Yes	49.4%
3	365 (Hand lamp)	2h	N_2, pH 4	Yes	34.7%
4	365 (Hg lamp)	2h	In N_2	No	17.2 %
5	365 (Hand lamp)	2h	N_2, pH 4	No	1%
6	365 (Hg lamp)	2h	25°C, pH 4	No	12.11%
7	254 (Hand lamp)	2h	N2, pH 4	No	39.8 %
8	254 (Hand lamp)	2h	pH 4	No	35.25%
9	254 (Hand lamp)	2h	pH 4	Yes	76.8%
10	254 (Hand lamp)	2h	N_2, pH 4	Yes (1/2)	45.5%
11	254 (Hand lamp)	1h	N_2, pH 4	Yes	45.3%

Table 3.7. Degree of reduction of thiol group by irradiation of Thiolated Glycol Chitosan in presence of Allylamine.

Comparing tests 5 and 8, results show that the use of irradiation at 254 nm behaves better than 365 nm as expected by literature [**133**]. It is also clear that natural light (test 1) has no effects on the reaction, as well as the presence of oxygen (comparing tests 7 and 8) does not significantly affect the final reaction. Instead, comparing tests 4 and 5 it is evident that by increasing the power of the lamp it is possible to obtain cross-linkage also with 365nm wavelength even though much less than 254 nm. Moreover, comparing tests 2 and 4, tests 3 and 5 and tests 8, 9 and 10 it is clear how the yield is positively affected as expected from the presence of photoinitiator. However, the yields obtained with no photoinitiators are quite high too with the advantage to avoid the photoinitiator.

After these preliminary results it was tested directly the reaction between the two modified polymers according to the scheme presented in previous **Figure 3.8**.

Finally, thiolated glycol chitosan and allylated heparin or alginate was successfully deposited on PS NPs by LbL technique (**Figure 3.25**).
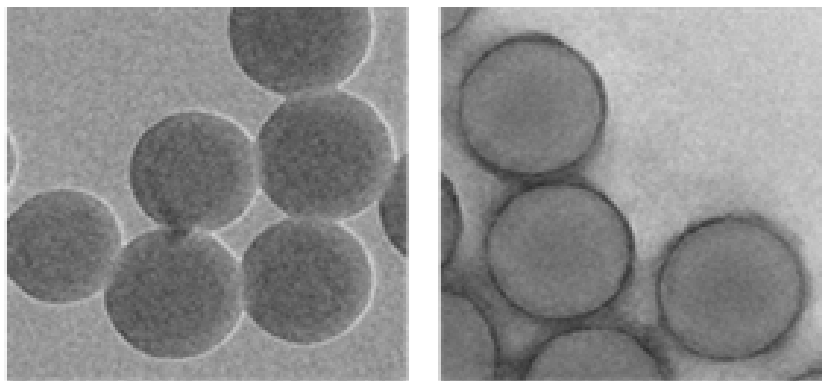
Figure 3.25. TEM image of beads of PS beads non coated (a) and coated with chitosan and heparin.

The bilayer was then irradiated using UV light at 254 nm. Also in this case Ellman's test was used to determine the reduction of free thiol groups that corresponds to the amount of bonds formed. The test was opportunely modified in order to apply it to a system containing particles which can produce scattering effects affecting the final results. For this reason, after irradiation of half amount of nanoparticles suspension, we proceeded by adding the Ellman's reagent to both suspensions, letting them to react for two hours, and centrifuging the suspensions before measurement with spectrophotometer. In this way measurements were carried out on the supernatant containing only TNB^{2-}, collected for UV measurement. The reduction of free thiol group could be determined by comparing sample irradiated and not irradiated (see Appendix **Figure A.E.8**). The results are reported in **Table 3.8**.

Test	Polyelectrolyts	Conditions	Reduction % of free thiols
1	Glicol chitosan-NAC Alg-P6	254 nm (TLC), 2h, with PI	40.7
2	Glicol chitosan -NAC Hep-P6	254 nm (TLC), 2h, with PI	66.5
3	Glicol chitosan -NAC Hep-P6	254 nm (TLC), 2h, without PI	24.4

Table 3.8. Degree of reduction of free thiols on bilayer nanoparticles.

Table clearly shows the effectiveness of the photo-reaction both in the case of sodium alginate and heparin even though better in the latter one as expected by the higher modification degree of heparin. Moreover, by comparing tests 2 and 3 it is evident how the photoreaction can happen also in absence of photo-initiator, even though with lower yield, which is an enormous advantage

in bio-applications as it was meant to be. It is finally noteworthy that irradiation is effective at 254 nm even if it was used a TLC (or compact) lamp, that provides low power. The advantage of using low intensity light is that reaction can be carried out with no need for a temperature control of the solution. To further improve the reaction yield, the solution was directly irradiated, using open containers. This is possible because, as reported in literature [**133, 134**] and as demonstrated in our preliminary experiments (see **Table 3.7**), the presence of oxygen has no negative effects on the reaction.

Only preliminary results were produced on the use of such reaction applied to the oil core based nanocapsules. However, by making a comparison between a cross-linked and not cross-linked trilayer with modified polymers and with the outer layer of chitosan at a saturation concentration (Tri4) (pH 4, 20 mM of acetic acid) it was observed an increase in stability. Indeed after one day of preparation first sample was already not stable whereas the cross-linked one after few days was still stable. Of course these are preliminary results which have to be confirmed and explored at different and also more aggressive conditions like the physiological environment of blood.

Appendix

A.E. Experimental

A.E.1. TGA on chitosan

On all chitosan samples (un-funtionalized and functionalized) a termogravimetric analysis was carried out to obtain the total content of water. Specifically, 3-5 mg of each sample were put into an alumina crucible and brought up to 600°C with a constant ramp from 25°C to 600°C at 20°C/min. At around 100°C, in the graph of wt % versus temperature, a step followed by a plateau can be seen and this loss of weight corresponds to a loss in water content that was not eliminated during the freeze drying procedure. This water content was found to be variable, ranging from 8 to 15 % and dependent on the specific freeze drying process from which the samples have been recovered. The water content was taken into account in the calculation of masses used in functionalization and LbL experiments. The instrument used was simultaneuos DSC/TGA - TA instruments SDT2960. As an example TGA of LMW chitosan is reported below (**Figure A.E.1**) showing in this case a weight loss at around 100° of 10% wt.

Sample: CT usato per stock cont h2o
Size: 5.5152 mg
Comment: CTin aria 20_ al min fino a 600

DSC-TGA

File: ...\CTpurified contenuto d'h2o 3 ott.001

Run Date: 3-Oct-11 13:05
Instrument: 2960 SDT V3.0F

weight loss 10,02%

Universal V3.3B TA Instruments
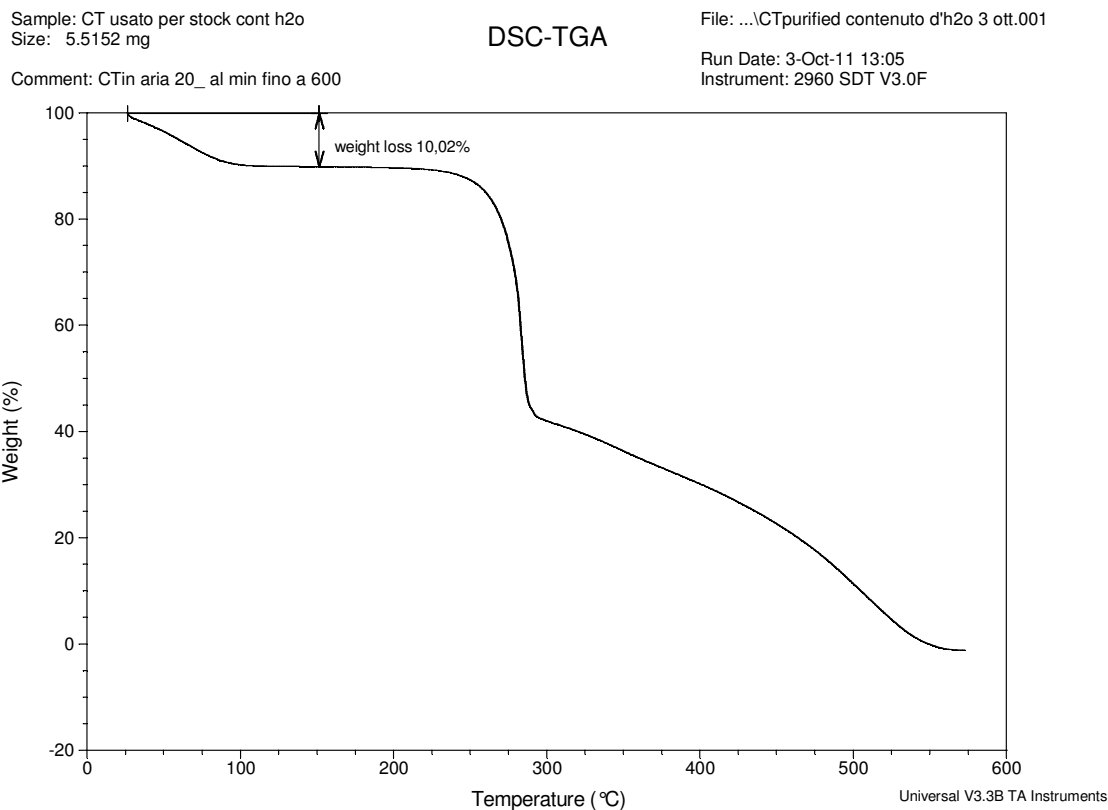
Figure A.E.1. TGA on chitosan samples.

A.E.2. Fluorescence emission of FITC with pH

The effect of pH on the fluorescence intensity of FITC was measured and it is reported in **Figure A.E.2**.
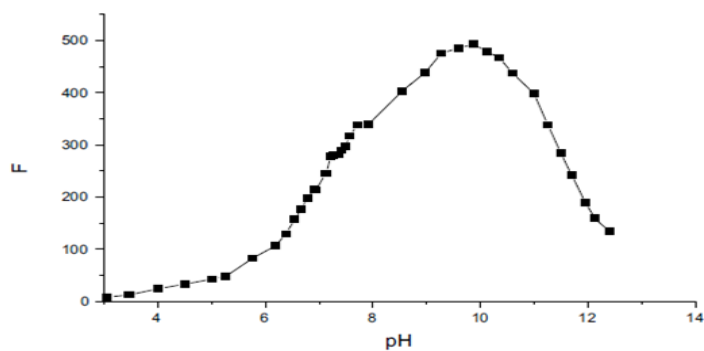
Figure A.E.2. Effect of pH on the fluorecscence intensity of FITC.

A.E.3. Degree of chitosan functionalization with FITC

To determine degree of chitosan functionalization with FITC, a calibration line was calculated by considering FITC concentrations from 6 µg/ml to 1.2 µg/ml in a solution 8:2 water/DMSO (Dimethylsulfoxide) with water phase at pH 6.13 (HAc/Ac buffer). At this pH, FITC's ε was $4.71 \cdot 10^4$ $M^{-1}cm^{-1}$. Calibration line is reported in **Figure A.E.3**.
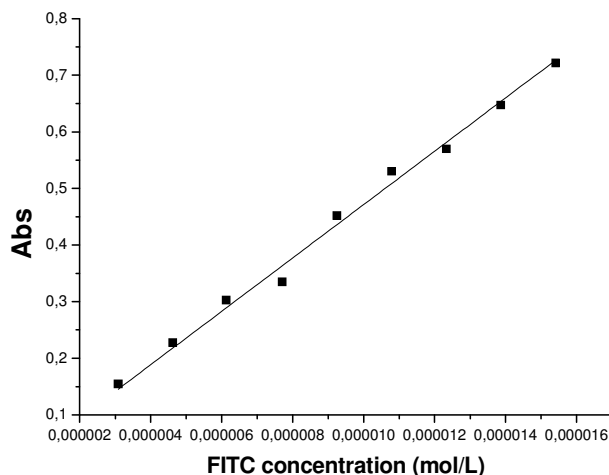
Figure A.E.3. FITC calibration line for determination of chitosan-FITC degree of functionalizaton.

The absorbance of FITC modified chitosan sample was recorded in the same conditions and from this absorbance, taking into account the calibration line, it was calculated a degree of functionalization of around 1.3 %.

A.E.4. DLS results on primary and secondary emulsions

In Table A.E.1 the DLS characterization, in terms of size and PDI, is reported for the different lecithin formulations and both in the case of 10 and 20 % wt of oil. It is possible to see how the increase of lecithin concentration brings to lower sizes even though with an increase of the PDI and that at the same concentration of lecithin in oil the higher viscosities (case of 20 % wt of oil) helps in further reducing size.

Process conditions	L1			L2			L3			L4			L5		
	Size (nm)	PDI	Z-pot (mV)	Size (nm)	PDI	Z-pot (mV)	Size (nm)	PDI	Z-pot (mV)	Size (nm)	PDI	Z-pot (mV)	Size (nm)	PDI	Z-pot (mV)
10 % wt oil															
Cycle 0	315	0.41	-43.3	248	0.34	-40	272	0.37	-44.1	280	0.39	-43.3	264	0.48	-39
Cycle1	222	0.14	-39.9	192	0.12	-40.6	182	0.13	-41.3	176	0.13	-46.9	160	0.15	-41.7
Cycle 2	204	0.09	-30.8	183	0.10	-35.8	169	0.11	-34.6	163	0.11	-37.2	150	0.11	-38.8
Cycle 3	199	0.09	-40.2	168	0.08	-42.2	154	0.10	-36.3	153	0.09	-36.2	139	0.12	-36.8
Cycle 3 + 50 steps	186	0.07	-42.1	153	0.06	-43.4	133	0.09	-38.7	127	0.75	-36.4	112	0.11	-38.3
Cycle 3 + 100 steps	178	0.06	-42.4	142	0.07	-33.2	114	0.11	-30.8	112	0.09	-33	95	0.09	-37.1
Cycle 3 + 150 steps	176	0.07	-41.8	138	0.08	-41.1	112	0.09	-34.1	103	0.08	-33.9	89	0.09	-32.7
Cycle 3 + 200 steps	173	0.04	-41	136	0.10	-32.9	107	0.09	-30.9	101	0.14	-32.1	85	0.10	-35.1
20 % wt oil															
Cycle 0	437	0.44	-42.7	317	0.38	-43.8	299	0.41	-42.9	261	0.37	-46.3	265	0.39	-42.9
Cycle1	239	0.14	-48.9	201	0.17	-43.8	181	0.13	-40.9	156	0.14	-40.1	151	0.15	-43
Cycle 2	212	0.09	-40	180	0.12	-43.1	167	0.09	-40.9	143	0.13	-43.6	141	0.14	-45.6
Cycle 3	206	0.08	-40.3	172	0.09	-41.9	161	0.10	-34.1	134	0.11	-43.4	134	0.13	-43.1
Cycle 3 + 50	181	0.06	-43.9	150	0.07	-41.4	132	0.08	-40.2	109	0.12	-43.4	107	0.12	-37.9
Cycle 3 + 100	168	0.04	-42.5	133	0.07	-39.5	115	0.07	-37.4	97	0.11	-44.2	94	0.13	-28.5
Cycle 3 + 150	164	0.05	-40.3	127	0.06	-35.9	107	0.06	-37.2	88	0.10	-52.1	83	0.11	-42.9
Cycle 3 + 200	159	0.03	-42.1	119	0.06	-37.6	100	0.06	-36.2	82	0.09	-36.3	77	0.10	-38

Table A.E.1. Primary emulsions at 10 and 20% wt of oil for the five different concentration of lecithin (L1÷L5) at the different processes cycles and cycles + steps.

In **Table A.E.2** it is reported the DLS characterization of secondary NEs at different chitosan concentrations for samples re-dispersed once (after 1 day) and twice (after 1 month) of preparation (for all the five templates L1÷L5), and as an example, for L1 not re-dispersed at all.

	L1 re-dispersed once through high pressure homogenizer (A)															
Chitosan concentration [%]	0.005		0.01		0.0175		0.025		0.05		0.1		0.175		0.25	
TIME (days)	Size [nm]	PDI	Size [nm]	PDI	Size [nm]	PDI	Size [nm]	PDI	Size [nm]	PDI	Size [nm]	PDI	Size [nm]	PDI	Size [nm]	PDI
0	188.4	0.07	172.4	0.06	180.7	0.05	174.2	0.04	173.2	0.05	182.9	0.1	199.3	0.11	197.6	0.11
1	215.9	0.12	195.6	0.08	192.7	0.08	185.8	0.09	186.7	0.10	191.2	0.13	220.4	0.12	249.1	0.16
3	199.2	0.09	193.1	0.1	210.8	0.20	190.8	0.08	191.1	0.09	200	0.1	237.2	0.13	250	0.14
7	208.6	0.08	197.1	0.09	200.2	0.08	189.4	0.07	191.3	0.09	195.2	0.12			249.2	0.17
14	209.5	0.11	205.6	0.08	207.1	0.1	203.8	0.09	196.7	0.1	202.5	0.15			242.2	0.11
28	215.1	0.10	204.1	0.06	206.8	0.07	204.6	0.07	202.1	0.09	199.5	0.10			247.2	0.12
75					638.8	0.41	198.6	0.08	211	0.08	214.8	0.08			254.2	0.08
90							338.7	0.35	205.5	0.04	224.8	0.06			248.3	0.07
160									208.9	0.12	214	0.09			229	0.12
190									286.4	0.32	197.1	0.1			201.7	0.1
270											211.6	0.04			219.3	0.06
360											214.3	0.1			214.2	0.07
510											210.7	0.09			219.4	0.1
	L1 re-dispersed twice through high pressure homogenizer after 1 month (B)															
28	214.4	0.1	195.6	0.08	183.9	0.06	187	0.06	185.7	0.08	186.5	0.07	179.7	0.09	206.4	0.07
31	247.4	0.11	189.4	0.09	194.1	0.08	190.1	0.08	181.9	0.07	184.4	0.07	182.6	0.08	200.7	0.06
42			193.7	0.09	191.2	0.07	190.8	0.07	193	0.15	178.8	0.08	181.4	0.08	206	0.12
60					189.7	0.06	183	0.1	184.5	0.07	182.3	0.08	181.9	0.07	196.7	0.08
95							182.2	0.08	181.2	0.09	177.7	0.08	170.5	0.08	192.5	0.12
160									175	0.11	174	0.09	167.8	0.09	177.5	0.09
190									178.2	0.07	174.4	0.12	168	0.07	181.5	0.12
270											180.2	0.08	170.8	0.08	185.9	0.09
360											178.7	0.12	165	0.06	174.2	0.07
510											182.8	0.1	169	0.05	182	0.06

L2 re-dispersed once through high pressure homogenizer (C)																
Chitosan concentration [%]	0.005		0.01		0.0175		0.025		0.05		0.1		0.175		0.25	
TIME (days)	Size [nm]	PDI	Size [nm]	PDI	Size [nm]	PDI	Size [nm]	PDI	Size [nm]	PDI	Size [nm]	PDI	Size [nm]	PDI	Size [nm]	PDI
0	134.8	0.11	128.4	0.08	128.7	0.06	127	0.06	125.1	0.1	139.5	0.12	162	0.17	196.8	0.17
1	134.4	0.10	130.3	0.09	131.3	0.06	132.2	0.07	128.7	0.09	138.3	0.11	167.6	0.16	189.1	0.17
3	143.3	0.07	138.1	0.06	139.1	0.09	139.1	0.06	136.8	0.09	148.8	0.12	179.7	0.16	206.6	0.16
7	148.2	0.11	135.7	0.09	131.9	0.07	141.7	0.08	143	0.09	155.1	0.11	185.4	0.14	203.8	0.15
14	165.6	0.07	139.3	0.08	149.8	0.12	142.7	0.07	142.8	0.08	148.7	0.13	172.9	0.14	198	0.16
28			134.9	0.05	137.4	0.07	145.5	0.07	150.1	0.09	154.7	0.08	171.9	0.12	193.6	0.15
75							190.1	0.1	148.8	0.08	165.8	0.07	179.5	0.07	194.3	0.13
90									144.7	0.06	166.8	0.06	177	0.09	187.7	0.13
160									262.3	0.36	163.3	0.12	160.5	0.07	197.9	0.22
190											142.4	0.13	146	0.09	151.6	0.11
270											159.5	0.08	163.7	0.07	165.2	0.09
360											160.4	0.1	152.9	0.07	162.8	0.17
510													158.6	0.08	159.3	0.09
L2 re-dispersed twice through high pressure homogenizer after 1 month (D)																
28			134.1	0.06	134.4	0.08	132.3	0.03	127	0.07	128.3	0.08	145.3	0.09	156.7	0.09
31			134.1	0.07	135	0.06	136.1	0.04	135.7	0.07	134.6	0.08	147.6	0.09	158.2	0.09
42					132	0.06	130.6	0.05	131.2	0.08	135.5	0.11	141.5	0.09	153.4	0.09
60							128.9	0.06	127.9	0.04	131	0.06	137.6	0.09	145.8	0.09
95									129.9	0.11	131.3	0.12	136.5	0.14	142.9	0.14
160									121.6	0.07	122.5	0.04	124.8	0.09	133.3	0.15
190									128.7	0.06	125	0.09	125.1	0.06	136.4	0.16
270											127.8	0.06	117.8	0.17	137.7	0.14
360											129.7	0.09	126.3	0.12	131.2	0.14
510											131.1	0.08	129.5	0.09	131.1	0.1

L3 re-dispersed once through high pressure homogenizer (E)																
Chitosan concentration [%]	0.005		0.01		0.0175		0.025		0.05		0.1		0.175		0.25	
TIME (days)	Size [nm]	PDI	Size [nm]	PDI	Size [nm]	PDI	Size [nm]	PDI	Size [nm]	PDI	Size [nm]	PDI	Size [nm]	PDI	Size [nm]	PDI
0	102.5	0.08	101.9	0.08	103.4	0.1	102.6	0.10	108.7	0.12	115.4	0.13	126.4	0.18	142	0.2
1	103.2	0.1	105.4	0.09	106.1	0.09	101.6	0.08	111.4	0.12	122	0.15	134.1	0.18	156	0.19
3	108.6	0.09	107	0.09	110.2	0.08	111.2	0.13	110.2	0.11	125.4	0.14	144	0.17	167.3	0.12
7	117.4	0.06	107.9	0.08	114	0.09	111.7	0.01	111.7	0.11	123.9	0.15	147.1	0.17	170.2	0.17
14	226.3	0.32	111.2	0.07	111.5	0.06	109.5	0.07	106.4	0.08	123.2	0.13	128.4	0.15	127.9	0.14
28			126.3	0.07	115.8	0.08	120.6	0.06	125	0.08	132	0.12	149.4	0.14	169.5	0.15
L3 re-dispersed twice through high pressure homogenizer after 1 month (F)																
28			139	0.1	111	0.07	109.9	0.07	111.3	0.08	113.6	0.1	121	0.11	131.7	0.12
31			218.9	0.12	108.5	0.1	106.5	0.07	108.2	0.07	110.8	0.09	121	0.13	131.5	0.1
42					280.7	0.17	104.2	0.07	109.2	0.07	109.3	0.09	114.1	0.11	124.2	0.1
60							155.3	0.05	107.8	0.08	107.4	0.1	111.7	0.11	115.2	0.1
95									106	0.1	105.9	0.09	110.3	0.11	123.3	0.18
160									101.7	0.07	99.09	0.06	103.9	0.01	104.6	0.08
190									113.9	0.07	100.2	0.074	102.1	0.07	106.3	0.1
270											105.3	0.09	102	0.07	101.8	0.06
360											115.7	0.14	106.2	0.09	100.7	0.07
510											120.2	0.23	105.3	0.08	104.9	0.07

L4 re-dispersed once through high pressure homogenizer (G)

Chitosan concentration [%]	0.005		0.01		0.0175		0.025		0.05		0.1		0.175		0.25	
TIME (days)	Size [nm]	PDI	Size [nm]	PDI	Size [nm]	PDI	Size [nm]	PDI	Size [nm]	PDI	Size [nm]	PDI	Size [nm]	PDI	Size [nm]	PDI
0	87.81	0.01	88.28	0.12	89.78	0.13	89.28	0.11	91.57	0.15	95.81	0.15	104.8	0.19	110.3	0.2
1	89.78	0.09	91.08	0.11	91.96	0.11	91.8	0.12	94.73	0.14	107.4	0.2	111.9	0.19	131.2	0.22
3	106.3	0.09	94.03	0.10	95.66	0.11	96.23	0.11	103	0.17	110	0.17	131.9	0.1	149.6	0.19
7	172.8	0.13	104.5	0.09	101.4	0.1	93.59	0.11	104.7	0.17	119.1	0.21	146.3	0.23	193.8	0.35
14			113.1	0.08	100.1	0.11	101.9	0.1	108.9	0.15	111.4	0.16	132.3	0.17	151.9	0.18
28					102.3	0.08	103.2	0.09	110.9	0.11	117.3	0.13	131.5	0.16	142.9	0.16
75									110.8	0.15	115	0.09	135.6	0.14	144.9	0.11
90									167.4	0.13	117.2	0.11	126.1	0.1	138.5	0.1
160											119.3	0.07	118.7	0.08	122	0.08
190											137.6	0.09	123.5	0.08	127.7	0.06
270											219.6	0.26	128.6	0.06	127.4	0.06
360													134.5	0.1	122.4	0.09
510													161.5	0.13	131.3	0.07

L4 re-dispersed twice through high pressure homogenizer after 1 month (H)

Chitosan concentration [%]	0.005		0.01		0.0175		0.025		0.05		0.1		0.175		0.25	
TIME (days)	Size [nm]	PDI	Size [nm]	PDI	Size [nm]	PDI	Size [nm]	PDI	Size [nm]	PDI	Size [nm]	PDI	Size [nm]	PDI	Size [nm]	PDI
28			252.9	0.05	97.48	0.1	95.56	0.08	96.8	0.1	98.13	0.11	105.3	0.13	113.9	0.13
31					95.51	0.07	94.37	0.08	96.51	0.08	96.83	0.12	104	0.14	114	0.14
42							91.58	0.07	90.49	0.09	92.92	0.1	97.72	0.11	106.8	0.12
60									91.19	0.11	91.34	0.11	99.12	0.13	104.6	0.14
95									90.26	0.14	91.3	0.12	85.68	0.12	105.4	0.19
160									101.4	0.06	84.88	0.08	87.62	0.01	91.19	0.01
190									175.5	0.1	89.93	0.15	88.32	0.11	92.6	0.13
270											91.73	0.12	88.98	0.1	89.45	0.1
360											98.59	0.15	92.53	0.1	91.08	0.1
510											120.7	0.3	98.14	0.13	96.02	0.1

L5 re-dispersed once through high pressure homogenizer (I)

Chitosan concentration [%]	0.005		0.01		0.0175		0.025		0.05		0.1		0.175		0.25	
TIME (days)	Size [nm]	PDI	Size [nm]	PDI	Size [nm]	PDI	Size [nm]	PDI	Size [nm]	PDI	Size [nm]	PDI	Size [nm]	PDI	Size [nm]	PDI
0	84.58	0.1	83.19	0.12	83.61	0.13	82.27	0.12	81.87	0.12	88.42	0.17	95.38	0.18	108.2	0.21
1	85.38	0.12	84.79	0.11	83.17	0.11	85.01	0.11	86.27	0.13	96.97	0.19	107.4	0.22	122.8	0.21
3	103.4	0.18	91.28	0.14	90.15	0.14	84.76	0.11	93.41	0.15	101	0.19	117.8	0.21	147	0.22
7	160.5	0.14	98.6	0.1	89.19	0.1	92.52	0.1	92.85	0.13	92.18	0.15	112.5	0.2	127.9	0.2
14			107.7	0.07	96.07	0.11	97.67	0.1	99.6	0.13	106.6	0.15	137.1	0.23	133.9	0.17
28					101.3	0.07	97.54	0.1	97.19	0.09	100.9	0.13	104.2	0.14	131.6	0.16
75									142.4	0.09	116	0.13	125.8	0.12	132.2	0.12
90											114.2	0.14	126.1	0.15	129	0.11
160											138.9	0.14	115.3	0.09	117.5	0.1
190											219.7	0.25	124.7	0.1	124.4	0.15
270													133.3	0.08	123.5	0.06
360													155.4	0.1		
510													240.1	0.34		

L5 re-dispersed twice through high pressure homogenizer after 1 month (L)

Chitosan concentration [%]	0.005		0.01		0.0175		0.025		0.05		0.1		0.175		0.25	
TIME (days)	Size [nm]	PDI	Size [nm]	PDI	Size [nm]	PDI	Size [nm]	PDI	Size [nm]	PDI	Size [nm]	PDI	Size [nm]	PDI	Size [nm]	PDI
28					96.98	0.1	90.44	0.09	88.33	0.11	92.05	0.13	98.16	0.13	107.6	0.15
31					98.5	0.12	92.05	0.13	91.28	0.09	92.97	0.13	98.49	0.13	112.7	0.16
42							125	0.06	87.07	0.08	85.53	0.1	93.93	0.11	101.1	0.14
60									86.53	0.08	88.08	0.09	90.94	0.11	101.8	0.13
95									82.65	0.11	83.52	0.12	89.13	0.13	94.01	0.11
160											79.13	0.09	81.07	0.07	84.59	0.09
190											82.13	0.11	89.04	0.19	84.88	0.09
270											92.59	0.15	88.05	0.12	85.89	0.09
360											104.7	0.19	96.62	0.18	91.64	0.12
510											166.6	0.5	108.6	0.28	101.8	0.19

L1 no re-dispersion process (M)																
Chitosan concentration [%]	0.005		0.01		0.0175		0.025		0.05		0.1		0.175		0.25	
TIME (days)	Size [nm]	PDI	Size [nm]	PDI	Size [nm]	PDI	Size [nm]	PDI	Size [nm]	PDI	Size [nm]	PDI	Size [nm]	PDI	Size [nm]	PDI
0	192	0.22	182.7	0.08	184.5	0.11	179.3	0.08	187.7	0.12	190.9	0.13	203	0.15	236.1	0.22
1	210.9	0.26	188.6	0.12	197.2	0.11	184.4	0.1	181.3	0.11	187.3	0.12	253.9	0.2	296.5	0.4
3			178.4	0.05	183.2	0.09	176.2	0.07	185.5	0.1	188.2	0.1	232.6	0.19	324.9	0.29
7			197.5	0.13	191.1	0.15	186.2	0.11	203.8	0.11	203.3	0.11	254.2	0.23	324.8	0.4
14			194	0.15	183.8	0.1	185.2	0.06	205.6	0.12	225.6	0.14	275.5	0.17	372.1	0.3
28			186.2	0.14	188.4	0.07	210	0.13	239.4	0.14	291	0.19	409.8	0.4		

Table A.E.2. Stability tests on secondary emulsions reprocessed once (A, C, E, G, I), reprocessed twice (B, D, F, H, L) and no re-processed (M). Some Notes: The data missing in A for the 0.175 % wt of CT are due to a mistake for which the sample was completely re-processed for the second time after three days; The sample in B corresponding to 0.175 % wt of chitosan as said was re-processed after three days instead of 1 month. As it is possible to see in this case the size is slightly less than the samples just above and below in terms of concentration; maybe the earlier processing avoided some aggregations ending up with a smaller average size; All the samples L3 in E were reprocessed after 1 month as planned but they were completely processed by mistake without keeping the sample for further stability tests. The times for measurements are rounded of few days. The red is related to double peaks. Missing boxes indicated destabilization.

A.E.5. Analysis of chitosan coverage on NEs by Spectrofluorimetry

Chitosan (% wt)	Emission at 510 nm (AU)		
	NE + Chitosan	NE + Chitosan	Chitosan
0.001	1604		
0.00175	2869		
0.0025	6332		
0.005	26686		
0.01	71921	80194	181224
0.0175	168359	158939	266550
0.025	214812	214773	322734
0.0375		301693	400490
0.05	368064	348130	434998
0.0625		420170	491428
0.075		445800	496268
0.0875		490375	494367
0.1	529369		526043
0.25	531200		

Table A.E.3. Fluorescence emission at 510nm for L4 secondary emulsions coated with chitosan-FITC and free chitosan at the same concentrations. Samples were diluted 1:4 to limit the emission of the more concentrated samples.

A.E.6. Saturation method by z-potential analysis

In **Figure A.E.4** it is reported an example of saturation method by using z-potential technique of NEs (L4 based) coated at different concentration of chitosan (from 0 to 0.2 % wt).
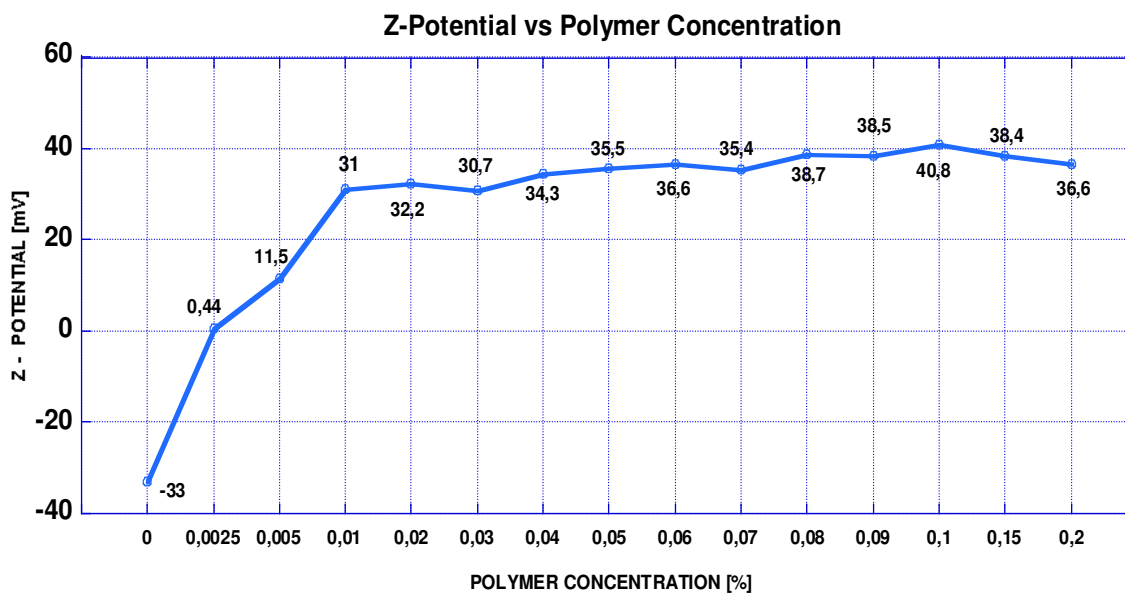
Figure A.E.4. Z-Potential analysis on L4 based secondary emulsiont at different chitosan % wt from 0 to 0.2 %.

As it is evident from the graph, there is not a very clear concentration which can be considered as saturation concentration.

A.E.7. Method to evaluate molecular weight of depolymerized chitosan

Five different concentrations were tested for each sample, each concentration measured five times. In particular, specific viscosity, η_{spec}, was determined using the following equation:

$$\eta_{spec} = \frac{t}{t_0} - 1$$

where t_0 is the flow time for solvent and t is the flow time for sample solution. The specific viscosity is related to a reduced viscosity, η_{rid}, by means of the concentration:

$$\eta_{rid} = \frac{\eta_{spec}}{C}$$

Intrinsic viscosity, [η] is then defined as:

$$[\eta] = \lim_{C \to 0} \frac{\eta_{spec}}{C}$$

and can be determined plotting on graph C versus η_{rid} and extrapolating the value for C = 0. As a representative example, the intrinsic viscosity calculation method of chitosan-B is shown in **Figure A.E.5**. Chitosan-B is the chitosan used for trilayer deposition.
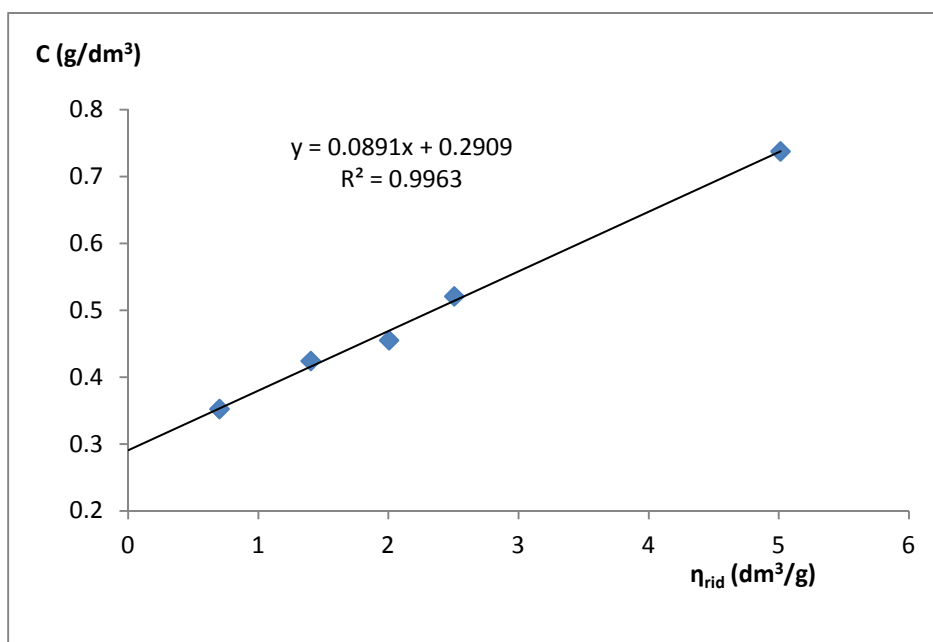
Figure A.E.5.Graphical determination of intrinsic viscosity.

The viscosity-average molecular weights (M_v), at different degree of de-polymerisation, were then calculated using the Mark-Houwink equation:

$$[\eta] = K \, (M_v)^a$$

where [η] is the intrinsic viscosity, a and K are constants for a given solute-solvent system and temperature. The latter constant have been identified ($K = 1.38 \times 10^{-5}$ and $a = 0.85$) respect to the pH, solvent ionic strength and degree of deacetylation of chitosan used (see material section). **Table A.E.4** summarizes the different concentrations utilized and the molecular weights obtained.

Name	NaNO$_2$ amount	M$_v$
Chitosan-LMW		126.0 kDa
Chitosan -A	1.73 mg	26.0 kDa
Chitosan -B	4.30 mg	17.5 kDa
Chitosan -C	9.70 mg	6.7 kDa
Chitosan -D	17.25 mg	2.1 kDa

Table A.E.4. Summary of the different concentrations utilized and the molecular weights obtained.

A.E.8. Analysis of magnetic beads residue after purification

It was tried to purify without dilution starting from 0.6 ml of magnetic nanobeads at 3 % w/v and a secondary emulsion (L4) not diluted (oil 1 % wt; chitosan 0.1 % wt), following then the usual procedure in terms of mixing, stirring, beads separation. DLS results are reported in the **Table A.E.5**.

Emulsion	Average size =86 PDI= 0.108 Z-pot = -34.2 ± 6.26 mV
Monolayer separation (Sample 1)	Average size = 95.31 nm PDI= 0.075 Z-pot = 37.5 ± 10.9 mV
Monolayer separation (Sample 2)	Average size = 93.24 nm PDI= 0.088 Z-pot = 35.2 ± 10.7 mV
Bilayer	Average size=115.4 nm PDI= 0.109 Z-pot = -39.8 ± 12.4 mV

Table A.E.5. DLS results on purification without dilution.

In order to verify if magnetic nanobeads were completely removed from the purified sample, EDX spectroscopy analysis was carried out at different magnetic beads amounts. Samples, after purification with beads, were first lyophilized before introducing in the scanning electron

microscopy (SEM) to eliminate oil phase. **Table A.E.6** summarizes the DLS results of purified L1 based secondary emulsions (with an initial stability concentration of chitosan of 0.1 % wt) and corrisponding amount of Co residue, for different amounts of magnetic beads used for purification, specifically from 60 to 180 µl (at 1 % w/v) brought to 0.5 ml and mixed with 0.5 ml of secondary emulsion diluted ten times.

		60 µl	90 µl	120 µl	150 µl	180 µl
Monolayer L1 0.1% CT-lmw_2 p	**Size (nm)**	192.1	195.9	177.6	182.7	200.9
	PDI	0.04	0.06	0.04	0.07	0.05
	Z.pot (mV)	38.5	35.8	31.9	39.9	44.1
Co by EDX spectroscopy	**% wt**	0		5.5		18

Table A.E.6. Summary of DLS and EDS analysis on purified L1 secondary emulsions.

As it is possible to see in terms of DLS all the trials in the range from 60 to 180 µl were fine. However in terms of magnetic beads residue it was necessary to use the minimum possible amount of beads to avoid any final contamination.

A.E.9. Spectra of absorbance of TNB^{2-}

To quantify the degree of functionalization of NAC modified chitosans as well as the degree of reticulation induced into the bilayer built on PS NPs, it was first calculated the calibration line by using NAC as standard. In particular, DTNB, at different concentrations, was dissolved by using acetic acid buffer solution at pH 3. Then 0.5 ml of each standard was added to 3.5 ml of a 0.5 M buffer phosphate at pH 8.03. The final pH is 7.4, a value necessary for the essay. The baseline was registered at t = 0 in order to subtract the absorbance due to DTNB at 412 nm. Then, standards were stored in the dark at 25 °C under stirring for 150 minutes. Finally, absorbance was measured for each sample following a known method [131] and the value at 412 nm was used to obtain the calibration line (see **Figure A.E.6**); the ε value of TNB^{2-} at 412 nm was $1.0320 \cdot 10^4$ M^{-1} cm^{-1}.
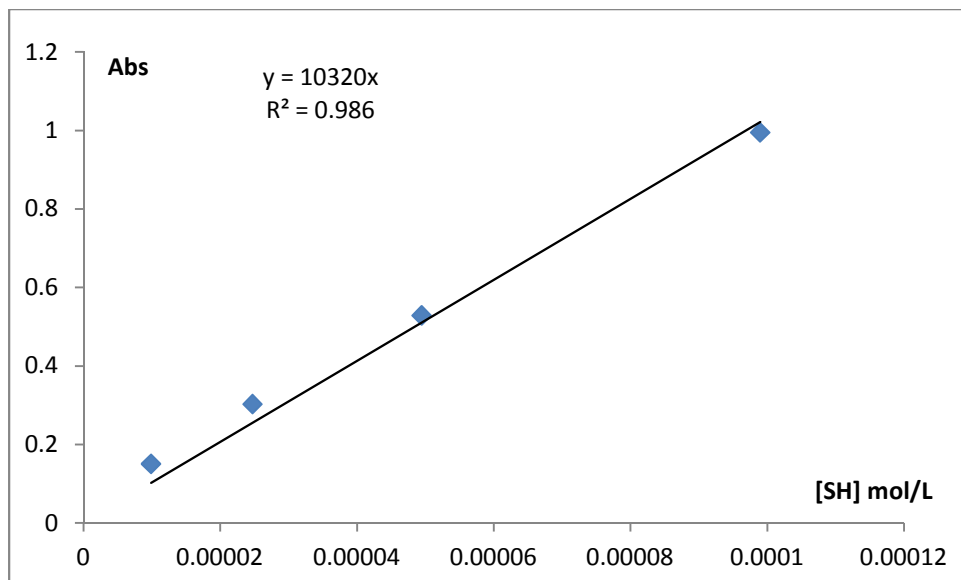
Figure A.E.6. Calibration line for determination of chitosan-NAC degree of functionalizaton.

Figure A.E.7 and **Figure A.E.8** report respectively the absorbance spectrum for the modified glycol chitosan to determine functionalization degree and the two spectra of irradiated and not irradiated bilayer to determine free thiol reduction, therefore reticulation degree.
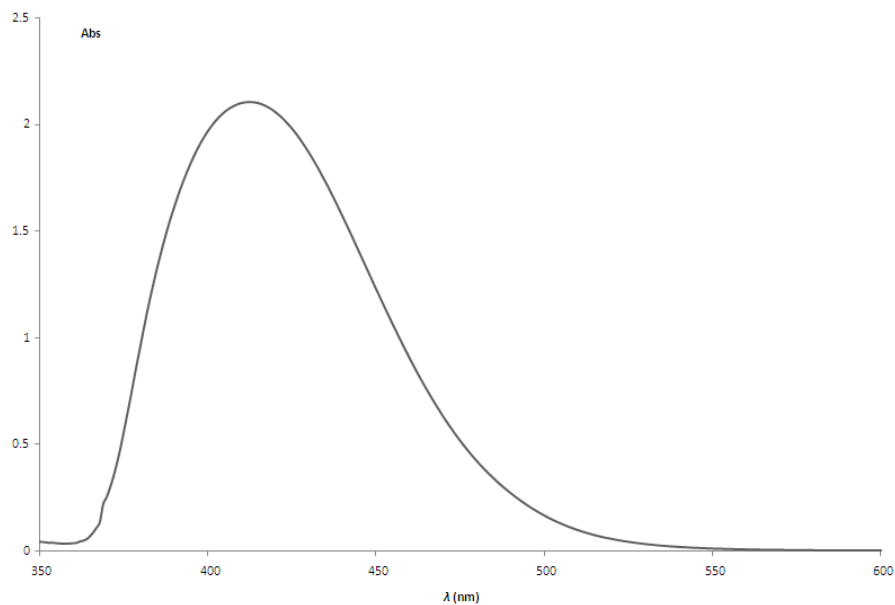

Figure A.E.7. Absorbance spectrum of a modified chitosan (sample GC-NAC 10).
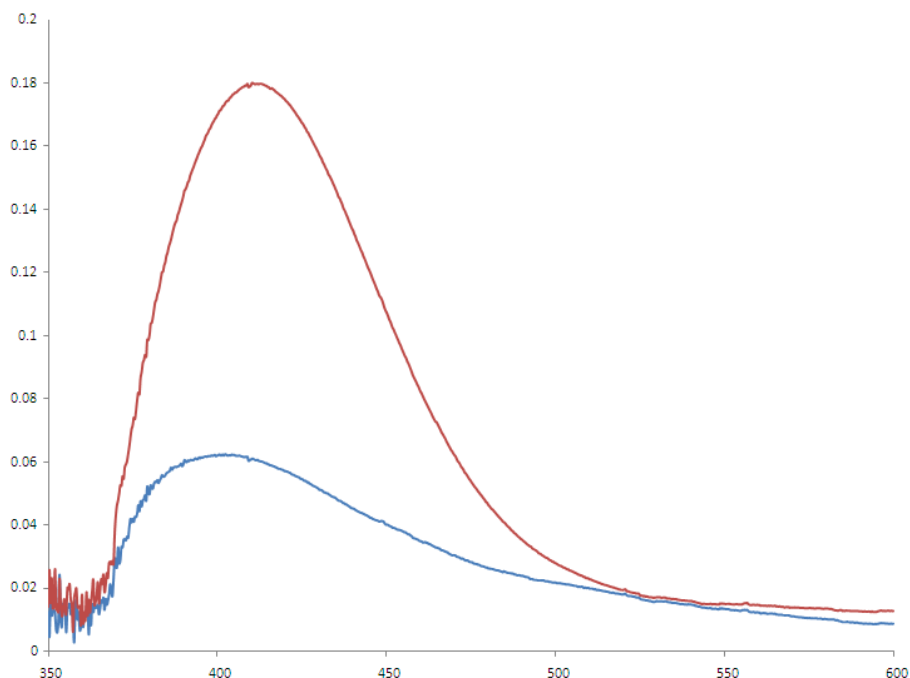
Figure A.E.8. Absorption spectra of irradiated (blu line) and not irradiated (red line) bilayer on PS NPs.

A.E.10. Sodium Alginate modification with allylamine

The first two attempts were carried out without HOBt and with the same molar concentration of sodium alginate, allylamine and EDC. In the first case, (AlgP1), EDC was added to sodium alginate before adding allylamine whereas in the second case, (AlgP2), after adding allylamine and the modification degree in both cases was low as quantified by NMR. Actually, a marked increase in functionalization was obtained with the use of HOBt together with EDC coupling agent, as it was for chitosan functionalization. Alginate and allylamine were dissolved together at different molar concentrations (30:1 molar ratio in AlgP3, 10:1 in AlgP4 and AlgP6). The pH was adjusted to a 6.8 value with the use of HCl and NaOH. The EDC/COO⁻ ratio was 4:1 for samples AlgP3, AlgP4 and AlgP6, while HOBt/COO⁻ ratio was mantained 4:1 as summarized in **Table A.E.7**. The only difference between AlgP4 and AlGP6 is due to the higher dilution of reagents in water as also reported in the table. The 6.8 pH was chosen as good compromise for activated ester formation (the optimal pH for EDC reaction would be around 5) and deprotonated allylamine reaction (the more the pH the lower the protonation at NH_3^+ of allylamine respect to NH_2 that is much more reactive with ester).

Alginate sample	HOBt:Allylamine:Alginate:EDC (molar ratio of functional groups)	Alginate concentration	pH of reaction	Degree of functionalization
AlgP1	0:3:1:2	10mg/ml	4-6	~10%
AlgP2	0:3:1:2	10mg/ml	5	~8%
AlgP3	4:30:1:4	3mg/ml	6.8	~40%
AlgP4	4:10:1:4	10 mg/ml	6.8	~62%
AlgP6	4:10:1:4	5mg/ml	6.8	~ 71 %

Table A.E.7. Alginate functionalization: conditions of reaction and degree of functionalization.

A.E.11. Preparation of oil core silica shell nanocapsules

As anticipated in the first chapter, NEs were also used in this work to build hybrid organic inorganic nanocapsules. In particular, once prepared a bilayer with chitosan and heparin it was functionalized with 3-(aminopropyl)triethoxysilane (APTS) and then TEOS was added to allow the synthesis of a silica shell. The functionalization of heparin with APTS was ment to ensure silica synthesis just around oil based template. Oil core can embed tracers for imaging while silica shell which is a biocompatible interface can be used to insulate such tracers. Indeed some people can be allergic to tracers and exposure of body to them can cause in the worst case to death. On the other side silica shell could be used also as drug delivery where the function of the silica in that case would be the protection of the inner oil core and drug [**135**]. A remarkable advantage of inorganic NCs, as anticipated, is that they are more resistant than polymer to environment conditions such as temperature pH and so on.

In terms of procedure it was prepared a primary emulsion based on L1 formulation. Chitosan was deposited at a final concentration of 0.01 % wt (at pH=4) whereas oil concentration was 1 % wt. Bilayer was prepared by mixing 4 ml of mono layer to 2.5 ml of heparin (0.044 % wt). After bilayer preparation heparin was activated with (APTS). Precisely, first 50 µl of EDC and NH_3 solution (with 1.23 mg EDC and 8.61 mg NH_3 per 1 ml of water) and then 50 µl of APTS solution (with 3.5 µL of APTS per ml of 2-proponol), were added to 1 ml of bilayer at 4°C in ice bath. After 15 min under stirring silica synthesis was started by adding to the dispersion first 2.3 ml of NH3 solution (18.5 µl of NH_3) in 2-propanol and then, dropwise, 2.3 ml of tetra ethyl orthosilicate (TEOS) solution (13.8 µL of TEOS).

In **Figure A.E.9** TEM images are reported as preliminary results on this kind of nanocapsules. It is possible to appreciate monodispersion (**Figure A.E.9.A)** and nanometric shell thickness (**Figure A.E.9.B**). In the analysis carried out and shown in upper part, samples were treated with osmium vapour to mark the inner oil core which indeed appears dark black.
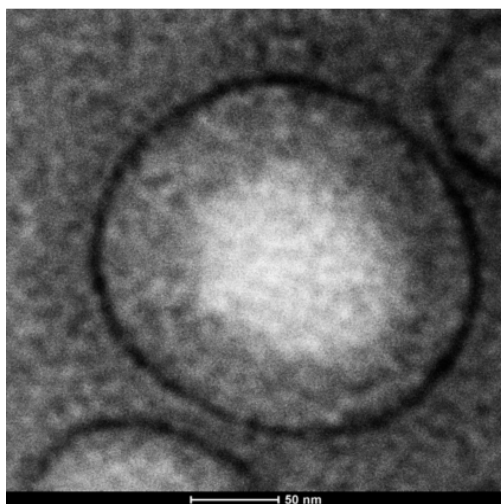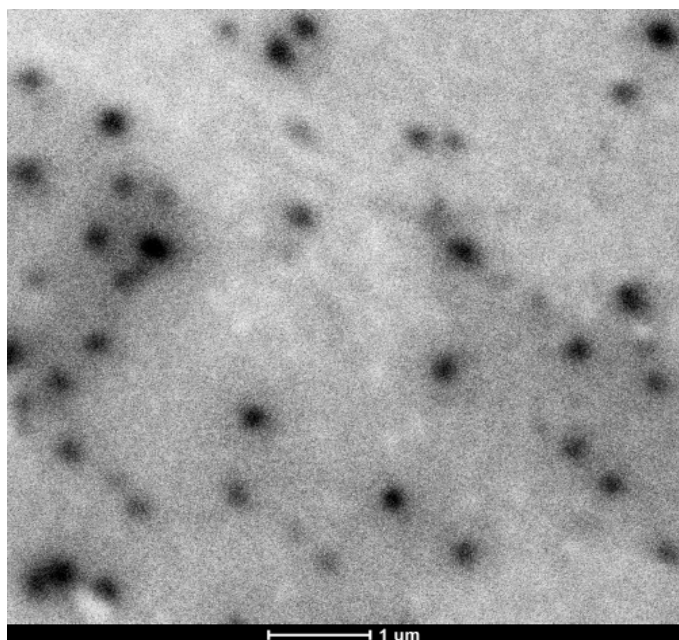

Figure A.E.9. TEM analysis of oil core based silica nanocapsules stained with osmium (top); magnified TEM image of one silica capsule (bottom) not stained.

A.I. Instruments

A.I.1. Immersion sonicator

One of the equipments used in the preparation of the pre-emulsions is the immersion sonicator. In **Figure A.I.1** it is reported the one used in the thesis which was the Ultrasonic Processor VCX500 Sonic and Materials.

Figure A.I.1. Picture of the Ultrasonic Processor VCX500 Sonic and Materials.

The ultrasonic power supply converts 50/60 Hz line voltage to high frequency electrical energy transmitted to the piezoelectric transducer within the converter, where it is changed to mechanical vibrations. The vibrations from the converter are intensified by the probe, creating pressure waves in the liquid. This action forms millions of microscopic bubbles which expand during the negative pressure excursion, and implode violently during the positive excursion. This phenomenon, referred to as cavitation, creates millions of shock waves in the liquid, as well as elevated pressures (about 500 atm) and temperatures (about 5000 °C) at the implosion sites. Although the cavitational collapse lasts a few microseconds and the amount of energy released by each individual bubble is minimal, the cumulative effect causes extremely high levels of energy to be released into the liquid. Temperature is monitored therefore if a pre-fixed threshold is overcome, sonication will stop. To avoid this condition it is possible to alternate pulse off and/or more effectively create an ice jacket to improve heat dissipation and keep temperature below the threshold. The Ultrasonic Processor is designed to deliver constant amplitude. As the resistance to the movement of the probe increases, additional power will be delivered by the

power supply to ensure that the excursion at the probe tip remains constant. Furthermore, the amplitude control allows the ultrasonic vibrations at the probe tip to be set to any desired level.

Probes consist of two sections each having different cross-sectional areas. Brought to resonant frequency, the probe expands and contracts longitudinally about its center. Amplification factor increases with the mass ratio between the upper section and the lower section. Probes with smaller tip (**Figure A.I.2.A**) diameters produce greater intensity of cavitation, but the energy released is restricted to a narrower, more concentrated field. Conversely, probes with larger tip (**Figure A.I.2.B**) diameters produce less intensity, but the energy is released over a greater area.
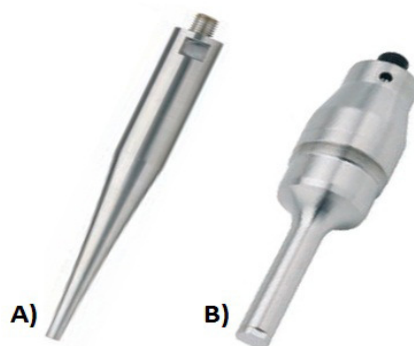
Figure A.I.2. Small (A) and large (B) types of probes.

High gain probes produce higher intensity than standard probes of the same diameter, and are usually recommended for processing larger volumes. Probes are fabricated from high grade titanium alloy Ti-6Al-4V because of its high tensile strength, good acoustical properties at ultrasonic frequencies, high resistance to corrosion, low toxicity, and excellent resistance to cavitation erosion. They are autoclavable and available with threaded ends to accept replaceable tips, microtips and extenders.

A.I.2. M-110PS series Microfluidizer

For the preparation of primary emulsions and for the re-dispersion of secondary emulsions it was used the Microfluidics M-110PS Series Microfluidizer (**Figure A.I.3**) that is a high pressure homogenizer designed for the high-performance micro-mixing of emulsions and dispersions.
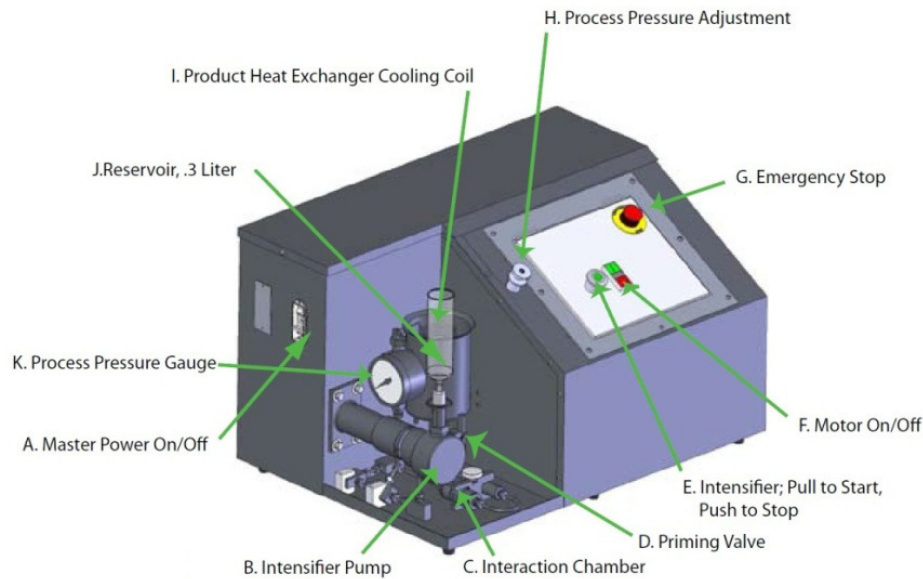
Figure A.I.3. Microfluidics M-110PS Series Microfluidizer.

The main components of the M-110PS model are following listed:

- the hydraulic power system, which supplies pressurized hydraulic oil to an intensifier pump;
- the intensifier pump which amplifies the hydraulic pressure and transfers it to liquid pressure in the process stream allowing pressure values as high as 2000 bar. During the suction stroke, the intensifier pump draws emulsion or dispersion from the inlet reservoir into the pressure chamber via the inlet check valve, which closes during the power stroke
- the interaction chamber which is where size reduction occurs; the emulsion or the dispersion is accelerated to a high velocity (up to 400 m\s) with shear rates approaching 10^7 s^{-1} therefore it is subjected to high forces capable to reduce size;
- a possible auxiliary processing module (APM) in series with the operation chamber and so called back pressure chamber which allows smooth reduction of pressure. This can be useful both for de-aggregation and to minimize risk of chamber breakage in consequence of a cavitation event due to undesired presence of air bubbles combined with sharp reduction of pressure at the exit of channel of the operation chamber.

- a possible cooling coil which cools the product back to ambient temperature or lower if surrounded by a liquid refrigerator as it exits from the interaction chamber. This can preserve the product from possible thermal degradation.

The operating principle is schematized in the following **Figure A.I.4**.
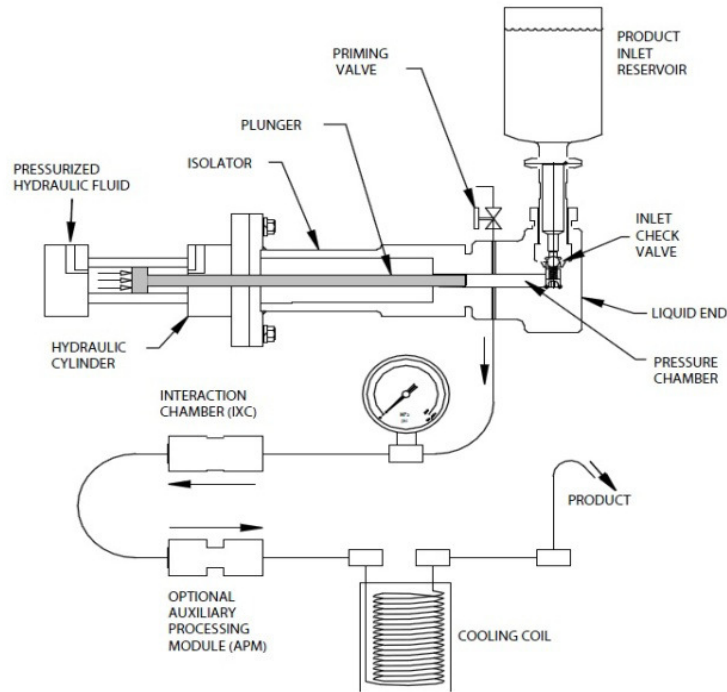
Figure A.I.4. Operating principle of M-110P Microfluidizer.

The schemes of a y and z chambers are following reported (**Figure A.I.5** and **Figure A.I.6**).
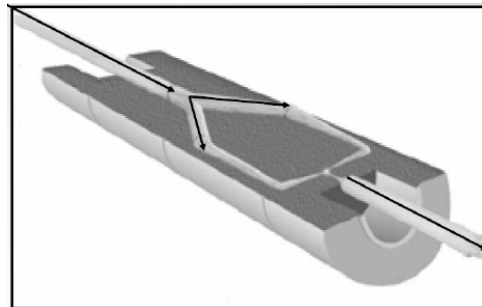
Figure A.I.5. Y-shaped interaction chamber: the pressurized emulsion stream enters the y-shaped interaction chamber and is split into two channels which then join in a central area where the impact allows the dispersed phase to reduce its size.
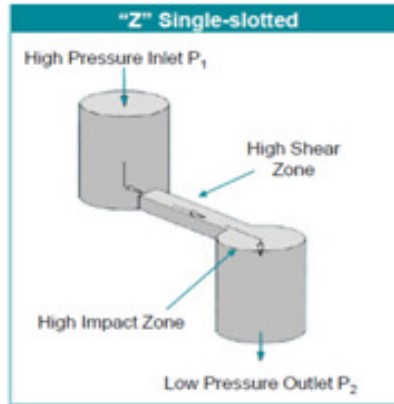
Figure A.I.6. Z-shaped interaction chamber: the pressurized fluid impacts against a stiff surface always at high speed, related to both the pressure and the section decreasing of the channel at the impact zone.

The channels of the chambers are made of zirconia or diamond. Typically diamond enhances the lifetime in terms of wear reduction and is particularly suggested for solid dispersions. In terms of sizes, in the case of y chamber the channel has a lateral size of 100 μm and a vertical size ranging from 75 to 100 μm whereas in the case of z chamber the channel has a lateral dimension of 100 μm and a vertical dimension ranging from 87 to 500 μm. For large scale productions multi-slotted chambers with channels in parallel are available.

A.I.3. Dynamic Light Scattering

Mean size, size distribution, given by the PDI, and Z-potential were measured by Zetasizer Nano Series, purchased from Malvern, using the DLS technique (**Figure A.I.7**).

Figure A.I.7. Zetasizer nano series.

A dynamic light scattering system, as schematized in **Figure A.I.8**, comprises six main components. Firstly, a laser (1) provides a light source to illuminate the sample contained in a cell (2). For dilute concentrations, most of the laser beam passes through the sample, but some is scattered by the particles within the sample at all angles. A detector (3) is used to measure the scattered light at one of different angles (for example 173° or 90° and so on). The intensity of scattered light must be within a specific range for the detector to successfully measure it. If too much light is detected, then the detector will become saturated. To overcome this, an attenuator (4) is used to reduce the intensity of the laser source and hence reduce the intensity of scattering. For samples that do not scatter much light, such as very small particles or samples of low concentration, the amount of scattered light must be increased. In this situation, the attenuator will allow more laser light through to the sample.
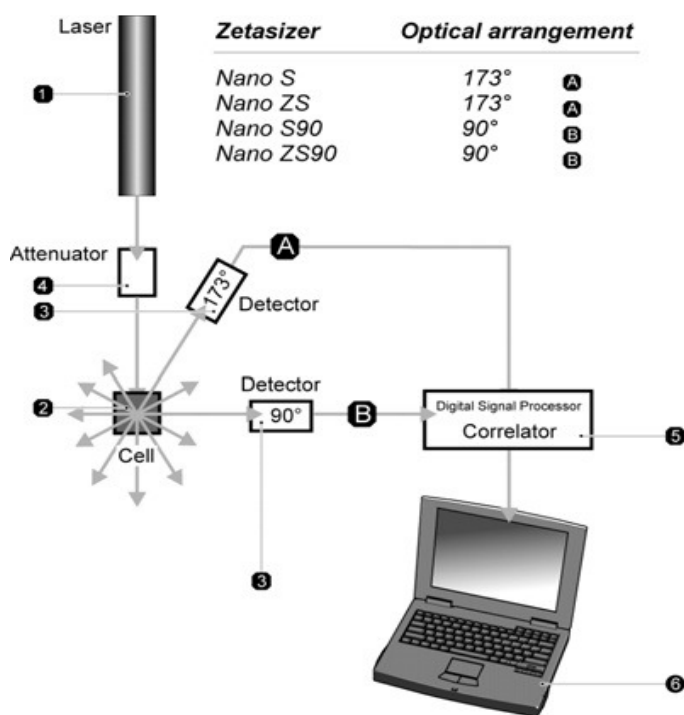
Figure A.I.8. Configuration of a dynamic light scattering system.

The appropriate attenuator position is automatically determined by software and covers a transmission range of 100% to 0.0003%. The scattering intensity signal from the detector is passed to a digital processing board called correlator (5). The correlator compares the scattering intensity at successive time intervals to derive the rate at which the intensity is varying. This

information, so called correlation function, coming from the correlator is then passed to a computer (6), where the software will analyze the data.

A.I.3.1. Particle size measurements

 DLS (sometimes referred to as photon correlation spectroscopy or quasi-Elastic light scattering) technique measures the size of particles typically in the sub micron region. Particularly, it measures Brownian motion and relates this to the size of the particles. Brownian motion is the random movement of particles due to the bombardment by the solvent molecules that surround them. The larger the particle, the slower the Brownian motion is. Smaller particles are "kicked" further by the solvent molecules and move more rapidly. An accurately known temperature is necessary for DLS because knowledge of the viscosity is required. Moreover, temperature also needs to be stable otherwise convection currents in the sample will cause non-random movements that will prevent the correct interpretation of size. The size of a particle is calculated from the translational diffusion coefficient by using the Stokes-Einstein equation:

$$d(H) = \frac{KT}{3\pi\eta D}$$

 where d(H) is the hydrodynamic diameter, D is the translational diffusion coefficient, k is the Boltzmann's constant, T is the absolute temperature and η is the viscosity. The diameter that is obtained by this technique is the diameter of a sphere that has the same translational diffusion coefficient as the particle. The translational diffusion coefficient will depend not only on the size of the particle "core", but also on any surface structure, as well as the concentration and type of ions in the medium. Any change to the surface of a particle that affects the diffusion speed will correspondingly change the apparent size of the particle.

 A real system is made of different sizes therefore the size given from the calculation is an average size (also known as the "cumulants mean"). The polydispersity of the system can be more or less wide; a parameter that provides this information is the polydispersity index (PDI). Both average size and PDI are given by cumulant analysis. It is the fit of a polynomial to the log of the G1 correlation function:

 Ln [G1] = a + bt +ct^2+dt^3 +et^4 + ...

The value of b is known as the second order cumulant, or the z-average diffusion coefficient. This is converted to a size using the dispersant viscosity and some instrumental constants. The coefficient of the squared term, c, when scaled as $2c/b^2$ is the PDI. It corresponds actually to the square of the standard deviation divided by the square of the average size.

Only the first three terms a, b, c are used in the standard analysis to avoid over-resolving the data; however this means that the average size is likely to be interpreted incorrectly if the distribution is very broad (i.e. has a high polydispersity). Conversely, if polydispersion is very low, the distribution can be considered monodisperse. More precisely according to the standards of the National Institute of Standards and Technology (NIST) "particle distribution may be considered monodisperse if at least 90% of the distribution lies within 5% of the median size".

As previously mentioned, the Zetasizer nano series system detects the scattering information at 173°. This is known as backscatter detection (**Figure A.I.9**).
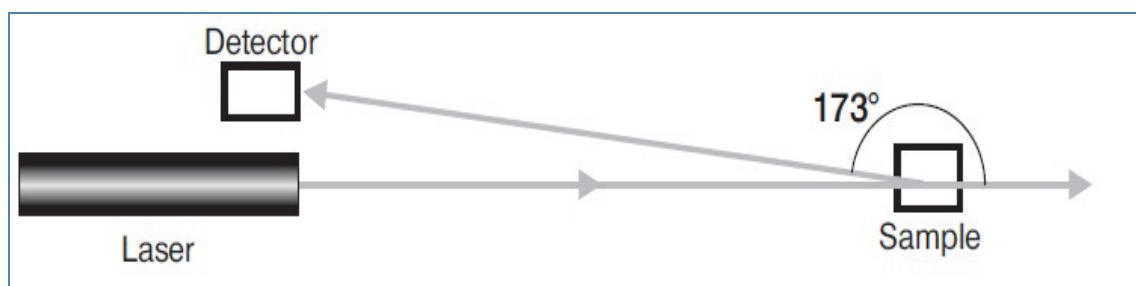
Figure A.I.9. Backscatter detection.

In addition, the optics are not in contact with the sample and hence the detection optics are said to be non invasive. There are several advantages in using non-invasive backscatter (NIBS) detection. For example, high concentrated samples can be measured due to the fact that the laser does not have to travel through the entire sample therefore multiple scattering, where light from one particle is itself scattered by other particles, is reduced. Then, the effects of dust are greatly reduced. Indeed, large particles mainly scatter in the forward direction therefore not detected by using backscatter detection. Finally, the measurement position within the cuvette of the Zetasizer can be changed by moving the focusing lens and is determined automatically by the software. For small particles, or samples at low concentrations, it is beneficial to maximize the amount of scattering from the sample moving the measurement point away from the cuvette wall towards the centre of the cuvette (**Figure A.I.10.A**). Conversely, large particles or samples at high

concentrations scatter much more light. In this situation, measuring closer to the cuvette wall will reduce the effect of multiple scattering by minimizing the path length over which the scattered light has to pass (**Figure A.I.10.B**).
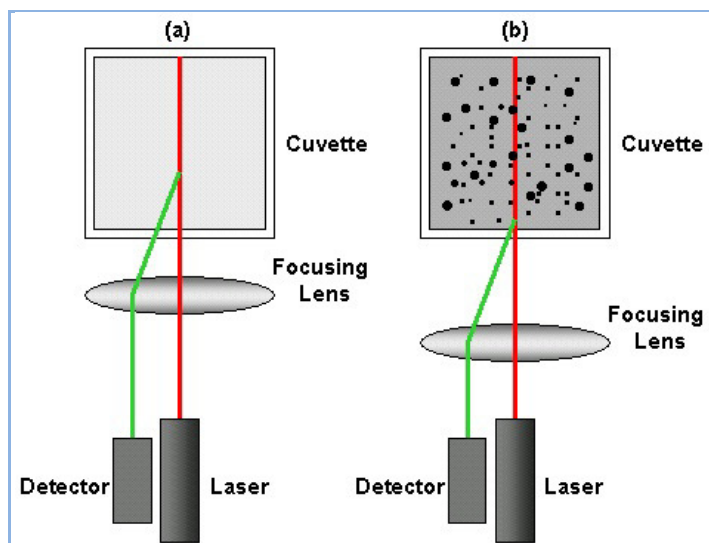
Figure A.I.10. Schematic diagram showing the measurement position for (a) small, weakly scattering samples and for (b) concentrated, opaque samples.

It is also worth making some other considerations. First it is necessary that particles are small compared to the wavelength of the laser used (typically less than d = λ/10), so that the scattering from a particle illuminated by a vertically polarized laser will be essentially isotropic, i.e. equal in all directions. Laser can be of various types, according to the wavelength desired for the experiment, in our case it is a He-Ne laser at a wavelength of 633 nm. Second, it is important to consider the Rayleigh approximation which tells us that $I \propto d^6$ and also that $I \propto 1/\lambda^4$ where I is the intensity of light scattered, d is the particle diameter and λ is the laser wavelength. Therefore a 50 nm particle will scatter light 10^6, in other words one million times, more than a 5 nm particle. The inverse relationship to λ^4 means that a higher scattering intensity is obtained as the wavelength of the laser used decreases.

A.I.3.2. Particle Z-potential measurements

Zeta potential is a physical property which is exhibited by any particle in suspension and is related to the surface charge of the particle itself. This charge at the particle surface affects the

distribution of ions in the surrounding interfacial region, resulting in an increased concentration of counter ions (ions of opposite charge to that of the particle) close to the surface. Thus an electrical double layer exists around each particle (**Figure A.I.11**).
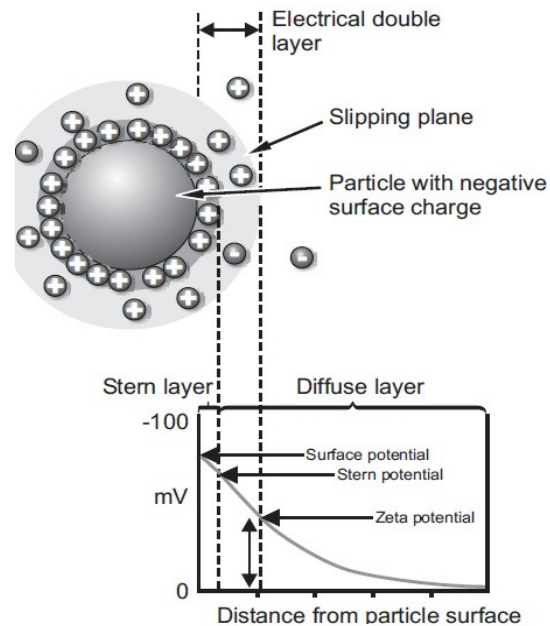
Figure A.I.11. Schematic illustration of Z-potential.

The liquid layer surrounding the particle exists as two parts; an inner region, called the Stern layer, where the ions are strongly bound and an outer, diffuse, layer where they are less firmly attached. Within the diffuse layer there is a notional boundary inside which the ions and particles form a stable entity. When a particle moves (e.g. due to gravity), ions within the boundary move with it, but any ions beyond the boundary do not travel with the particle. This boundary is called slipping plane and is the distance at which it is determined the z-potential.

It has long been recognized that the zeta potential is a very good index of the magnitude of the interaction between colloidal particles and measurements of zeta potential are sometimes used to assess the stability of colloidal systems. If all the particles in suspension have a large negative or positive zeta potential then they will tend to repel each other and there will be no tendency for the particles to come together. However, if the particles have low zeta potential values then there will be no force to prevent the particles coming together and flocculating. The dividing line between stable and unstable suspensions is generally taken at either +30 or -30 mV. Particles

with zeta potentials more positive than +30 mV or more negative than -30 mV are normally considered stable. However, if the particles have a density different from the dispersant, they will eventually sediment forming a close packed bed (i.e. a hard cake).

One of the most important factors that affect the z-potential is the pH of the sample. A zeta potential value on its own without defining the solution conditions is a virtually meaningless number. For instance, if we consider a particle in suspension with a negative zeta potential, by adding alkali to this suspension then the particles tend to acquire more negative charge whereas, by adding acid to this suspension then a point will be reached where the charge will be neutralized. Further addition of acid can cause a building up of positive charge. There may be a point where the zeta potential passes through zero. This point is called isoelectric point and is practically very important being normally the point where the colloidal system is least stable.

Also ions in solution can affect the zeta potential. They can interact with charged particle surfaces in one of two distinct ways:

1)   non-specific ion adsorption where they have no effect on the isoelectric point;

2)   specific ion adsorption, which will lead to a change in the value of the isoelectric point.

The specific adsorption of ions onto a particle surface, even at low concentrations, can have a dramatic effect on the zeta potential of the particle dispersion. In some cases, specific ion adsorption can lead to charge reversal of the surface.

The Zetasizer Nano series calculates the zeta potential by determining the electrophoretic mobility and then applying the Henry equation. The electrophoretic mobility is obtained by performing an electrophoresis experiment on the sample and measuring the velocity of the particles using Laser Doppler Velocimetry (LDV).

An important consequence of the existence of electrical charges on the surface of particles is that they will exhibit certain effects under the influence of an applied electric field. When an electric field is applied across an electrolyte, charged particles suspended in the electrolyte are attracted towards the electrode of opposite charge (**Figure A.I.12**).
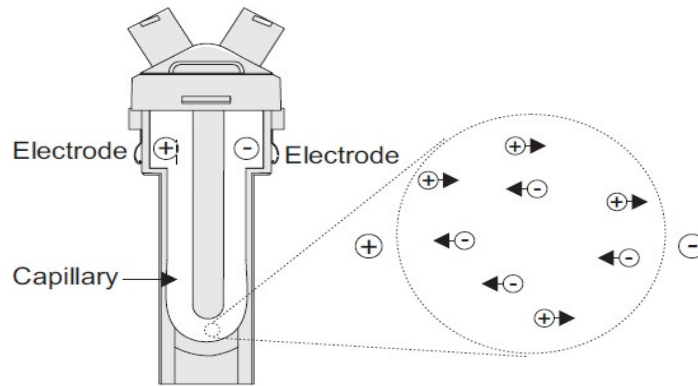
Figure A.I.12. Zetasizer cell with electrodes at either end to wich a potential is applied.

Viscous forces acting on the particles tend to oppose this movement. When equilibrium is reached between these two opposing forces, the particles move with constant velocity. The velocity of the particle is dependent on strength of electric field or voltage gradient, the dielectric constant of the medium, the viscosity of the medium and the Zeta potential. The velocity of a particle in an electric field is commonly referred to as its electrophoretic mobility. With this knowledge it is possible to obtain the zeta potential of the particle by application of the Henry equation:

$$U_E = \frac{2 \; \varepsilon \; z \; f(K_a)}{3\eta}$$

where z is the zeta potential, U_E the electrophoretic mobility, ε the dielectric constant, η the viscosity and f(Ka) the Henry's function. Two values are generally used as approximations for f(Ka): 1.5 when electrophoretic determinations of zeta potential are made in aqueous media with a moderate electrolyte concentration and 1.0 for small particles in low dielectric constant media.

Finally, to evaluate the electrophoretic mobility it is used the LDV. This is a well established technique to measure the velocity of particles moving through a fluid in an electrophoresis experiment. The light scattered at an angle of 17° respect to the incident beam is collected by the detector (**Figure A.I.13**). This produces a fluctuating intensity signal where the rate of fluctuation is proportional to the speed of the particles. A digital signal processor is used to extract the characteristic frequencies in the scattered light.
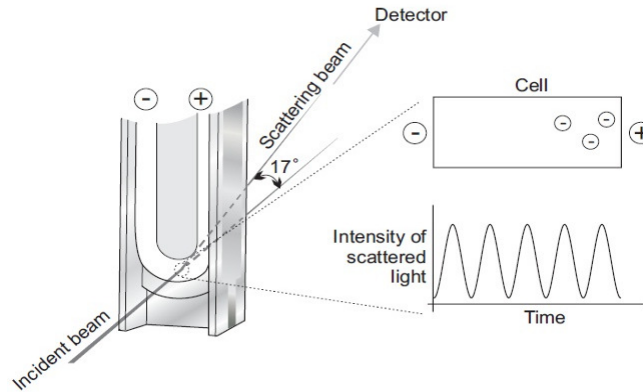
Figure A.I.13. Laser Doppler Velocimetry technique.

A.I.4. Confocal Microscopy

Confocal microscopy is an optical imaging technique invented by Marvin Minsky in 1957 while he was trying to study neural networks to understand how brain learns and needed a way to image these connections in their natural state (in three dimensions) [**136**]. Today, confocal microscopy is widely used in many fields of science.

Illuminating and observing a sample, two physical processes significantly limit the sharpness of the observed image:

1)   by illuminating the entire sample, the light spreads in it disturbing the image of the focus plane: to solve this problem it is needed to illuminate only small areas of the sample.

2)   while it is possible to observe a focus plane of the sample, also the light reflected from the plans not in focus comes to the eyes, making a confusing picture: the revolutionary idea compared to conventional microscopy is to block as much as possible the information derived from the above and below planes to the desired through a small opening.

Confocal microscopy allows overcoming the limits of conventional optical microscopy such as resolution, focus and contrast. Indeed it significantly improves the image resolution at the expense of field of view [**137**]. Confocal microscope consists of a pinhole in input and in output, which is a shutter that allows to illuminate only a very limited part of the sample and to collect only light coming from it. The image therefore is not disturbed by unwanted reflections or fluorescences by the plans not in focus and the points of focus plane that are not observed. As it

is possible to see from the **Figure A.I.14**, the beam excitation passes through the illuminating pinhole, irradiating only a small region of the sample.
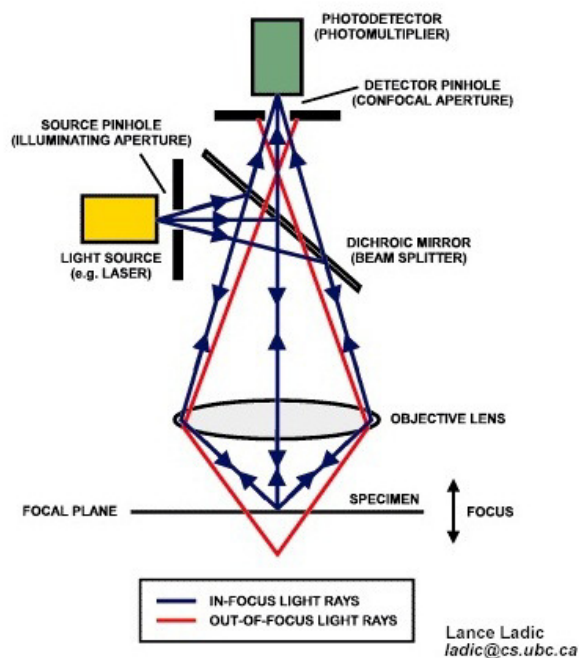
Figure A.I.14. Simplified optics of a Laser Scanning Confocal Microscope (LSCM).

   Before detection a second confocal aperture, a detector pinhole, reduces the contributions of the above and below planes to the focus. By scanning techniques, it is possible to study the entire sample surface. The fundamental principle of any scanning microscope is to illuminate a point of the sample at a time; the signal resulting from the interaction between the incident radiation and the sample is recorded and processed to form a reproduction of the sample to visualize. Compared to a conventional microscope that immediately provides the full image, with the confocal microscope the sample is probed point by point.

   In confocal microscopy, as excitation source it is often used a laser beam. This provides a high intensity and monocromatic light source. It is first filtered and attenuated so to use a correct intensity and proper excitation spectrum to produce fluorescence that is the emission of a secondary photon upon absorption of a photon of higher wavelength (**Figure A.I.15**) [**136**]. Most molecules at normal temperatures are at the lowest energy state, the so-called 'ground state'. Occasionally, a molecule may absorb a photon and increase its energy to the excited state. From here it can very quickly transfer some of that energy to other molecules through collisions (red)

and spontaneously emits the remaining energy by emitting a photon (green) with a lower wavelength to return to the ground state.
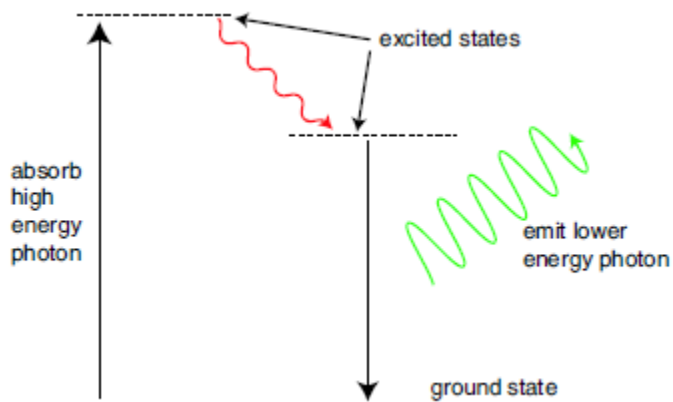
Figure A.I.15. Scheme of the fluorescence mechanism.

In fluorescence microscopy, fluorescent molecules, in order to increase the signal, are designed to be attached to specific parts of a sample, thus identifying them when imaged. Multiple fluorophores can be used to simultaneously identify different parts of a sample. There are two options when using multiple fluorophores:

1)   fluorophores can be chosen that respond to different wavelengths of a multi-line laser;

2)   fluorophores can be chosen that respond to the same excitation wavelength but emit at different wavelengths.

However one limit is about the presence of too many fluorophores near the surface of the sample that may absorb enough light to limit the one available to the rest of the sample. While the intensity of incident radiation can be increased, fluorophores may become saturated if the intensity is too high. Moreover, they can present photobleaching that is an irreversible fade when they are exposed to excitation light for a long time being able to emit only a limited number of photons. This may be due to reaction of the molecules' excited state with oxygen or oxygen radicals. Photobleaching can be limited by reducing the oxygen available or by using free-radical scavengers. Some fluorophores are more robust than others, so choice of fluorophore is very important.

The confocal microscope used in this work was the version capable to perform also STED - which technique will be described in the next paragraph- that is a Leica TCS STED-CW microscope (Leica-Microsystems, Mannheim, Germany).

A.I.5. Stimulated emission depletion microscopy

STED microscopy, is a fluorescence microscopy technique that uses the non-linear de-excitation of fluorescent dyes to overcome the resolution limit imposed by light diffraction [138]. As previously described, the resolution of a confocal microscope is limited to the spot size to which the excitation can be focused. This size depends on system parameters, but is limited by approximately half the wavelength of the light used (for example at about 200 nm if a blue light is used). Within the STED microscope the diffraction limit is surmounted by switching off dye molecules by means of a targeted strong de-excitation mechanism. Super resolutions beyond the diffraction limit can be achieved as shown in **Figure A.I.16**.
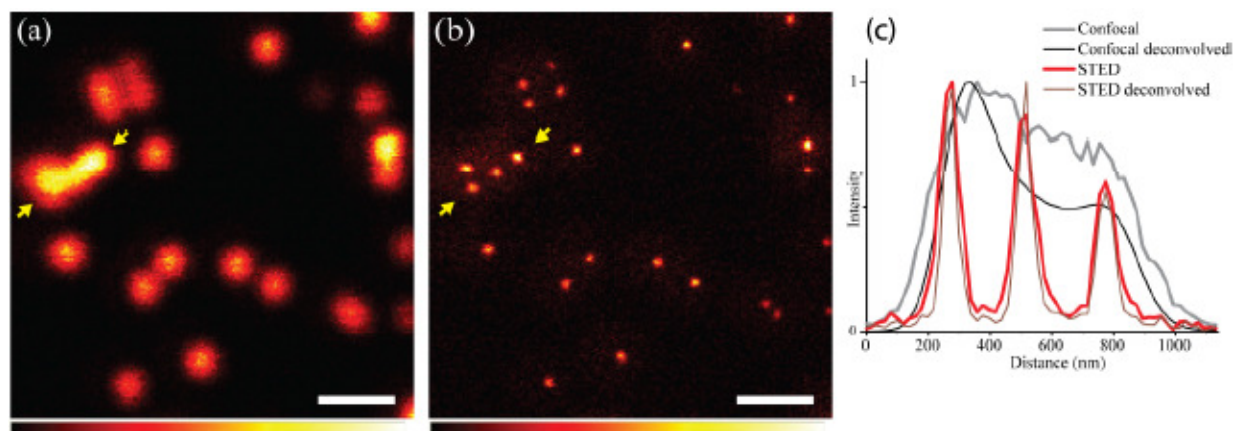
Figure A.I.16. The Comparison of the confocal (a) and the STED (b) image demonstrates the superior resolution of STED microscopy. Scale bar 0.5μm.

STED microscopy uses fluorescent dyes to label specific sites of a sample (such as Alexa 488, FITC Oregon Green and established fluorescent proteins such as yellow fluorescent protein (YFP)). Such dyes can be excited by light of certain wavelengths. Instead of spontaneous relaxation and fluorescence emission, the molecules of the sample can also return to their ground state by stimulated emission (**Figure A.I.17**) [139].
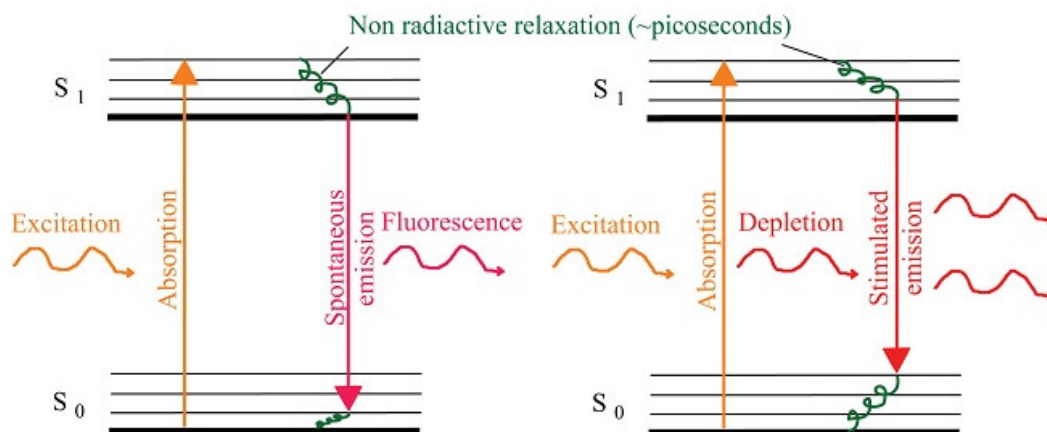
Figure A.I.17. Spontaneous emission (left), stimulated emission (right) by adding a depletion laser.

The fluorophore at S_1 can absorb a depletion photon, and go back to S_0 by releasing two photons that have the same wavelength as the absorbed one. Since it is possible to precisely control the wavelength of stimulated emission output, it can be chosen significantly different from the typical wavelength of fluorescence (to avoid interferences with absorption and emission). Therefore the sample is excited with two spot lasers, one useful for spontaneous emission (**Figure A.I.18.a**) and one centered to this spot (**Figure A.I.18.b**) useful for depletion. Of course the objective is to deplete only a ring of the sample to keep the center part useful for emission (**Figure A.I.18.c**). To do that the de-excitation spot has a shape of a doughnut obtained by making pass the laser through a lens with an optical vortex which reduces the intensity of the laser in the central part (**Figure A.I.19**). This reduction can be decided by the rotation of this lens therefore tuning the final resolution of the analysis.
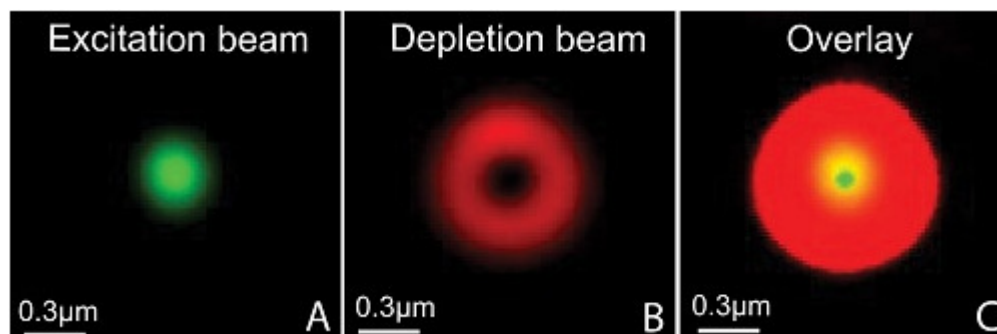
Figure A.I.18. Excitation spot (A), doughnut-shaped de-excitation spot (B) and overlay with small green spot allowing fluorescence (C).
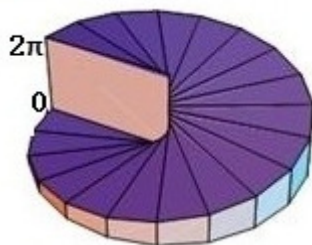
Figure A.I.19. Optical vortex to create doughnut-shaped de-excitation spot.

Therefore structures which are smaller than the diffraction-limit can be made visible with STED and resolution can easily reach 70 nm with conventional equipments and go below this size with some optimization in terms of instrument and choice of phluorophores.

A.I.6. Transmission electron microscopy

TEM operates on the same basic principles as the light microscope but using electrons as light source [**140**]. Electrons have much lower wavelength than light, which makes possible to get a resolution of thousand times better than with a light microscope. By means of TEM it is possible to observe objects at nanometer resolution and for this reason electron microscopy is a powerful technique in medical, biological and materials science. After electrons are emitted from the electron gun, they travel over a vacuum column and pass through electromagnetic lenses that focus the electrons into a very thin beam that then travels to the sample. The objective lenses and the projector lenses magnify the transmitted beam and project it onto the fluorescent viewing screen. Impact of electrons excites the screen and produces a visible magnified image of the sample. This image is recorded with a CCD camera. Cryo-electron microscopy is a form of transmission electron microscopy where the sample is studied at cryogenic temperatures (generally liquid nitrogen temperatures). Indeed only in the early 80's it was demonstrated the possibility to produce vitreous ice by different means, such as high pressure freezing or flash freezing. This gave the possibility to develop Cryo-TEM technology, which represents a great opportunity for very delicate samples like biological samples as well as liquid dispersions or nano-capsules with a small shell around liquid core (like ours) thanks to the fact that they are fixed in their own environment. Sample has to be prepared in a very accurate way since a thin layer of liquid has to be frozen in cryogenic conditions on the TEM grid. To do that it was used

specific equipment, the VITROBOT of FEI, reported in **Figure A.I.20**. First the grid is mounted onto sharp tweezers then vitrification parameters are set by using the display of the VITRIBOT and the sample is put with a pipette on the grid which communicates from the back with a filter paper. It follows the blot of the sample to obtain a thin film typically sub micrometric and the grid is instantaneously immersed in the cryogenic liquid.

Figure A.I.20. Picture of the VITROBOT (right) and magnification of the pistons used for sample blotting (left).

So the grid is ready to be mounted in the equipment. Transferring phase is also critical; indeed if the sample gets molten during this phase then it will freeze again in the sample holder of the TEM but this time not in a controlled way. Therefore the presence of abundant crystals will prevent a correct analysis.

In particular we used a Tecnai 12 electron microscope (Philips, Eindhoven, Netherlands) which is represented in the **Figure A.I.21**.

Figure A.I.21. Picture of the Tecnai 12 electron microscope.

A.I.7. Fluorescence Spectroscopy

Fluorescence occurs when a substance that has absorbed light or other electromagnetic radiation, emits light with different wavelength. The emission process can be explained on the basis of the different electronic states of the molecules called energy levels. If light is absorbed by a substance, the electronic state of the molecule changes from the ground electronic state (low energy state) to a one of the vibrational states of the excited electronic state. Excited molecule can collide with other molecules causing as a result lose of energy until the molecule reaches the lowest vibrational state of the excited electronic state, and finally, as consequence of collisions, the molecule drops again into one of the various vibrational levels of the ground electronic state, emitting a photon in the process. Because the molecules can drop in any of the different vibrational levels of the ground state, the emitted photons will have different energies and in consequence, different frequencies [**137**]. In this work, fluorescence spectroscopy was used to characterize the emission of chitosan labeled with FITC both as free polymer and in the case of secondary emulsion for comparison. In the following **Figure A.I.22** it is reported the EnSpire Multimode Plate Reader 2300-0000, Perkin Elmer used in this work.

Figure A.I.22. Picture of the spectrofluorimeter EnSpire Multimode Plate Reader 2300-0000, Perkin Elmer.

A.I.8. UV Visible

In some molecules and atoms, photons of UV and visible light have enough energy to cause transitions between the different electronic energy levels [**141**]. The wavelength of light absorbed is that having the energy required to move an electron from a lower energy level to a higher energy level. When light passes through or is reflected from a sample, the amount of light absorbed is the difference between the incident radiation (I_0) and the transmitted radiation (I). The amount of light absorbed is expressed as either transmittance or absorbance. Transmittance usually is given in terms of a fraction of 1 or as a percentage and is defined as $T=I/I_0$, whereas absorbance is defined as A=-logT.

For most applications, absorbance values are used since the relationship between absorbance and both concentration and path length normally is linear. The presence of an absorbance band at a particular wavelength often is a good indicator of the presence of a chromophore.

However, the position of the absorbance maximum is not fixed but depends partially on the molecular environment of the chromophore and on the solvent in which the sample may be dissolved. Other parameters, such as pH and temperature, also may cause changes in both the intensity and the wavelength of the absorbance maxima.

The equipment we have used is the Cary® 100/300 UV-Vis from Varian (**Figure A.I.23**).
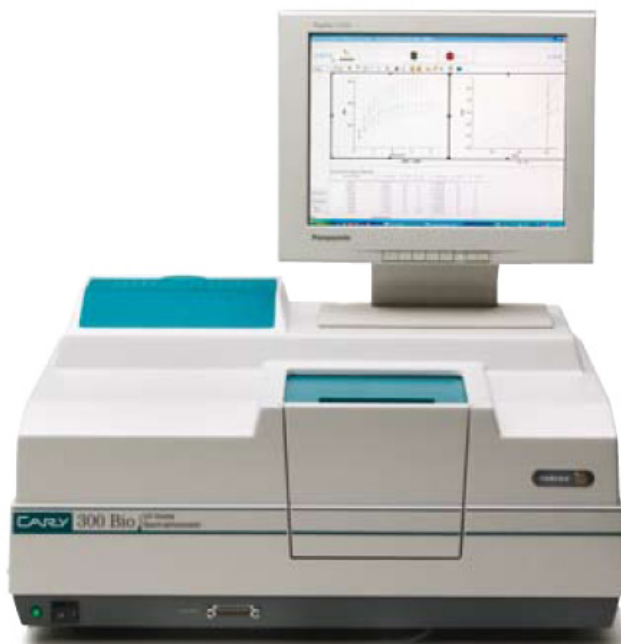
Figure A.I.23. Picture of the spectrophotometer Cary® 100/300 UV-Vis from Varian.

A.I.9. Thermogravimetric analysis

  TGA is a method in which changes in physical and chemical properties of materials are measured as a function of increasing temperature (with constant heating rate), or as a function of time (with constant temperature and/or constant mass loss). TGA is commonly used to determine selected characteristics of materials that exhibit either mass loss or gain due to decomposition, oxidation, or loss of volatiles (such as moisture). It is an especially useful technique for the study of polymeric materials, including thermoplastics, thermosets, elastomers, composites, plastic films, fibers, coatings and paints.

  In terms of apparatus, TGA relies on a high degree of precision in three measurements: mass change, temperature, and temperature change. Therefore, the basic instrumental requirements for TGA are a precision balance with a pan loaded with the sample, and a programmable furnace. The furnace can be programmed either for a constant heating rate, or for heating to acquire a constant mass loss with time. Regardless of the furnace programming, the sample is placed in a small, electrically heated furnace equipped with a thermocouple to monitor accurate measurements of the temperature by comparing its voltage output with that of the voltage-versus-temperature table stored in the computer's memory. A reference sample may be placed on

another balance in a separate chamber. The atmosphere in the sample chamber may be purged with an inert gas to prevent oxidation or other undesired reactions. **Figure A.I.24** represents the DSC/TGA - TA instruments SDT2960.

Figure A.I.24. Picture of the DSC/TGA - TA instruments SDT2960.

A.I.10. Nuclear magnetic resonance spectroscopy

NMR spectroscopy exploits the magnetic properties of certain atomic nuclei. It is used by chemists and biochemists to investigate the properties of organic molecules, though it is applicable to any kind of sample that contains nuclei possessing spin. When placed in a magnetic field, NMR active nuclei (such as ^{1}H or ^{13}C) absorb electromagnetic radiation at a frequency characteristic of the isotope.[142]. The resonant frequency (energy of the absorption) and the intensity of the signal are proportional to the strength of the magnetic field measured in Tesla. From the strength of the magnet (B_0) it is possible to evaluate the operating frequency ω_0 of the spectrometer by Larmor equation:

$$\omega_0 = \gamma B_0$$

where γ is the gyromagnetic ratio of the nucleus being tested.

From the formula it arises that a range of magnetic strengths between 1 and 21 Tesla corresponds to operation frequencies between 42.5 and 900 MHz. Typically the higher the operating frequency the higher the sensitivity. Indeed, it has to be considered that upon application of an external magnetic field, electrons surrounding the proton in covalent

compounds move in response to the field and generate local magnetic fields that oppose the much stronger applied field for the Lenz's law. This local field thus "shields" the proton from the applied magnetic field, which must therefore be increased in order to achieve resonance (absorption).

Moreover, given that the location of different NMR signals is dependent on the external magnetic field strength and the rf frequency, the signals are usually reported relative to a reference signal, usually that of TMS (tetramethylsilane). Additionally, being the distribution of NMR signals field dependent, these frequencies are divided by the spectrometer frequency. However, since we are dividing Hz by MHz, the resulting number would be too small, and thus it is multiplied by a million. This operation therefore gives a locator number called the "*chemical shift*" with units of parts per million. To detect such small frequency differences the applied magnetic field must be constant throughout the sample volume. High resolution NMR spectrometers use shims to adjust the homogeneity of the magnetic field to parts per billion (ppb) in a volume of a few cubic centimeters. "Shimming" refers to the process of adjusting a series of electromagnets to maximize the homogeneity of the magnetic field. Indeed, possible in-homogeneities cause broad peak in the NMR spectrum because nuclei from the top portion of the NMR tube have a different resonance frequency than nuclei from the bottom portion.

For what concerns quantitative part, via software it is possible to analyze the size of peaks to understand how many protons give rise to the peak. In particular, by integrating the peak it is possible to evaluate the number of protons, or any other observed nucleus, at least in the case of simple one-dimensional NMR experiments.

Some of the most useful information for structure determination in a one-dimensional NMR spectrum comes from *scalar coupling* between NMR active nuclei. This coupling arises from the interaction of different spin states through the chemical bonds of a molecule and results in the splitting of NMR signals. These splitting patterns can be complex or simple and, likewise, can be straightforwardly interpretable or deceptive. This coupling provides detailed insight into the connectivity of atoms in a molecule. Coupling to n equivalent nuclei splits the signal into a n+1 multiplet with intensity ratios following Pascal's triangle. It has to be noted that coupling between nuclei that are chemically equivalent, or in other words with the same chemical shift, has no effect on the NMR spectra. At the same way, couplings between nuclei that are distant

(usually more than 3 bonds apart for protons in flexible molecules) are usually too small to cause observable splittings.

In particular, the NMR used to analyze modified chitosans and alginates structures was a DRX 600 Bruker NMR spectrometer (**Figure A.I.25**).

Figure A.I.25. Picture of the Bruker 600 MHz NMR spectrometer.

In general, nuclear magnetic resonance spectroscopy can be used not only to study the structure of molecules but also the interaction of various molecules, the kinetics or dynamics of molecules and the composition of mixtures of biological or synthetic solutions or composites. NMR's advantage is the unique ability of a nuclear spectrometer to allow both the non-destructive and the quantitative study of molecules in solution and in solid state, as well as to enable the study of biological fluids.

Conclusions

Nowadays, nano-bio-technology is emerging as promising strategy to improve biodistribution of bioactive substances such as nutrients, drugs, therapeutics as well as tracers for diagnostics by means of engineered NCs which have to respect several specifications in terms of safety, loading capability, average size, monodispersion, multifunctionality and cost optimization depending on the kind of market.

Therefore, in this work we developed NCs made of completely biocompatible and biodegradable materials (vegetal oil, egg lecithin, polysaccharides like chitosan, heparin and sodim alginate) with final objective to build up NCs with no side effects by their own.

Moreover, we developed NCs with up-gradable complexity, in order to be able to engineer NCs suitable not only in terms of properties but also in terms of cost, depending on the final market specifications. To do that we started from the optimization of primary emulsions (in terms of size and PDI) made of soy-bean oil stabilized by a layer of chitosan (secondary emulsion) and then we used the layer by layer technique to build up more and more complex nanocapsules. From one side the oil core guaranties high loading capability of lipophilic bioactive molecules which are the most powerful ones but difficult to distribut into the body and from the other side layer-by-layer is recognized as the most controlled way to buil up multi-functional polymer shells (e.g. tunable thickness, tunable permeability, targeting properties, diagnostics capability, insulation of molecules or NPs between layers and so on).

The most original aspect of this work was to effectively combine the use of oil core and the layer by layer technique. Indeed, the layer by layer typically uses solid cores that are much monodisperse and stable than nanoemulsions. Instead, we were able to effectively use oil core templates by means of some original findings made during the path of the thesis also useful for a better exploitation of nanoemulsions as product ready to go on the market by their own.

We demonstrated that secondary emulsions showing unparalleled long-term stability can be produced with a control in size depending on the formulation (down to 100nm), and PDI (≤ 0.1), thanks to the implementation of a novel multi re-dispersion process. In particular, we showed

that, in order to get very stable secondary emulsions, a specific concentration is not sufficient, as it must be combined with an optimized post-process. Such process was indeed identified as a multi-re-dispersion over time by homogenizing at medium pressure (around 700 bar) which had to be combined with polymer concentrations typically excluded due to flocculation. Thanks to the re-dispersion we were able to uniform the system and obtain ultrastability with no flocculation. Such unique stability represents an adding value for nanoemulsions which by their own with affordable cost could be exploited in the emerging field of nutraceuticals. Multi-processed secondary emulsions at high concentrations (> 0.1%) were also proved to satisfy USP specifications even after several months, unlike bare emulsions which make these nanoemulsions also suitable in pharmacopeia.

Moreover, we investigated the saturation regime by employing a novel in fluorescence approach, with new insights on the evolution of the polymer deposition around primary emulsions. Indeed, with this new approach we demonstrated that saturation is a relative concept. More precisely, we noticed that there is always equilibrium between polymer on oil surface and polymer in solution even at very low polymer concentrations, and only at very high concentrations there is a real complete coverage of the emulsion which guaranties ultrastability (if not associated to flocculation). However, an optimal concentration corresponding to an almost complete coverage and no significant excess of polymer in solution can be identified by the proposed approach thanks to the presence of a clear peak in fluorescence.

For what concerns the preparation of polymer nanocapsules around oil in water nanoemulsions, we demonstrated not only the possibility to use secondary emulsions at the saturation concentration but also secondary emulsions in their ultrastability region. The latter is more advantageous considering that the liquid template is stable for more than one year compared to the few weeks of saturated emulsions. Its use was made possible after removal of the excess polymer by means of a nanobeads mediated fishing procedure. This procedure was also originally developed in during this thesis and it was made possible thanks to the monodispersion of the emulsion itself. Therefore, for the first time nanoemulsion can be stored and used like the solid ones but with all the well known advantages of oil templates like pre-loading with high payloads as well as stabilizing and carrying powerful lipophilic drugs. In addition, no harsh conditions are required to remove any solid template therefore the delicacy of the method allows the use of natural bio-polymers Moreover, due to the monodispersion and the small size down to

100nm these nanocapsules are also suitable for the EPR mechanism. In our opinion nanotechnology applied to drug delivery can highly benefit from the use of the proposed method offering a real alternative to the preparation of nanocapsules via solid core templating.

Both in the case of saturated or ultrastable emulsions it was demonstrated by fluorescence microscopy the capability to pre-load oil with lipophilic substances.

As known electrostatic interaction which link single polymer layers of the layer by layer nanocapsules can be easily weakened by certain physiological conditions (pH, oxidizing conditions). For this reason and also for a future aim to consolidate nanocapsules with shapes different from spheres in this thesis was also developed a thioene click chemistry reaction between polyelectrolytes modified with N-acethyl cysteine in the case of chitosan and allylammine in the case of heparine and sodium alginate. By adapting in an original way colorimetric Ellman test it was possible to evaluate cross-linkage efficiency between layers. Preliminary results on the stability over time of cross-linked and no cross-linked tri-layers show higher stability as expected in the first case.

Finally, it was also demonstrated capability to build up monodisperse oil core silica shell nanocapsules which could be exploited both in drug delivery and in diagnostics with the advantage of inorganic materials to be more resistant than polymers to environment conditions such as temperature, pH and so on. The synthetic strategy was based on a multi step process involving encapsulation of nanodroplets of oil in a bilayer of chitosan and heparin followed by in situ synthesis of silica by using TEOS as precursor. Since APTS was chemically linked to heparin this allowed formation reaction of TEOS and therefore formation of silica just around oil droplets. The inner core which is oil may include a variety of materials like high payloads of hydrophobic drugs, as well as fluorescent quantum dots (QDs), magnetic or gold NPs, among various other variants for drug delivery and multi-modal imaging. Therefore, we believe this is another innovative, low cost and effective way to produce new nanocarriers useful for nanomedicine.

Bibliography

[1] Jochen Weiss, Paul Takhistov, D. Julian McClements. *Functional Materials in Food Nanotechnology*, Journal of Food Science, 71(9):R107–R116, 2006.

[2] Pilar Rivera Gil, Loretta L. del Mercato, Pablo del_Pino, Almudena Muñoz_Javier, and Wolfgang J. Parak, *Nanoparticle-modified polyelectrolyte capsules*, Review Literature And Arts of the Americas, 3(3):12-21, 2008.

[3] Functional Food (2011)
http://www.wur.nl/UK/research/ResearchBlog/2010/11/01/foodphysics011110.htm [accessed June 2011].

[4] A Rajasekaran, G Sivagnanam and R Xavier, *Nutraceuticals as therapeutic agents: A Review*, Research J. Pharm. and Tech. 1(4): Oct.-Dec. 2008.

[5] Edgar Acosta, *Bioavailability of nanoparticles in nutrient and nutraceutical delivery*, Current Opinion in Colloid & Interface Science 14 (2009) 3–15.

[6] Li Mu, R. Sprando, *Application of nanotechnology in cosmetics*, Pharmaceutical Research, 27(8):1746-1749, 2010.

[7] Tin-hinan Kabri, Elmira Arab-Tehrany, Nabila Belhaj and Michel Linder, *Physico-chemical characterization of nanoemulsions in cosmetic matrix enriched on omega-3*, Journal of Nanobiotechnology 2011, 9:41.

[8] Zibin Gao, Linan Zhang, Yongjun Sun, *Nanotechnology applied to overcome tumor drug resistance*, Journal of Controlled Release 162 (2012) 45–55.

[9] Suphiya Parveen, Ranjita Misra, Sanjeeb K. Sahoo, *Nanoparticles: a boon to drug delivery, therapeutics, diagnostics and imaging*, Nanomedicine: Nanotechnology, Biology, and Medicine 8 (2012) 147–166.

[10] Ki Young Choi, Hyunjin Chung, Kyung Hyun Min, Hong Yeol Yoon, Kwangmeyung Kim, Jae Hyung Park, Ick Chan Kwon, Seo Young Jeong, *Self-assembled hyaluronic acid nanoparticles for active tumor targeting*, Biomaterials 31 (2010) 106–114.

[11] Marie Gaumet, Angelica Vargas, Robert Gurny, Florence Delie, *Nanoparticles for drug delivery: The need for precision in reporting particle size parameters*, European Journal of

Pharmaceutics and Biopharmaceutics 69 (2008) 1–9.

[12] Dan Peer, Jeffrey M. Karp, Seungpyo Hong, Omid C. Farokhzad, Rimona Margalit and Robert Langer, *Nanocarriers as an emerging platform for cancer therapy*, Nature Nanotechnology, Vol 2, December 2007.

[13] Andrew I. Minchinton and Ian F. Tannock, *Drug penetration in solid tumours*, Nature Reviews, Cancer Volume 6, August 2006, 583-592.

[14] Olivier Trédan, Carlos M. Galmarini, Krupa Patel, Ian F. Tannock, *Drug Resistance and the Solid Tumor Microenvironment*, J Natl Cancer Inst 2007; 99:1441–54.

[15] Andrew J. Primeau, Augusto Rendon, David Hedley, Lothar Lilge, and Ian F.Tannock, *The Distribution of the Anticancer Drug Doxorubicin in Relation to Blood Vessels in Solid Tumors*, Clin Cancer Res December 15 2005; 11(24):8782-8.

[16] Cliff Wong, Triantafyllos Stylianopoulos, Jian Cui, John Martin, Vikash P. Chauhan, Wen Jiang, Zoran Popovic, Rakesh K. Jain, Moungi G. Bawendi, and Dai Fukumura, *Multistage nanoparticle delivery system for deep penetration into tumor tissue*, 2426–2431, PNAS, February 8, 2011, 108(6):2426–2431.

[17] Rakesh K. Jain and Triantafyllos Stylianopoulos, *Delivering nanomedicine to solid tumors*, Nat Rev Clin Oncol. 2010 November; 7(11): 653–664.

[18] Naoyuki Kohno, Takao Ohnuma, Peter Truog, *Effects of hyaluronidase on doxorubicin penetration into squamous carcinoma multicellular tumor spheroids and its cell lethality*, J Cancer Res Clin Oncol (1994) 120:293-297.

[19] "DOXIL Product Information" Ortho Biotech Products, L.P. Archived September 21, 2007 at the Wayback Machine.

[20] "Liposomal doxorubicin (Caelyx, Myocet)", Macmillan Cancer Support. April 1, 2009.

[21] "Doxorubicin liposomal", Chemocare. Cleveland Clinic.

[22] Abuchowski A., McCoy J. R., Palczuk N. C., van Es T., Davis F. F., *Effect of covalent attachment of polyethylene glycol on immunogenicity and circulating life of bovine liver catalase*, Journal of Biological Chemistry 1977, 252, 11, 3582–3586.

[23] Veronese F. M., Pasut G., *PEGylation, successful approach to drug delivery*, Drug Discovery Today 2005, 10, 21, 1451–1458.

[24] Ryan S. M., Giuseppe M., Wang X., Haddleton D. M., Brayden D. J., *Advances in PEGylation of important biotech molecules: delivery aspects*, Expert Opinion on Drug Delivery 2008, 5(4):371-383.

[25] Damodaran V. B. Fee C. J., *Protein PEGylation: An overview of chemistry and process considerations*, European Pharmaceutical Review 2010, 15, 1, 18-26.

[26] Bjugstad K. B., Redmond Jr. D. E., Lampe K. J., Kern D. S., Sladek Jr. J. R., Mahoney M. J., *Biocompatibility of PEG-Based Hydrogels in Primate Brain*, Cell Transplantation 2008, 17, 4, 409-415.

[27] PEG-ylated products (2011), *http://www.pegasys.com/pegasys/about-pegasys/pegasys-interferon.htm* [accessed September 2011].

[28] Graham, M. L., *Pegaspargase: a review of clinical studies*, Advanced Drug Delivery Review 2003, 55(10):1293–1302.

[29] Rabinov, B.E., *Nanosuspensions in drug delivery*, Nature Reviews of Drug Discovery 2004, 3, 785-796.

[30] Moghimi S.M., Sebeni J., *Stealth liposomes and long circulating nanoparticles: critical issues in pharmacokinetics, opsonization and protein-binding properties*, Progress in Lipid Research 2003, 42, 463-478.

[31] Monghimi, S.M.; Hunter, A.C., *Recognition by macrophages and liver cells of opsonized phospholipids vescicles and phospholipids headgroups*, Pharmaceutical Research 18, 1-8.

[32] Szebeni, J., Alving, C.R., Savay, S., Barenholtz, Y., Priev, A., Danino, D., Talamon, Y., *Formation of complement –activating particles in acquous solutions of Toxol: possible role in hypersensitivity reactions*, International Immunopharmacology 1, 721-735.

[33] P. Decuzzi, M. Ferrari. *The Receptor-Mediated Endocytosis of Nonspherical Particles*, Biophysical Journal 94(10):3790–3797, 2008.

[34] Arnaud Beduneau, Patrick Saulnier, Nicolas Anton, Francois Hindre, Catherine Passirani, Holisoa Rajerison, Nicolas Noiret, Jean-Pierre Benoit, *Pegylated Nanocapsules Produced by an Organic Solvent-Free Method: Evaluation of their Stealth Properties*, Pharmaceutical Research, 23(9):2190-2199, 2006.

[35] Julie A. Champion, Samir Mitragotri, *Role of target geometry in phagocytosis*, Proceedings of the National Academy of Sciences of the United States of America. 103(13):4930-4934, 2006.

[36] Wen Jiang, Betty Y. S. Kim, James T. Rutka, Warren C. W. Chan, *Nanoparticle-mediated cellular response is size-dependent*, Nature Nanotechnology, 3(3):145–150, 2008.

[37] Brian J. Hicke, Andrew W. Stephens, Ty Gould, Ying-Fon Chang, Cynthia K. Lynott, James Heil, Sandra Borkowski, Christoph-Stephan Hilger, Gary Cook, Stephen Warren, and Paul G. Schmidt, *Tumor Targeting by an Aptamer*, The Journal of Nuclear Medicine, 47(4), April 2006.

[38] M. Malvezzi, P. Bertuccio, F. Levi, C. La Vecchia & E. Negri, *European cancer mortality predictions for the year 2013*, Annals of Oncology Advance Access published February 12, 2013.

[39] Francois Quemeneur, Marguerite Rinaudo and Brigitte Pèpin-Donat, *Influence of Polyelectrolyte Chemical Structure on their Interaction with Lipid Membrane of Zwitterionic Liposomes*, Biomacromolecules. 9(8):2237–2243, 2008.

[40] Moghimi S. M., Hunter A. C., Murray J. C., *Nanomedicine: current status and future prospects*, The FASEB Journal, 2005, 19, 311-330.

[41] Hai-jian Xia, Zhen-hai Zhang, Xin Jin, Qin Hu, Xiao-yun Chen, Xiao-bin Jia, *A novel drug–phospholipid complex enriched with micelles: preparation and evaluation in vitro and in vivo*, International Journal of Nanomedicine 2013, 8, 545–554.

[42] Banerjee A, Onyuksel H., *Peptide delivery using phospholipid micelles*, Wiley Interdiscip Rev Nanomed Nanobiotechnol, 2012 Sep-Oct; 4(5):562-74.

[43] Francis M.F., Francis1, Mariana Cristea, Françoise M. Winnik, *Polymeric micelles for oral drug delivery: Why and how?*, Pure and Applied Chemistry, 76(7–8):1321–1335, 2004.

[44] Dongin Kim, Zhong Gao Gao, Eun Seong Lee, and You Han Bae, *In vivo evaluation of doxorubicin-loaded polymeric micelles targeting folate receptors and early endosomal pH in drug resistant ovarian cancer*, Mol Pharm. 2009, 6(5):1353–1362.

[45] Nelson A Ochekpe, Patrick O Olorunfemi and Ndidi C Ngwuluka, *Nanotechnology and Drug Delivery Part 2: Nanostructures for Drug Delivery*, Trop J Pharm Res, June 2009, 8(3):275-287.

[46] Gianella A, Jarzyna P. A, Mani V, Ramachandran S, Calcagno C, Tang J, Kann B, Dijk W. J. R., Thijssen V. L, Griffioen A. W, Storm G, Fayad Z. A, Mulder W. J. M, *A Multifunctional Nanoemulsion Platform for Imaging Guided Therapy Evaluated in Experimental Cancer*, ACS Nano 2011, 5(6):4422–33.

[47] Seyfoddin Ali, Shaw J., Al-Kassas R., *Solid lipid nanoparticles for ocular drug delivery*, Drug delivery, 2010, 17, 7, 467–489.

[48] Beezer A. E., King A. S. H., Martin I. K., Mitchel J. C., Twyman L. J., Wain C. F., *Dendrimers as potential drug carriers; encapsulation of acidic hydrophobes within water soluble PAMAM derivatives*, Tetrahedron, 2003, 59, 3873–3880.

[49] Rania Bakry, Rainer M Vallant, Muhammad Najam-ul-Haq, Matthias Rainer, Zoltan Szabo, Christian W Huck, Günther K Bonn, Medicinal applications of fullerenes, International Journal of Nanomedicine 2007:2(4) 639–649.

[50] Nazarov G. V., Galan S. E., Nazarova E. V., Karkishchenko N. N., Muradov M. M.,

Stepanov, V. A., *Drug synthesys method and manufacturing technology. Nanosized forms of drug (a review)*, Pharmaceutical Chemistry Journal, 2009, 43(3):163-170.

[51] Abdelbary M. A. Elhissi, Waqar Ahmed, Israr Ul Hassan, Vinod. R. Dhanak, and Antony D'Emanuele, *Carbon Nanotubes in Cancer Therapy and Drug Delivery*, Journal of Drug Delivery, Volume 2012, Article ID 837327.

[52] Takuya Yamashita, Kohei Yamashita, Hiromi Nabeshi, Tomoaki Yoshikawa, Yasuo Yoshioka, Shin-ichi Tsunoda and Yasuo Tsutsumi, *Carbon Nanomaterials: Efficacy and Safety for Nanomedicine*, Materials 2012, 5, 350-363.

[53] Gong-Yan Liu, Chao-Jian Chen and Jian Ji, *Biocompatible and biodegradable polymersomes as delivery vehicles in biomedical applications*, Soft Matter, 2012, 8, 8811.

[54] Charles Sanson, Odile Diou, Julie Thevenot, Emmanuel Ibarboure, Alain Soum, Annie Brulet, Sylvain Miraux, Eric Thiaudiere, Sisareuth Tan, Alain Brisson, Vincent Dupuis, Olivier Sandre, and Sebastien Lecommandoux, *Doxorubicin Loaded Magnetic Polymersomes: Theranostic Nanocarriers for MR Imaging and Magneto-Chemotherapy*, ACS Nano 5(2):1122–1140, 2011.

[55] Masayuki Yokoyama, *Clinical Applications of Polymeric Micelle Carrier Systems in Chemotherapy and Image Diagnosis of Solid Tumors*, J Exp Clin Med 2011, 3(4):151-158.

[56] S. J. Oldenburg, J. B. Jackson, S. L. Westcott, and N. J. Halas, *Infrared extinction properties of gold nanoshells*, Applied Physics Letters Vol. 75, No. 19.

[57] Gabriele Maiorano, Stefania Sabella, Barbara Sorce, Virgilio Brunetti, Maria Ada Malvindi, Roberto Cingolani, and Pier Paolo Pompa, *Effects of Cell Culture Media on the Dynamic Formation of Protein Nanoparticle Complexes and Influence on the Cellular Response*, ACS Nano 4(12):7481–7491, 2010.

[58] Neenu Singha, Gareth J.S. Jenkinsa, Romisa Asadib and Shareen H. Doak, *Potential toxicity of superparamagnetic iron oxide nanoparticles (SPION)*, Nano Reviews 2010, 1:5358.

[59] Rita E. Serda, Biana Godin, Elvin Blanco, Ciro Chiappini, and Mauro Ferrari, *Multi-stage delivery nano-particles system for therapeutic applications*, Biochim Biophys Acta. 2011 March, 1810 (3):317–329.
.
[60] Loretta L. del Mercato, Pilar Rivera-Gil, Azhar Z. Abbasi, Markus Ochs, Carolin Ganas, Inga Zins, Carsten Sonnichsenb and Wolfgang J. Paraka, *LbL multilayer capsules: recent progress and future outlook for their use in life sciences*, Nanoscale, 2010, 2, 458–467.

[61] Catarina Pinto Reis, Ronald J Neufeld, António J Ribeiro, Francisco Veiga, *Nanoencapsulation II. Biomedical applications and current status of peptide and protein nanoparticulate delivery systems*, Nanomedicine: nanotechnology, biology and medicine. 2(2):53-65, 2006.

[62] Jonathan Hadgraft and Majella E. Lane, *Skin: the ultimate interface*, Phys. Chem. Chem. Phys., 2011, 13, 5215–5222.

[63] Advancell (2013), Dermosome Technology, *http://www.advancell.net/?page_id=327*, [accessed January 2013].

[64] K. Egbaria and N. Weiner, *Liposomes as a topical drug delivery system*, Advanced Drug Delivery Reviews, 5 (1990) 287-300.

[65] Jana Pardeike, Aiman Hommoss, Rainer H. Müller, *Lipid nanoparticles (SLN, NLC) in cosmetic and pharmaceutical dermal products*, International Journal of Pharmaceutics 366 (2009) 170–184.

[66] Charles Lovelyn, Anthony A. Attama, *Current State of Nanoemulsions in Drug Delivery*, Journal of Biomaterials and Nanobiotechnology, 2011, 2, 626-639.

[67] Sílvia S. Guterres, Marta P. Alves and Adriana R. Pohlmann, *Polymeric Nanoparticles, Nanospheres and Nanocapsules for Cutaneous Applications*, Drug Target Insights 2007: 2 147–157.

[68] Shah P, Bhalodia D, Shelat P., *Nanoemulsion: a pharmaceutical review*, Systematic reviews in pharmacy 2010; 1:24-32.

[69] Arora N, Agarwal S, Murthy RSR, *Latest Technology Advances in Cosmaceuticals*, International Journal of Pharmaceutical Sciences and Drug Research 2012; 4:168-82.

[70] Sonneville-Aubrun O, Simonnet JT, L'Alloret F, *Nanoemulsions: a new vehicle for skincare products*, Advances in Colloid and Interface Science 2004; 108-109:145-49.

[71] Fei Xiong, Hao Wang, Yue-Jian Chen, Kun-Kun Geng, Ning Gu, and Jia-Bi Zhu, *Characterization, biodistribution and targeting evaluation of breviscapine lipid emulsions following intravenous injection in mice*, Drug Delivery, 2011; 18(2):159-165.

[72] Sanguansri, L., Oliver, C. M. and Leal-Calderon, F. (2013) Nanoemulsion Technology for Delivery of Nutraceuticals and Functional-Food Ingredients, in Bio-Nanotechnology: A Revolution in Food, Biomedical and Health Sciences (eds D. Bagchi, M. Bagchi, H. Moriyama and F. Shahidi), Blackwell Publishing Ltd., Oxford, UK. doi:10.1002/9781118451915 chapter38.

[73] A. Forgiarini, J. Esquena, C. Gonzalez, C. Solans, *Formation of Nano-emulsions by Low-Energy Emulsification Methods at Constant Temperature*, Langmuir 17(7):2076-2083, 2001.

[74] Isabel Solè, Carmen M. Pey, Alicia Maestro, Carmen González, Montserrat Porras, Conxita Solans, José M. Gutiérrez, *Nano-emulsions prepared by the phase inversion composition method: Preparation variables and scale up*, Journal of Colloid and Interface Science 344 (2010) 417–423.

[75] Richard J. Farn, *Chemistry and Technology of Surfactants*, Blackwell publishing Ltd, 2006, Wiley online book.

[76] Satoshi Ogawa, Eric A. Decker, D. Julian McClements, *Production and Characterization of O/W Emulsions Containing Droplets Stabilized by Lecithin−Chitosan−Pectin Mutilayered Membranes*, Journal of Agricultural and Food chemistry, 52(11):3595-3600, 2003.

[77] Iva Kralova; Johan Sjöblom, *Surfactants Used in Food Industry: A Review*, Journal of Dispersion Science and Technology, 30:1363–1383, 2009.

[78] D. Julian McClements, *Theoretical Analysis of Factors Affecting the Formation and Stability of Multilayered Colloidal Dispersions*, Langmuir 2005, 21, 9777-9785.

[79] Demet Guzey, D. Julian McClements, *Formation, stability and properties of multilayer emulsions for application in the food industry*, Advances in Colloid and Interface Science 128–130 (2006) 227–248.

[80] Lydie Moreau, Hyun-Jung Kim, Eric A. Decker, and Julian McClements, *Production and Characterization of Oil-in-Water Emulsions Containing Droplets Stabilized by â-Lactoglobulin-Pectin Membranes*, J. Agric. Food Chem. 2003, 51, 6612-6617.

[81] Satoshi Ogawa, Eric A. Decker, and D. Julian McClements, *Production and Characterization of O/W Emulsions Containing Cationic Droplets Stabilized by Lecithin-Chitosan Membranes*, J. Agric. Food Chem. 2003, 51, 2806-2812.

[82] Muzzarelli, R. A. A., *Depolymerization of chitins and chitosans with hemicellulase, lysozyme, papain and lipases*. In R. A. A. Muzzarelli, & M. G. Peter (Eds.), Chitin handbook (pp. 153–164). Grottammare: Atec Edizioni (1997).

[83] Muzzarelli, R. A. A, *Chitin nanostructures in living organism's chitin: Formation and diagenesis*, Topics in Biogeology, 34, 1–34 (2011).

[84] M. Dasha, F. Chiellini, R.M. Ottenbrite, E. Chiellini, *Chitosan-A versatile semi-synthetic polymer in biomedical applications*, Progress in Polymer Science 36 (2011) 981–1014.

[85] Krzysztof Szczepanowicz, Dorota Dronka-Gora, Grazyna Para and Piotr Warszynski, *Encapsulation of liquid cores by layer-by-layer adsorption of polyelectrolytes*, Journal of Microencapsulation, 2010; 27(3):198-204.

[86] Claudia Preetz, Andrea Rübe, Ines Reiche, Gerd Hause, Karsten Mäder, *Preparation and characterization of biocompatible oil-loaded polyelectrolyte nanocapsules*, Nanomedicine: Nanotechnology, Biology, and Medicine 4 (2008) 106–114.

[87] Saehun Mun, Eric A. Decker, D. Julian McClements, *Influence of droplet characteristics on the formation of oil-in-water emulsion stabilized by surfactant-chitosan layers*, Langmuir: the ACS journal of surfaces and colloids. 21(14):6228-6234, 2005.

[88] C. E. Mora-Huertasa, H. Fessi, A. Elaissari, *Polymer-based nanocapsules for drug delivery*, International Journal of Pharmaceutics 385 (2010) 113–142.

[89] Catarina Pinto Reis, Ronald J. Neufeld, Antonio J. Ribeiro, Francisco Veiga, *Nanoencapsulation I. Methods for preparation of drug-loaded polymeric nanoparticles*, Nanomedicine: Nanotechnology, Biology, and Medicine 2 (2006) 8– 21.

[90] Mi-Yeon Lee, Sang-Gi Min, Sandrine Bourgeois, Mi-Jung Cholang, *Development of a novel nanocapsule formulation by emulsion-diffusion combined with high hydrostatic pressure*, Journal of Microencapsulation 26(2):122–129, 2009.

[91] Isabel M. Martins, Sofia N. Rodrigues, Filomena Barreiro, Alırio. E. Rodrigues. *Microencapsulation of thyme oil by coacervation*, Journal of Microencapsulation, 26(8):667–675, 2009.

[92] Svetlana A. Sukhishvili, *Responsive polymer films and capsules via layer-by-layer assembly*, Current opinion in Colloid & Interface Science 10 (2005) 37-44.

[93] Hye Young Koo, Ha-Jin Lee, Jun Kyung Kim and Won San Choi, *UV-triggered encapsulation and release from polyelectrolyte microcapsules decorated with photoacid generators*, Journal of Materials and Chemistry, 2010, 20, 3932-3937.

[94] Yan Yan, Georgina K. Such, Angus P. R. Johnston, Hannah Lomas, and Frank Caruso, *Toward Therapeutic Delivery with Layer-by-Layer Engineered Particles*, ACS nano 5(6):4252–4257, 2011.

[95] Gero Decher, *Fuzzy Nanoassemblies: Towards Layered Polymeric Multicomposites*, Science, Vol. 277 29 August 1997.

[96] Piotr Kujawa, Patricia Moraille, Jacqueline Sanchez, Antonella Badia, and Francoise M.Winnik, *Effect of Molecular Weight on the exponential Growth and Morphology of Hyaluronano/Chitosan Multilayers: A surface Plasmon Resonance Spectroscopy and Atomic Force Microscopy Investigation*, J. Am. Chem. Soc. 2005, 127, 9224-9234.

[97] Volodkin D. V., Larionova N. I., Sukhorukov G. B., *Protein Encapsulation via Porous CaCO3 Microparticles Templating*, Biomacromolecules 2004, 5, 1962-1972.

[98] Di Cui A. S., Dubreuil F., De Geest B. G., De Cock L. J., Picart C., R. Auzely-Velty, *Designing Hyaluronic Acid-Based Layer-by-Layer Capsules as a Carrier for Intracellular Drug Delivery*, Biomacromolecules 2010, 11, 3, 713-720.

[99] Hu B. Y., Cai K., Luo Z., Jandt K.D., *Layer-By-Layer Assembly of β -Estradiol Loaded Mesoporous Silica Nanoparticles on Titanium Substrates and Its Implication for Bone Homeostasis*, Advanced Materials 2010, 22, 4146–4150.

[100] Sukhorukov G. B., Donath E., Lichtenfeld H., Knippel E., Knippel M., Budde A.,

Mohwald H.; *Layer-by-layer self assembly of polyelectrolytes on colloidal particles*, Colloids Surfaces A: Physicochemical Eng. Aspects 1998, 137, 253-266.

[101] Gao C. Y., Moya S., Lichtenfeld H., Casoli A., Fiedler H., Donath E., Mohwald H., *The Decomposition Process of Melamine Formaldehyde Cores: The Key Step in the Fabrication of Ultrathin Polyelectrolyte Multilayer Capsules*, Macromolecular Materials Engineering 2001, 286, 6, 355-361.

[102] I. I. Slowing, J. L. Vivero-Escoto, C. W. Wu, V. S. Lin, *Mesoporous silica nanoparticles as controlled release drug delivery and gene transfection carriers*, Advanced Drug Delivery Review 2008, 60, 1278-1288.

[103] Angus P. R. Johnston, Christina Cortez, Alexandra S. Angelatos, Frank Caruso, *Layer-by-layer engineered capsules and their applications*, Current Opinion in Colloid & Interface Science 11 (2006) 203–209.

[104] Stefaan De Koker, Richard Hoogenboom and Bruno G. De Geest, *Polymeric multilayer capsules for drug delivery*, Chem. Soc. Rev., 2012, 41, 2867–2884.

[105] Sri Sivakumar, Vipul Bansal, Christina Cortez, Siow-Feng Chong, Alexander N. Zelikin, and Frank Caruso, *Degradable, Surfactant-Free, Monodisperse Polymer-Encapsulated Emulsions as Anticancer Drug Carriers*, Adv. Mater. 2009, 21, 1820-1824.

[106] Sukhorukov G. B., Dahne L., Hartmann J., Donath E., Mohwald H., *Controlled precipitation of dyes into hollow polyelectrolyte capsules based on colloids and biocolloids*, Advanced Materials 2000 12, 112–115.

[107] Caruso F., Fiedler H., Haage K., *Assembly of b-glucosidase multilayers on spherical colloidal particles and their use as active catalysts*, Colloids and Surfaces -A 2000,169,287–293.

[108] Schuler C., Caruso F., *Decomposable hollow biopolymer-based capsules*, Biomacromolecules 2001, 2, 921–926.

[109] Georgieva, R., Moya, S., Donath, E., Baumler, H., *Permeability and conductivity of red blood cell templated polyelectrolyte capsules coated with supplementary layers*, Langmuir 2004 20, 1895–1900.

[110] Donath E., Moya S., Neu B., Sukhorukov G. B., Georgieva R, Voigt A., *Hollow polymer shells from biological templates: Fabrication and potential applications*, Chemistry-A European Journal 2002, 8, 5481–5485.

[111] Radtchenko I.L., Giersig M., Sukhorukov G.B., *Inorganic particle synthesis in confined micron-sized polyelectrolyte capsules*, Langmuir 2002, 18, 8204–8208.

[112] Shchukin D.G., Radtchenko I.L., Sukhorukov G.B., *Synthesis of nanosized magnetic ferrite particles inside hollow polyelectrolyte capsules*, Journal Physical Chemistry- B 2003, 107,

86–90.

[113] Shchukin D. G., Shutava T., Shchukina E., Sukhorukov B. G., Lvov Y. M., *Modified polyelectrolyte microcapsules as smart defense systems*, Chemistry of Materials 2004, 16, 3446–3451.

[114] Shchukin D. G., Sukhorukov G. B., Mohwald H., *Smart inorganic/organic nanocomposite hollow microcapsules*, Angewandte Chemie International Edition English 2003, 42, 4472–4475.

[115] Shchukin D. G., Sukhorukov G. B., Mohwald H., *Fabrication of fluorescent rare earth phosphates in confined media of polyelectrolyte microcapsules*, Journal Physical Chemistry-B 2004, 108, 19109–19113.

[116] Tong W., Gao C., Mohwald H., *Poly(ethyleneimine) microcapsules: Glutaraldehyde-mediated assembly and the influence of molecular weight on their properties*, Polymer Advanced Technolgy, 2008, 19, 817–823.

[117] Tomihata K., Ikada Y., *Crosslinking of hyaluronic acid with water-soluble carbodiimide*, Journal of Biomedical Materials Research, 1997 37, 243–251.

[118] Luke A. Connal, Cameron R. Kinnane, Alexander N. Zelikin, and Frank Caruso, *Stabilization and Functionalization of Polymer Multilayers and Capsules via Thiol-Ene Click Chemistry*, Chem. Mater. 2009, 21, 576–578.

[119] Mauro Ferrari, *Beyond drug delivery*, Nature Nanotechnology, vol. 3 March 2008.

[120] Vijapur L. S. et al., *Thiolated Chitosans: a novel mucohadesive polymers: a review*, International Research Journal of Pharmacy, (2012), 3 (4):51-57.

[121] Shujun Shu, Xinge Zhang, Zhongming Wu, Zhen Wang, Chaoxing Li, *Gradient cross-linked biodegradable polyelectrolyte nanocapsules for intracellular protein drug delivery*, Biomaterials 31(2010) 6039-6049.

[122] P. Lertsutthiwong, P. Rojsitthisak, U. Nimmannit, *Preparation of turmeric oil-loaded chitosan-alginate biopolymeric nanocapsules*, Materials Science and Engineering: C. 29(3):856-860, 2009.

[123] Kyuri Lee, Hyukjin Lee, Ki Hyun Bae, Tae Gwan Park, *Heparin immobilized gold nanoparticles for targeted detection and apoptotic death of metastatic cancer cells*, Biomaterials 31 (2010) 6530-6536.

[124] Qichao Ruan, Yingchun Zhu, Fang Lia, Junwu Xiao, Yi Zeng, Fangfang Xu, *Investigation of layer-by-layer assembled heparin and chitosan multilayer films via electrochemical spectroscopy*, Journal of Colloid and Interface Science 333 (2009) 725–733.

[125] Abdallah Makhlof, Martin Werle, Yuichi Tozuka, Hirofumi Takeuchi, *Nanoparticles of*

glycol chitosan and its thiolated derivative significantly improved the pulmonary delivery of calcitonin, International Journal of Pharmaceutics 397 (2010) 92–95.

[126] Knight D. K., Shapka S. N., Amsden B. G., *Structure, depolymerization, and cytocompatibility evaluation of glycol chitosan*, Journal of Biomedical Materials Research - Part A, 1 November 2007, 83(3):787-798.

[127] Ali Al-Saadi, Chih Hao Yu, Vitaliy V. Khutoryanskiy, Shao-Ju Shih, Alison Crossley, and Shik Chi Tsang, *Layer by-Layer Electrostatic Entrapment of Protein Molecules on Superparamagnetic Nanoparticle: A New Strategy to Enhance Adsorption Capacity and Maintain Biological Activity*, J. Phys. Chem. C 2009, 113, 15260–15265.

[128] G. Graham Allan, Mark Peyron, *Molecular weight manipulation of chitosan I: kinetics of depolymerization by nitrous acid*, Carbohydrate Research 277 (1995) 257-272.

[129] G. Graham Allan, Mark Peyron, *Molecular weight manipulation of chitosan II: prediction and control of extent of depolymerization by nitrous acid*, Carbohydrate Research 277 (1995) 273-282.

[130] Shirui Mao, Xintao Shuai, Florian Unger, Michael Simon, Dianzhou Bi, Thomas Kissel, *The depolymerization of chitosan: effects on physicochemical and biological properties*, International Journal of Pharmaceutics 281 (2004) 45–54.

[131] Riddles P., Blakeley R., Zerner B., *Ellman's Reagent: 5,5'-Dithiobis(2-nitrobenzoicAcid) a Reexamination*, Analytical Biochemistry 94, 75-81 (1979).

[132] Mirko X. Weinhold, Janelle C. M. Sauvageau, Nadia Keddig, Marianne Matzke, Bernd Tartsch, *Strategy to improve the characterization of chitosan for sustainable biomedical applications: SAR guided multi-dimensional analysis*, Green Chem., 2009, 11, 498–509.

[133] Neil B. Cramer, J. Paul Scott, and Christopher N. Bowman, *Thiol–Enes: Chemistry of the Past with Promise for the Future*, Macromolecules 2002, 35, 5361-5365.

[134] Cherles E. Hoyle, Tai Yeon Lee, Todd Roper, *Thiol–Enes: Chemistry of the Past with Promise for the Future*, Journal of Polymer Science: Part A: Polymer Chemistry, Vol. 42, 5301–5338 (2004).

[135] Aleksa V. Jovanovic, Royale S. Underhill, Tracy L. Bucholz, and Randolph S. Duran, *Oil Core and Silica Shell Nanocapsules: Toward Controlling the Size and the Ability To Sequester Hydrophobic Compounds*, Chem. Mater. 2005, 17, 3375-3383.

[136] Denis Semwogerere, Eric R. Weeks, *Confocal Microscopy*, Encyclopedia of Biomaterials and Biomedical Engineering Copyright 2005 by Taylor & Francis.

[137] *Multiphoton Excitation Microscopy*, MPE Tutoria, Copyright 2000 Coherent, Inc.

[138] Silvia Galiani, Benjamin Harke, Giuseppe Vicidomini, Gabriele Lignani, Fabio Benfenati, Alberto Diaspro, and Paolo Bianchini, *Strategies to maximize the performance of a STED microscope*, Optics Express 26 March 2012 20(7):7362.

[139] John J. Bozzola, Lonnie D. Russell, *Electron Microscopy* Second edition, Jones and Bartlett Publishers.

[140] Stefani E., Wu Y., Rodriguez P. F. G., *http://www.anes.ucla.edu/sted/principle.html* [accessed January 2013]

[141] Tony Owen, *Fundamentals of UV-visible spectroscopy*, Chapter 1, Copyright Hewlett-Packard Company, 1996.

[142] James Keeler, *Understanding NMR Spectroscopy*, James Keeler, 2002 & 2004.

Acknoweledgments

It is unbelievable I am getting a PhD considering that just after my degree I went working for companies and only after 9 years I decided to come back to University to apply for a Doctorate. For that I thank my innate desire to do research.

My first "thanks" goes to my grandfather Raffaele who was an example of life for me. He worked hard during all his life reaching the top but staying modest and generous towards everybody asking for help and, most of all, close to his family to which he dedicated his entire life. Whenever I feel tired and discouraged it is enough to think about him and I get the strength to face every difficulty. I also want to thank all my relatives in particular, my aunt Nunzia - from up there- who has always had a high opinion of me, which is a daily motivation and incitation. I thank my parents Francesco and Luisa for all the values they gave me and for being always present when needed as well as my little brother Nico and my sister Anna who are always very nice to me and are an important part of my life.

Then, I want to thank my future wife Antonella who supported me in this journey with her love understanding when I had to spend most of my time to the last experiments of the day and being patient listening to my little work discovery stories. It was thanks to her if I was able to achieve this important goal serenely. I take also the occasion to thank my four kind sisters-in-law, Mita, Chiara, Paola and Teresa.

Furthermore, I wish to thank prof. Netti for his valuable advice and for believing in me even if older than average and with a different background and career. He offered me the opportunity to join his group committing me to a challenging and new project in the field of nanomedicine. I am happy to work with him because I see we are on the same page in trying to do something useful for humankind.

Finally, a special "thanks" goes to past collaborators Ugo, Angela, and a present collaborator, Enzo, who directly contributed to this work as well as all the IIT and Unina collaborators and colleagues. I also want to thank Bianchini and Formiggini for STED analysis, Cossi for granulometric tests, Matthijn for cryo-TEM analysis and De Castro for helping with the interpretation of NMR spectra.

Raffaele Vecchione
April 2